# Low-Rank Distributed Control with Application to Wind Energy

Madjidian, Daria

2014

*Document Version:*
Publisher's PDF, also known as Version of record

# Low-Rank Distributed Control with Application to Wind Energy

Daria Madjidian


LUND
UNIVERSITY

Department of Automatic Control

The picture on the upper part of the cover shows wake effects at Horns Rev offshore wind farm located in the North Sea. Courtesy of Vattenfall.

PhD Thesis
ISRN LUTFD2/TFRT--1103--SE
ISBN 978-91-7623-003-9 (print)
ISBN 978-91-7623-004-6 (web)
ISSN 0280–5316

Department of Automatic Control
Lund University
Box 118
SE-221 00 LUND
Sweden


Printed in Sweden by Media-Tryck.
Lund 2014

*To Layla and Freya*

# Abstract

This thesis addresses three different topics in wind power plant operation.

Most of the research is focused on controlling a wind farm that is required to meet a power set-point. In this mode of operation, the wind turbines are able to vary their power production as long as the total power demand is met. The research investigates how this freedom can be used in order to reduce the fatigue loads experienced by the wind turbines. The problem is studied in a linear-quadratic control setting where the objective is to minimize the total fatigue load experienced by the turbines, while satisfying a requirement on their joint power production. It is shown that, under certain assumptions, the design problem can be drastically simplified. In particular, the computational effort needed to obtain the solution is independent of the number of wind turbines and the only centralized operation required to implement the optimal control law is a single summation. The research also explains the mechanisms that make power allocation schemes useful for load reduction.

Part of the research addresses wake effects in wind farms by developing a low-complexity model of the aerodynamic interaction between wind turbines. The model is used in a series of examples, where the wind turbines coordinate their power productions in order to maximize the power production of the wind farm. The examples indicate that the benefit of power coordination increases with the number of turbines in the wind farm. They also identify the underlying mechanisms behind this effect.

The last topic of the thesis is to investigate the benefits of using preview of the incoming wind speed in order to reduce structural loads on the wind turbine tower. The main focus is to understand how measurement distortion influences the achievable load reduction as well as the required length of preview. Results from high-fidelity simulations based on real wind turbine measurements indicate that the use of preview can lead to a significant reduction of tower fatigue loads and that the length of preview needed to attain the reduction does not exceed a few seconds.

# Acknowledgments

I have had the privilege of working with some very skilled and interesting people and this thesis would not have been possible without their help. First, I would to thank my supervisor, Anders Rantzer, for his support and encouragement, and for allowing me to pursue my interests. He is a constant source of ideas and guidance. He has also created opportunities for me to work with others. I am especially grateful to my collaborators, Leonid Mirkin and Maxim Kristalny. Their role in this this thesis can not be overstated. Their technical savvy and attitude towards research has been a real source of inspiration. Thank you both for being so pleasant to work with and so generous with your time. During my time at the department, I had the privilege of sharing offices with two colleagues: Erik Johannesson and Mahdi Ghazaei. I thoroughly enjoyed their company and our discussions, both technical and not. A special thanks to Erik for learning enough Chinese so that we could eat well during our stay in China, and to Mahdi for his Farsi lessons. I am also very grateful to those that keep the department running with such efficiency. Especially to Eva Westin, Ingrid Nilsson, Eva Schildt and Britt-Marie Mårtensson for their (endless?) patience with my sea of questions and requests, and to Leif Andersson for his help with typesetting the thesis and for saving me from several computer related crises. To all the current and former staff in our department, thank you for the great working environment and many friendships.

To my parents, thank you for always making sure I had the possibility to choose my direction. Without your guidance and support, my life would not have been the same.

Most of all, I would like to thank my wife Layla for her constant love and support, especially during the last stages of writing. This would not have been possible without you.

*Daria*

# Contents

# Preface

## Contributions of the Thesis

This thesis consits of two introductory chapters and six papers. This section describes the contents of the introductory chapters and the contributions of each paper.

### Chapter 1 – Wind Energy

The objective of this chapter is twofold. First, it aims to contextualize the research in this thesis and discuss its contributions in a wind energy setting. Second, it provides necessary background information to readers who are not familiar with wind energy applications.

### Chapter 2 – Linear-Quadratic Control Theory

The first section of this chapter reviews some fundamental results in linear-quadratic control that are frequently used in the papers. Section 2.2 summarizes the author's view of the contributions of this thesis in the context of linear quadratic control theory.

### Paper I

Madjidian, D., M. Kristalny, and A. Rantzer (2013). "Dynamic power coordination for load reduction in dispatchable wind power plants". In: *Proceedings of the 2013 European Control Conference*. Zürich, Switzerland, pp. 3554–3559.

The paper assumes a setting where a wind farm is required meet a pre-specified power set-point. In such situations, there is freedom in how the total power demand is distributed over the individual wind turbines. The focus of the paper is to investigate the benefits of dynamic power allocation schemes in terms of reducing fatigue loads on the turbines. In particular, the paper assesses the potential for load reduction at different

operating points and explains the mechanisms that make power allocation useful.

### Paper II

Madjidian, D. and L. Mirkin (2014). "Distributed control with low-rank coordination". *IEEE Transactions on Control of Network Systems* **1**:1, pp. 53–63.

The paper studies coordination among a homogeneous group of linear systems. The systems are coupled by a requirement on the dynamics of an average system and the objective is to minimize a sum of quadratic costs functions for the individual systems. The main result of the paper is that the coordination problem can be decomposed in terms of the uncoordinated problems for the individual systems. In particular, it is shown that the computational effort needed to obtain the solution is independent of the number of systems and that the only global operation required to implement the optimal control law is an averaging operation. Furthermore, the solution is transparent in the sense that both the control law and the resulting performance of each system can be expressed analytically in terms of the optimal uncoordinated control laws and performances. The results are demonstrated on a simplified version of the wind farm application discussed in Paper I.

### Paper III

Madjidian, D. and L. Mirkin (2014). "Optimal coordination of homogeneous agents subject to delayed information exchange". Submitted to the *2014 IEEE Conference on Decision and Control*.

The paper revisits the coordination problem in Paper II with the additional restriction that the information exchange between the systems is subject to a time-delay. It is shown that the properties of the optimal control law in the delay-free case extend to the case with delayed information exchange. The paper also contains a more detailed discussion on how the coordination constraint and the delay impact the performance of the individual systems.

### Paper IV

Madjidian, D. (2014). "Distributed control of dispatchable wind power plants". Manuscript prepared for submission.

This paper is written primarily for a wind energy audience. The purpose is to show how the theory developed in Paper II nd Paper III can be used to control a dispatchable wind power plant. A large part of the paper

is devoted to explaining the properties of the controller that are especially useful for wind farm control. In the last part of the paper, a controller is designed and evaluated in a simulation study based on real wind farm data. The simulations show fatigue reductions in the range of 30-40%.

### Paper V

Madjidian, D. and A. Rantzer (2011). "A stationary turbine interaction model for control of wind farms". In: *Proceedings of the* 18th *IFAC World Congress*. Milano, Italy.

The paper develops a steady-state model of the aerodynamic coupling between wind turbines that are positioned in a row. The main underlying assumptions are that merged wakes are formed by superimposing individual wind turbine wakes and that the effect of each turbine on the wind field decays exponentially with distance. Based on these assumptions, the model can be stated in a compact recursive form where the wind conditions at each wind turbine are functions of the state of the closest upwind neighbor. The model is used in a series of examples, where the wind turbines coordinate their power productions in order to maximize the power production of the wind farm. The examples indicate that the benefit of power coordination increases with the number of turbines in the wind farm. They also identify the underlying mechanisms behind this effect.

### Paper VI

Kristalny, M., D. Madjidian, and T. Knudsen (2013). "On using wind speed preview to reduce wind turbine tower oscillations". *IEEE Transactions on Control Systems Technology* **21**:4, pp. 1191–1198.

The paper investigates the benefits of using preview of the incoming wind speed in terms of reducing the fatigue loads on the wind turbine tower. A large part of the paper is devoted to analyzing how measurement distortion effects the achievable load reduction as well as the required length of preview. The analysis is carried out by designing controllers in an optimal control framework and evaluating their performance through high fidelity simulations based on real wind turbine measurements. The last part of the paper examines the possibility of using upwind wind turbines as a source of preview for downwind turbines.

### Additional peer-reviewed publications

Biegel, B., D. Madjidian, V. Spudić, A. Rantzer, and J. Stoustrup (2013). "Distributed low-complexity controller for wind power plant in derated operation". In: *Proceedings of the 2013 IEEE Multi-Conference on Systems and Control*. Hyderabad, India, pp. 146–151.

Kristalny, M. and D. Madjidian (2011). “Decentralized feedforward control of wind farms: prospects and open problems”. In: *Proceedings of the 50th IEEE Conference on Decision and Control and European Control Conference*. Orlando, FL, USA, pp. 3464–3469.

Madjidian, D. (2014). “A decomposition result in linear-quadratic coordinated control”. In: *Proceedings of the* 19th *IFAC World Congress*. To appear. Cape Town, South Africa.

Madjidian, D. and L. Mirkin (2014). “Distributed control with low-rank coordination”. To appear in *the 21st International Symposium on Mathematical Theory of Networks and Systems*. Groningen, The Netherlands.

Madjidian, D., K. Mårtensson, and A. Rantzer (2011). “A distributed power coordination scheme for fatigue load reduction in wind farms”. In: *Proceedings of the 2011 American Control Conference*. San Francisco, CA, USA, pp. 5219–5224.

# 1

# Wind Energy

The objective of this chapter is twofold. First, it aims to contextualize the research in the thesis and discuss its contributions in a wind energy setting. Second, it provides necessary background information to readers who are not familiar with wind energy applications.

## 1.1 Global wind energy statistics

Wind power is a rapidly growing source of energy. The annual average growth rate has been about 20% over the past ten years and the total installed wind power capacity world-wide reached 318 GW at the end of 2013. See Figure 1.1. China accounts for most of the installed capacity (91.4 GW), followed by the U.S. (61.1 GW), Germany (34.3 GW), Spain (23.0 GW) and India (20.2 GW) [Global Wind Energy Council, 2014]. The total installed capacity in the EU is 121.5 GW and accounts for approximately 8% of total electricity consumption [European Wind Energy Association, 2014]. In terms of actual penetration (percent of electricity production), in 2012 Denmark topped the list with about 27%, followed by Portugal at 17%, Spain at 16%, Ireland at 13% and Germany at 11% [European Wind Energy Association, 2013]. In Sweden, the total installed capacity at the end of 2013 amounted to 4.4 GW and the penetration in 2012 was 5%.

In an attempt to reduce emission of green-house gases, several regions have set goals on renewable energy production. In particular, the European Union aims to produce 20% of its electricity from renewable sources by 2020 [European Comission, 2006], the United States is looking into 20% wind energy penetration by 2030 [U.S. Department of Energy, 2008], and Denmark plans to have all of its energy supplied by renewable sources in 2050 [Danish Government, 2011]. Wind energy widely considered to be a clean source of power and is expected to be a key resource in attaining these goals.

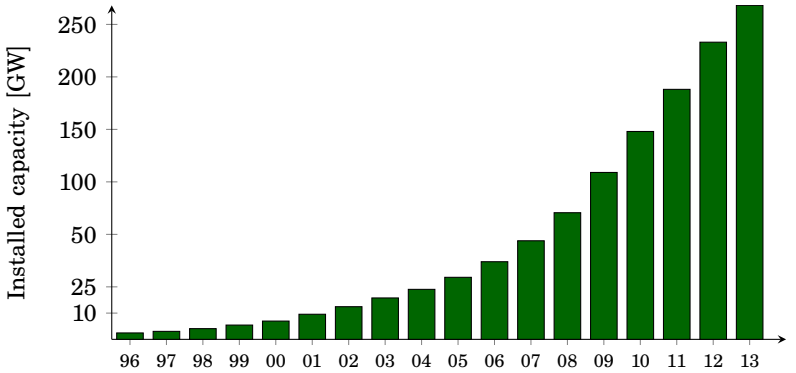


**Figure 1.1** Global cumulative installed wind power capacity.

## 1.2 Context and contributions

The purpose of this section is to discuss the contributions of the thesis in the context of wind energy. The first three subsections discuss different control challenges in wind energy and the last subsection describes how they are addressed by the different papers.

### Wake effects in wind farms

To take advantage of economies of scale, especially at sea, wind turbines are often placed relatively close to each other [Pao and Johnson, 2011]. However, close placement leads to performance loss due to aerodynamic coupling between the turbines. More specifically, when a wind turbine extracts power from the wind, it emits a wake, which is characterized by a lower wind speed and a higher level of turbulence compared to the ambient wind flow. Therefore, wind turbines that operate in the wake of other turbines experience lower mean power production and a higher level of structural loading [Burton et al., 2001].

The performance degradation caused by wake effects may be significant. In a study based on two years worth of data collected from two commercial wind farms, it was shown that in the dominant wind direction and in a certain range of ambient wind speeds, wind turbines located far downstream experienced a reduction in produced power of roughly 40% compared to the most upstream turbine [Barthelmie et al., 2013]. Similar observations were made in [McKay et al., 2012], where 6 months worth of data from a commercial Canadian wind-farm were analyzed. The results showed that for certain unfavorable wind conditions, the loss in power production and the increase in wind speed standard deviation could be in

the order of 70% and 240%, respectively.

The studies above are based on situations where the wind turbines individually maximize their power production. Considering the magnitude of the performance degradation due to wake effects, a natural question is whether these effects can be mitigated by coordinating wind turbine power production. For instance, by extracting less power at the most upwind turbine it might be possible to increase power production at several down wind turbines and thus increase the overall power production. Some evidence for this, based on relatively simple simulation models, was provided in [Johnson and Thomas, 2009] for a two-turbine example and in [Marden et al., 2013] for a larger farm. However, in general, wakes effects have received little attention from the control community, and wind turbines in wind farms continue to be operated individually without regard to their effect on down-wind turbines. A reason for this is the difficulty in obtaining wind farm wake models suitable for control design.

### Structural loads

Wind speeds are generally higher at higher altitudes and the power extracted by a wind turbine is proportional to the area swept by its rotor. This has led to a rapid growth of wind turbines dimensions and modern-day turbines typically stand more than 100 meters tall and have a rotor diameters which exceed 120 meters [Manwell et al., 2009]. As a consequence, wind turbines have become more sensitive to structural loads caused by wind speed fluctuations.

A wind turbine is typically designed to have a life-span of over twenty years. Due to its flexible structure and the uncertain environment in which it operates, a significant amount of effort in the design process is devoted to ensuring that it is able to withstand the various loads that it will experience. A high tolerance to structural loads requires a more rigid structure, which in turn implies higher material costs [Manwell et al., 2009]. Therefore, by designing control laws that reduce structural loads, it may be possible to cut the overall cost of wind energy by reducing the amount of materials used. Since the bulk of the capital costs in wind energy are material cost [Krohn et al., 2009], even a small reduction in materials can lead to substantial savings. Alternatively, given a turbine with a structure of a certain rigidity, a reduction in structural loads may increase the life-span of the turbine and reduce operation and maintenance costs.

### Grid integration of wind power

In the electric power system, the transmission system carries power from the generation units to the consumers (loads). As the transmission sys-

tem does not have any significant ability to store energy, generation must continuously match the load on the network. In most countries this load-balancing problem is the responsibility of the transmission system operator (TSO). It is typically handled by scheduling the generation units based on the predicted load profile and the generation capabilities and costs of each unit. This scheduling is performed on several time scales. For instance in the Nordic power system electricity is traded on the day-ahead and intra-day markets, which clear twenty-four hours and one hour before delivery, respectively [Nord Pool Spot, 2014]. Since the actual load profile cannot be perfectly predicted, the TSO also purchases additional regulation capacity to balance mismatches in real-time [Glover et al., 2008].

The wind resource is inherently random in nature and the randomness applies to all time scales. If wind power plants operate at maximum power production, which is currently the case in many regions [Couture et al., 2010], the variability would be directly fed-through to the power system. This implies that, unlike conventional generation units, which are a balancing resource for the TSO, wind power plants add to the uncertainty in all stages of the load-balancing problem. Moreover, if wind power plants replace conventional generators, a higher amount of variability has to be handled by a smaller generation fleet. Therefore, as wind power penetration increases, an important question is how to absorb the additional variability that it presents.

Several different approaches have been proposed to integrate larger amounts wind power production into the power system. One option is for the TSO to acquire larger amounts of operational reserve, which is how it is typically handled at present [Ela et al., 2010]. It is also possible to absorb power variations by using energy storage devices or to increase the capacity of the transmission system to even out variations between different geographical regions [Kanoria et al., 2011]. Another option that has received significant attention recently is to reduce the variability on the demand side by making a portion of the load controllable [Biegel et al., 2014]. The option adopted in this thesis is to let the wind power plants manage the additional variability. In this case, wind power plants would behave as dispatchable power plants, meaning that they regulate their output power production according to the balancing needs of the electrical power system. Such policies are already in place in Spain and the United Kingdom, where large wind-power providers bear full responsibility for forecasting and balancing their own production [Klessmann et al., 2008].

## Relation to papers

Paper V addresses the problem of wake effects by developing a simple model of the aero-dynamic interaction between wind turbines. The focus

of Paper VI is to exploit wind speed preview in order to reduce structural loads on the wind-turbine tower. Papers I–IV address a combination of reducing structural loads and integrating wind power into the power system. This is further explained below.

When operating a wind farm as a power plant, the sum of the power production of the wind-turbines should match the power set-point to the wind-farm. Since there are several turbines in the farm, there is a certain degree of freedom in distributing the power over the turbines, which can be used to reduce the structural loads experienced by the turbines. The idea is to continuously redistribute power among the turbines in order to to give them as much flexibility as possible in responding to local wind speed variations. Since wind speeds are not the same across the wind farm, changes in power production that benefits one wind turbine can be compensated for by changes in turbines with opposite needs. A natural question is then: how does the ability to vary power production help reduce structural loads? This is the topic of Paper I. To adjust its power production, a wind-turbine must coordinate with other turbines so that the total power production matches the set-point. This coordinated control problem is studied in a more general setting in Paper II and Paper III. In Paper IV the theoretical results derived in Paper II and Paper III are used to control a wind farm.

## 1.3 Background

This section provides the wind-energy background needed in order to read this thesis. This is done by describing the wind power plant model used in the papers.

### Model of a wind turbine

All wind-turbine models in this thesis describe a horizontal-axis, variable-speed and collective-pitch wind-turbine. *Horizontal-axis* means that the rotor is mounted so that the rotor plane is perpendicular to the wind direction (as in Figure 1.2). The property *variable-speed* implies that the rotational speed of the rotor and generator can be adjusted. Variable speed operation requires the use of power electronics, but leads to more power extraction compared to fixed-speed operation, where the generator is directly connected to the power network [Manwell et al., 2009]. *Collective pitch* refers to the fact that the pitch angle is modified simultaneously and equally at all blades. Some modern turbines also have ability to pitch each blade individually, but this is not considered in this thesis. Figure 1.2 shows the layout for a typical horizontal-axis wind turbine.

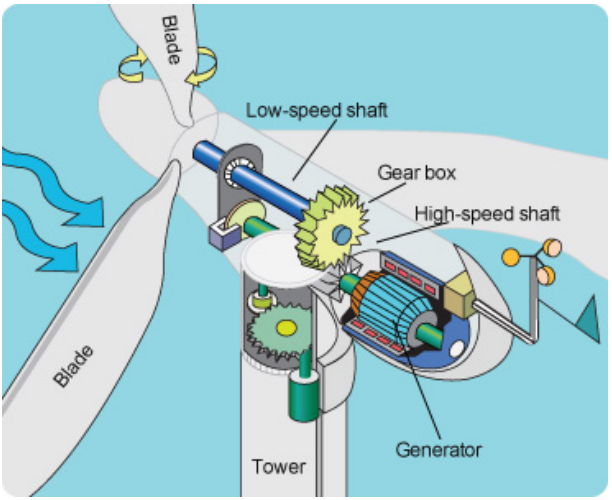


**Figure 1.2** A typical composition of a horizontal-axis wind turbine. The incoming wind interacts with the blades of the wind turbine, causing the rotor to spin. The rotational energy is transferred to the generator through the drive-train, which consists of the low-speed and high-speed shafts as well as the gear-box. When the generator spins, electricity is produced. The figure is used with the permission of the Government of the Hong Kong Special Administrative Region

.

Whenever simulations are performed, they are always run using the NREL 5-MW wind turbine described in [Jonkman et al., 2009]. Its design specifications are publicly accessible and it is a common reference in the wind energy literature. The models in this thesis are based on the model of the NREL 5-MW described in [Grunnet et al., 2010], which consists of the different components in Figure 1.3. Below, we describe each of these components.

***Wind speed*** It is common practice to model the incoming wind speed as

$$v = \bar{v} + w,$$

where $\bar{v}$ can be considered constant over a limited period of time and $w$ describes fluctuations around this mean.

For control purposes, $w$ is typically modeled as a stationary stochastic process and there are several suggestions on how to model its spectral density. See [Burton et al., 2001, Chapter 2] and references therein. However, most of these models describe wind speed fluctuations only in a single

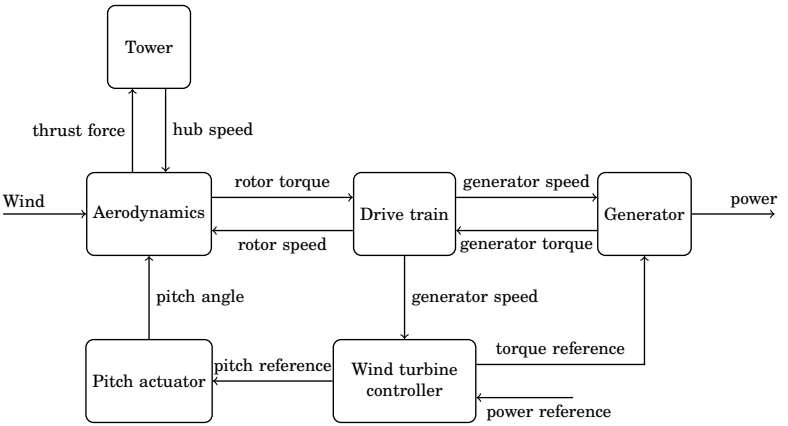


**Figure 1.3** Schematic overview of the NREL wind turbine mode. The arrows show through which variables the different blocks interact with each other.

point in space. On their own, these so called *point wind speed* models are not suitable for describing the incoming wind to a wind-turbine. This is because relevant turbine variables, such as rotor torque and thrust force, depend on wind speed variations along the entire rotor.

In this thesis, we adopt the concept of *effective wind speed*. It can be interpreted as spatially constant wind field that produces the same rotor torque and thrust force as the actual spatially varying field. See [Soltani et al., 2013] for more information. The effective wind speed model used in this thesis was identified from real data in Section 5 of Paper VI.

***Aerodynamics*** The power in the wind that passes through the area swept by a wind turbine rotor is given by

$$P_{\text{wind}} = \frac{1}{2}\rho\pi R^2 v_r^3,$$

where $\rho$ is density of the air, $R$ is the radius of the turbine, and $v_r = v - \dot{z}$ is the wind speed experienced by the rotor. Here, $z$ refers to the fore-aft position of the hub and is described further down. The turbine extracts a portion of the total wind power

$$P_{\text{ext}} = C_p(\lambda, \beta) P_{\text{wind}},$$

where $C_p$ is the *power coefficient* of the turbine and determines the portion of the wind power extracted. The power coefficient is a function of the pitch angle of the blades, denoted $\beta$, and the tip-speed ratio

$$\lambda = \frac{R\omega_r}{v},$$

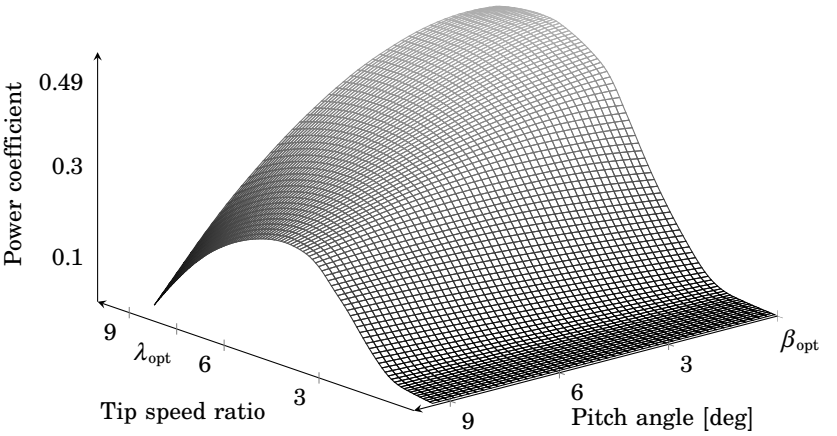


**Figure 1.4** Power coefficient for the NREL 5 MW wind turbine.

where $\omega_r$ is the rotational speed of the rotor. The tip-speed ratio describes the speed of blade-tips in relation to the incoming wind speed. The aerodynamic torque acting on the rotor is given by

$$m_r = \frac{P_{\text{ext}}}{\omega_r}. \tag{1.1}$$

When the turbine extracts power from the wind it experiences a thrust force, $F_t$, on its rotor. It is given by

$$F_t = \frac{1}{2}\rho\pi R^2 C_t(\lambda, \beta) v_r^2, \tag{1.2}$$

where the *thrust coefficient*, $C_t$, is a function of the tip-speed ratio and the pitch-angle.

The power and thrust coefficients are typically provided as look-up tables by the manufacturer of a wind-turbine. For the NREL 5 MW used in this thesis, they are shown in Figure 1.4 and Figure 1.5, respectively.

For more information on wind-turbine aerodynamics, see [Manwell et al., 2009]

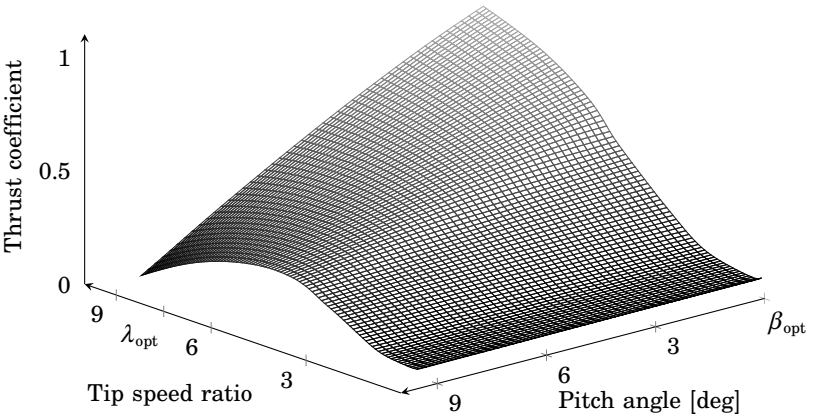


**Figure 1.5** Thrust coefficient for the NREL 5 MW wind turbine.

***Drive-train dynamics*** The drive-train connects the rotor to the generator. It is modeled as two rotating shafts connected through a gearbox:

$$\begin{aligned} J_r\dot{\omega}_r &= m_r - m_{\text{sh}} \\ J_g\dot{\omega}_g &= \frac{1}{n_g}m_{\text{sh}} - m_g \\ \dot{\theta} &= \omega_r - \frac{1}{n_g}\omega_g \end{aligned}$$

where $\omega_g$ is the generator speed, $m_r$ is the aerodynamic rotor torque defined by (1.1), $m_g$ is generator torque, $\theta$ is the torsion in the low-speed shaft and $m_{\text{sh}} = k_s\theta + b_s\dot{\theta}$ is the restoring shaft torque. The parameters $J_r$, $J_g$, $k_s$, $b_s$ and $n_g$ are the rotor inertia, generator inertia, shaft stiffness, shaft damping, and gear ratio, respectively.

***Tower dynamics*** The aerodynamic thrust force acting on the rotor of the turbine causes the entire turbine to sway back and forth. This process, often called tower nodding, is a source of structural loading to the wind turbine tower. The tower dynamics are modeled as a second order damped spring mass system

$$m_t\ddot{z} + b_t\dot{z} + k_s z = F_t,$$

where $z$ is the fore-aft (along the wind direction) displacement of the wind turbine hub, $F_t$ is the aerodynamic thrust force in (1.2), and the parameters $k_s$ and $b_s$ are the tower stiffness and damping, respectively.

***Generator*** The generator converts the kinetic energy in the high-speed shaft to electricity according to

$$p = m_g \omega_g,$$

where $p$ is the active power production. In variable-speed operation the generator torque can be adjusted. This process is modeled as a first order servo-system

$$\dot{m}_g = -\frac{1}{\tau_g}(m_g - m_{g\text{ref}}),$$

where $m_{g,\text{ref}}$ is the generator torque set-point. This is one of the two variables that can be directly manipulated by the wind turbine controller.

***Pitch actuator*** The pitch actuator is modeled as a first order servo-system

$$\dot{\beta} = -\frac{1}{\tau_{\text{pitch}}}(\beta - \beta_{\text{ref}}),$$

where $\beta_{\text{ref}}$ is the pitch angle set-point. This is one of the two variables that can be directly manipulated by the wind turbine controller.

***Wind turbine controller*** Standard wind turbine operation is illustrated by the solid power curve in Figure 1.6. The turbine has three main modes of operation, typically called operating regions [Pao and Johnson, 2011]. In Region 1, the wind speed is too low and no power is produced. In Region 2, the controller strives produce maximum power by maintaining optimal aerodynamic efficiency. This is done by fixing the pitch angle to $\beta_{\text{opt}}$, which is the pitch angle that corresponds to the optimal aerodynamic efficiency:

$$\max_{\lambda,\beta} C_p(\lambda, \beta) = C_p(\lambda_{\text{opt}}, \beta_{\text{opt}}).$$

The controller manipulates the generator torque in order to maintain the optimal rotor speed, which is defined as

$$\omega_{r|\text{opt}} = \frac{\lambda_{\text{opt}} v_r}{R},$$

where $v_r$ is the effective wind speed experienced by the wind turbine rotor, and $R$ is the rotor radius. The optimal pitch angle, $\beta_{\text{opt}}$, and the optimal tip-speed ratio, $\lambda_{\text{opt}}$, are marked in Figure 1.4.

In Region 2, the desired rotor speed, $\omega_{r|\text{opt}}$, is proportional to the effective wind speed. However, at some wind speed level, the rotor reaches its *rated speed*, which is the maximum design speed. At this point, the turbine has entered Region 3 and reached its *rated power* production. The controller then tracks the rated rotor speed, $\omega_{\text{rated}}$, by manipulating

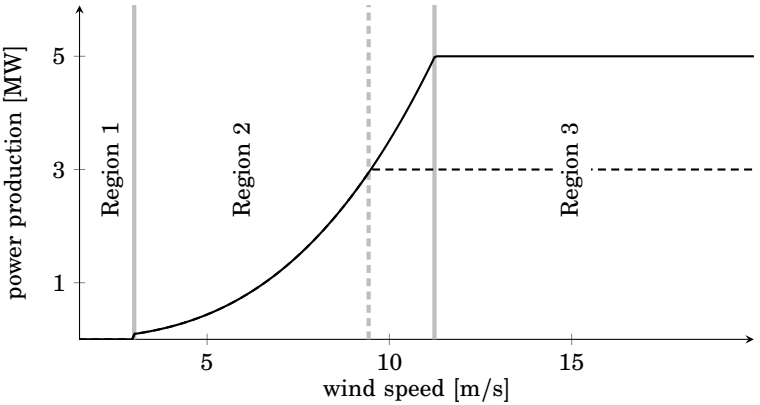


**Figure 1.6** Power curve of the NREL 5-MW wind turbine. The solid curve illustrates standard operation. The dashed curve shows the power production when the power reference to the turbine is 3 MW. The solid gray lines indicate transitions between operating regions. The effect of a power reference below rated power is to shift the transition point between Region 2 and Region 3 to the left as indicated by the dashed gray line.

the pitch angle of the turbine in order to adjust the aerodynamic torque on the rotor. In the NREL baseline controller, this is achieved by a gain-scheduled PI-control algorithm. The generator torque is set as

$$m_{g,\text{ref}} = \frac{p_{\text{rated}}}{\omega_g},$$

in order to maintain rated power production.

There is also an additional region dedicated to transitions between regions 2 and 3. However, this region is not considered in this thesis.

In derated operation, the wind turbine controller tries to follow a power reference, $p_{\text{ref}}$. This corresponds to the dashed line in Figure 1.6. As illustrated by the figure, derating is achieved by shifting the transition point between Region 2 and Region 3. This is handled by the exact same pitch and torque control loop as before, except for replacing $p_{\text{rated}}$ by $p_{\text{ref}}$ and $\omega_{\text{rated}}$ by a new rotor speed set point $\omega_{\text{ref}}$. Unless stated otherwise, the speed reference in the papers is set as

$$\omega_{\text{ref}} = \min(\omega_{\text{rated}}, \omega_{r|\max}),$$

where $\omega_{r|\max} \leq \omega_{\text{rated}}$ is defined as the highest rotor speed that can be sustained while still maintaining enough aerodynamic efficiency to achieve the set point That is:

$$C_p(\frac{R\omega_{r|\max}}{v_r}, \beta_{\text{opt}})P_{\text{wind}} = p_{\text{ref}}.$$

The benefit of maintaining a high speed in derated operation, is that more kinetic energy is stored and can be used to respond to changes in the power set point. Another option, is to set

$$\omega_{\text{ref}} = \min(\omega_{r|\text{opt}}, \omega_{\text{rated}}).$$

The advantage of this choice is that it results in a smaller thrust force for a given power production, which preferred in the context of reducing wake effects in Paper V. Another benefit is that by operating below rated rotor speed, a larger variation in rotor speed can be allowed. This additional flexibility can be used to address other control objectives, as in Paper I, where it is used to reduce structural loads.

### Aerodynamic interaction between wind turbines

Aerodynamic interaction between wind turbines is the topic of Paper V. The paper proposes a model that maps *mean* values of different variables at up-wind wind turbines to *mean* wind speeds at down-wind turbines.

Papers I and IV consider wind turbines operating in the vicinity of some operating point. In this case, it is the wind speed *variations* and not the mean wind speed levels that are important. In the papers, it is assumed that the wind speed variations experienced by different wind turbines are uncorrelated. This assumption is motivated by practical studies. In particular, in Section 5 of Paper VI, data collected from a real wind farm was used to investigate the correlation in wind speed variations between neighboring turbines. The result indicates that the wind speed variations are only correlated in a range of very low frequencies. This observation is consistent with the results in [Vigueras-Rodríguez et al., 2012], which are based on a larger data set. The frequencies at which the wind speed variations can be considered correlated are so low that we consider the dynamics of different turbines to be uncoupled.

### Evaluation of structural loads

Wind turbine components are designed with respect to two loads categories: ultimate loads and fatigue loads. Ultimate loads correspond to the maximum load levels that the turbine is expected to experience. These are normally associated with distinct events, such as gusts, start-ups and shutdowns. On the other hand, fatigue is related to a materials ability to withstand a certain number of stress cycles. In this thesis, only fatigue loads are considered. The presentation below is based on [Manwell et al., 2009; Hammerum, 2006], which are references for more information.

Fatigue can be thought of as the loss of strength of a material due to repeated stress cycles. A materials fatigue resistance is typically quantified

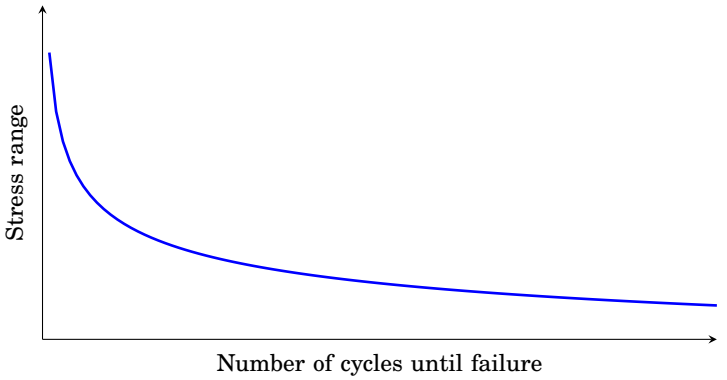


**Figure 1.7** An typical shape of an S–N curve.

by an S–N curve, illustrated in Figure 1.7. The S–N curve can conceptually be obtained by exposing a sequence of material samples to sinusoidal loads as follows. For material sample number $i$, a load with stress range (twice the amplitude of the sinusoid), $s_i$, is applied to the material. The load is maintained until the material fails, at which point the number of cycles, $N_i$, is recorded, The test is then repeated for many different stress ranges.

An often used model for the S–N curve, is $s^k N = K$, where $k$ and $K$ are material properties. The *fatigue damage* caused by one stress cycle with stress range $s_i$, is defined as

$$D_i = \frac{1}{K} s_i^k,$$

and can be interpreted as the portion of material strength that is lost due to the stress cycle. The total fatigue damage, $D$, from a sequence of cycles with different stress levels, $s_1, \ldots, s_r$, can then be computed by using Palmgren-Miner's damage accumulation rule:

$$D = \sum_{i=1}^{r} D_i = \frac{1}{K} \sum_{i=1}^{r} s_i^k.$$

The concepts introduced above are defined for sinusoidal stress histories. A standard method to evaluate the fatigue damage caused by a more realistic stress history, is to convert it to a number of equivalent stress cycles, which can then be added using Palmgren-Miner's rule. One of the most common methods for extracting equivalent cycles is the rain-flow counting algorithm [Manwell et al., 2009, Chapter 6].

# 2

# Linear-Quadratic Control Theory

The first section of this chapter reviews some fundamental results in linear-quadratic control that are frequently used in the papers. Section 2.2 summarizes the author's view of the contributions of this thesis in the context of linear quadratic control theory.

## 2.1 $\mathcal{H}_2$ Optimal Control

In optimal control problems, the task is to find the best possible controller with respect to some performance measure. Typically, the performance is quantified by a cost function, which maps the closed loop system to a real valued number called the cost. A lower cost corresponds to a better performance. Linear quadratic control problems are class of optimal control problems with linear plant dynamics and quadratic cost functions. These problems have been studied extensively and are the subject of many textbooks. This section gives a brief overview of linear quadratic control theory. The presentation is based on [Zhou et al., 1995], which is a reference for further details.

### Problem formulation

A standard form for linear-quadratic control problems is the feedback loop shown in Figure 2.1, where $G$ and $K$ are proper transfer functions associated with the *generalized plant* and the controller (which is yet to be designed), respectively. Recall that a transfer function proper if it corresponds to a causal system. The generalized plant models the physical process we wish to control as well as the associated control objectives and certain a-priori knowledge about the effect of the environment. The two input signals to the plant are the exogenous disturbance signal, $w$, and the

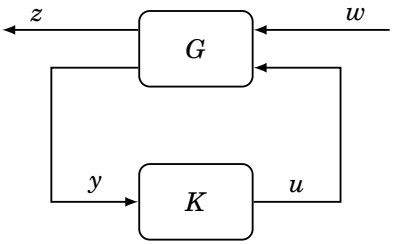


**Figure 2.1** General framework for linear-quadratic control problems.

control signal, $u$. The outputs are the regulated signal, $z$, which is used to express the control objectives, and the signal of available measurements, $y$.

We will assume that $G$ is a rational transfer function, which means that it has an associated state space realization

$$\begin{aligned} \dot{x}_i(t) &= Ax(t) + B_u u(t) + B_w w(t), \quad x(0) = 0 \\ z(t) &= C_z x(t) + D_{zu} u(t) \\ y(t) &= C_y x(t) + D_{yw} w(t) \end{aligned}$$

This is typically expressed using the notation

$$G = \left[\begin{array}{c|cc} A & B_w & B_u \\ \hline C_z & 0 & D_{zu} \\ C_y & D_{yw} & 0 \end{array}\right]. \tag{2.1}$$

Let $T_{zw}$ denote the closed loop transfer function from $w$ to $z$:

$$T_{zw} = \left[\begin{array}{c|c} A_{\text{cl}} & B_{\text{cl}} \\ \hline C_{\text{cl}} & D_{\text{cl}} \end{array}\right]$$

The controller, $K$, is said to be *internally stabilizing* if the matrix $A_{\text{cl}}$ is Hurwitz.

The objective in linear-quadratic control is to find an internally stabilizing and proper controller $K$, which minimizes

$$\|T_{zw}\|_2 := \left( \frac{1}{2\pi} \int_{-\infty}^{\infty} \operatorname{tr}\left( T_{zw}^T(-\mathrm{j}\omega) T_{zw}(\mathrm{j}\omega) \right) \mathrm{d}\omega \right)^{\frac{1}{2}}. \tag{2.2}$$

The quantity in (2.2) is called the the $\mathcal{L}_2$-norm of $T_{zw}$. It is finite if and only if $D_{\text{cl}} = 0$ and $T_{zw}$ does not have poles on the imaginary axis. Provided that this is true and that $A_{\text{cl}}$ is Hurwitz, it can be computed as $\|T_{zw}\|_2^2 =$

$\mathrm{tr}(B_{\mathrm{cl}}^T Q B_{\mathrm{cl}}) = \mathrm{tr}(C_{\mathrm{cl}} P C_{\mathrm{cl}}^T)$ where $P \geq 0$ and $Q \geq 0$ are the solutions to the Lyapunov equations

$$A_{\mathrm{cl}} P + P A_{\mathrm{cl}}^T + B_{\mathrm{cl}} B_{\mathrm{cl}}^T = 0 \tag{2.3}$$

$$A_{\mathrm{cl}}^T Q + Q A_{\mathrm{cl}} + C_{\mathrm{cl}}^T C_{\mathrm{cl}} = 0. \tag{2.4}$$

By Parseval's relation, the $\mathcal{H}_2$-norm of a system equals the energy in its impulse response. Thus, minimizing the expression in (2.2) is equivalent to minimizing

$$\int_0^\infty \mathrm{tr}\left(z^T(t) z(t)\right) \mathrm{d}t$$

when $w$ is an impulse.

The problem illustrated in Figure 2.1 is called the output-feedback $\mathcal{H}_2$-problem. A fundamental result, known as the separation principle, states that this problem can be decomposed in terms of two sub-problems, which can be solved separately. One problem is to find a solution assuming that the full state vector can be measured, and the other is to find an estimator, which estimates this solution by using the measurements, $y$. Before stating the solution to output-feedback case, we discuss these sub-problems.

### State-feedback

If the full state vector can be measured, that is, if $y = x$, the generalized plant takes the following shape

$$G = \left[\begin{array}{c|cc} A & B_w & B_u \\ \hline C_z & 0 & D_{zu} \\ I & 0 & 0 \end{array}\right]$$

We make the following assumptions:

$\mathcal{A}_1$: The pair $(A, B_u)$ is stabilizable. That is, there is a matrix $F$ such that $A + B_u F$ is Hurwitz.

$\mathcal{A}_2$: $D_{zu}$ has full column rank. Without loss of generality we also assume that $D_{zu}^T D_{zu} = I$

$\mathcal{A}_3$: The matrix $\begin{bmatrix} A - \mathrm{j}\omega I & B_u \\ C_z & D_{zu} \end{bmatrix}$ has full column rank for all $\omega$.

Introduce the algebraic Riccati equation (ARE)

$$A^T X + X A + C_z^T C_z - (X B_u + C_z^T D_{zu})(B_u^T X + D_{zu}^T C_z) = 0 \tag{2.5}$$

Its solution, $X \geq 0$ is said to be stabilizing if

$$F = -(B_u^T X + C_z D_{zu}) \tag{2.6}$$

is such that $A + B_u F$ is Hurwitz. It is well-known that assumptions $\mathcal{A}_{1\text{-}3}$ guarantee the existence of a stabilizing solution to (2.5).

The solution to the state feedback control problem is given by $u = Fx$, where $F$ is given by (2.6) and $X$ is the stabilizing solution to (2.5). The closed loop system under this control law is then

$$T_{zw} = \left[\begin{array}{c|c} A + B_u F & B_w \\ \hline C_z + D_{zu} F & 0 \end{array}\right].$$

According to the discussion above, the cost under the optimal state-feedback law satisfies $\|T_{zw}\|_2^2 = \mathrm{tr}(B_w^T Q B_w)$ where $Q$ is the solution to

$$(A + B_u F)^T Q + Q(A + B_u F) + (C_z + D_{zu} F)^T (C_z + D_{zu} F) = 0. \quad (2.7)$$

By inserting (2.6) into (2.7), it realized that $Q = X$. Hence, the optimal cost under the optimal control law in the state feedback problem is given by

$$\|T_{zw}\|_2^2 = \mathrm{tr}(B_w^T X B_w),$$

where $X$ is the stabilizing solution to (2.5).

***Linear quadratic regulator problem*** Perhaps the most basic and widely known optimal control problem formulation is the linear quadratic regulator (LQR) problem . It is similar to the state feedback problem discussed above, except that the plant has a non-zero initial state and no exogenous disturbance signal:

$$\dot{x} = Ax + B_u u, \quad x(0) = x_0.$$

The cost function is typically expressed as

$$\mathcal{J} = \int_0^\infty \begin{bmatrix} x(t) \\ u(t) \end{bmatrix}^T \begin{bmatrix} Q_x & Q_{xu} \\ Q_{xu}^T & I \end{bmatrix} \begin{bmatrix} x(t) \\ u(t) \end{bmatrix} \mathrm{d}t$$

for some matrices $Q_x \geq 0$ and $Q_{xu}$ such that the matrix inside the integral is positive semi-definite. This problem can be fit into the framework of Figure 2.1, by setting

$$G = \left[\begin{array}{c|cc} A & x_0 & B_u \\ \hline C_z & 0 & D_{zu} \\ I & 0 & 0 \end{array}\right]$$

for some matrices $C_z$ and $D_{zu}$ that satisfy

$$\begin{bmatrix} Q_x & Q_{xu} \\ Q_{xu}^T & I \end{bmatrix} = \begin{bmatrix} C_z^T \\ D_{zu}^T \end{bmatrix} \begin{bmatrix} C_z & D_{zu} \end{bmatrix}. \quad (2.8)$$

Note that the existence of $C_z$ and $D_{zu}$ in the equation above is guaranteed by the assumption that the matrix on the left hand side in (2.8) is positive semi-definite. It is readily seen that the solution to the LQR problem is given by $u = Fx$ where $F$ is given by (2.6) and that the optimal cost is $\mathcal{J} = x_0^T X x_0$, where $X$ is the stabilizing solution to (2.5).

## Output Estimation

Consider the following system

$$\begin{aligned} \dot{x}(t) &= Ax(t) + B_w w(t) \\ y(t) &= C_y x(t) + D_{yw} w(t) \end{aligned}$$

and consider the problem of finding an estimate $\hat{\eta}$ to $\eta := C_\eta x$ based on the available measurements $y$. Here, $C_\eta$ is some arbitrary but given matrix. If we think of $K$ in Figure 2.1 as an estimator or an observer, the problem can be cast in the generalized plant framework by setting $u = \hat{\eta}$ and $z = \eta - u$. In this case, the generalized plant takes the form

$$G = \left[\begin{array}{c|cc} A & B_w & 0 \\ \hline C_\eta & 0 & -I \\ C_y & D_{yw} & 0 \end{array}\right].$$

In solving the estimation problem we will assume that

$\mathcal{A}_4$: The pair $(C_y, A)$ is detectable. That is, there is a matrix $L$ such that $A + LC_y$ is Hurwitz.

$\mathcal{A}_5$: $D_{yw}$ has full row rank. Without loss of generality we also assume that $D_{yw} D_{yw}^T = I$.

$\mathcal{A}_6$: The matrix $\begin{bmatrix} A - j\omega I & B_w \\ C_y & D_{yw} \end{bmatrix}$ has full row rank for all $\omega$.

Note that, in the output estimation problem, the closed loop system is internally stable if and only if $A$ is Hurwitz. That is, the internal stability of the closed loop system cannot be effected by $K$. Therefore, in addressing the output estimation problem, we drop the requirement that $K$ must be internally stabilizing.

Introduce the algebraic Riccati equation

$$AY + YA^T + B_w^T B_w - (C_y Y + D_{yw} B_w^T)^T (C_y Y + D_{yw} B_w^T) = 0 \qquad (2.9)$$

It is well-known that assumptions $\mathcal{A}_{4\text{–}6}$ guarantee the existence of a stabilizing solution, $Y \geq 0$, to (2.9).

The solution to the output estimation problem is given by

$$\begin{aligned}\dot{\hat{x}}(t) &= (A + LC_y)\hat{x}(t) - Ly \\ \hat{\eta}(t) &= C_\eta \hat{x}(t)\end{aligned}$$

where

$$L = -(YC_y^T + B_w D_{yw}^T), \tag{2.10}$$

and $Y$ is the stabilizing solution to (2.9).

Let $\tilde{x} := x - \hat{x}$. Then

$$\dot{\tilde{x}}(t) = (A + LC_y)\tilde{x}(t) + (B_w + LD_{yw})w,$$

which implies that the closed loop system from $w$ to $z$ is given by

$$T_{zw} = \left[\begin{array}{c|c} A + LC_y & B_w + LD_{yw} \\ \hline C_\eta & 0 \end{array}\right].$$

To compute the estimation cost, we set $A_{\text{cl}} = A + LC_y$ and $B_{\text{cl}} = B_w + LD_{yw}$ in (2.3), which results in

$$(A + LC_y)P + P(A + LC_y)^T + (B_w + LD_{yw})(B_w + LD_{yw})^T = 0. \tag{2.11}$$

By inserting (2.10) into (2.11), it is readily seen that $P = Y$. Hence, the optimal estimation cost is given by

$$\|T_{zw}\|_2^2 = \text{tr}(C_\eta Y C_\eta^T),$$

where $Y$ is the stabilizing solution to (2.9).

### Solution to $\mathcal{H}_2$ problem

Consider the general plant in (2.1). Provided that assumptions $\mathcal{A}_{\mathbf{1\text{–}6}}$ are satisfied, the solution to the output-feedback problem is given by

$$K = \left[\begin{array}{c|c} A + B_u F + LC_y & -L \\ \hline F & 0 \end{array}\right] \tag{2.12}$$

where $F$ and $L$ are given by (2.6) and (2.10), respectively. In the expressions for $F$ and $L$, $X \geq 0$ and $Y \geq 0$ are the stabilizing solutions to the algebraic Riccati equations (2.5) and (2.9), respectively. The value of the cost function under (2.12) satisfies

$$\|T_{zw}\|_2^2 = \text{tr}(B_w^T X B_w) + \text{tr}(FYF^T).$$

Note that the optimal control law and the optimal cost are the result of solving two problems. The first is to find a state-feedback law $u = Fx$ that minimizes $\|T_{zw}\|_2$, whereas in the second problem the task is to find the best possible approximation to (or estimation of) this control signal based on available measurements.

## 2.2 Contributions

To illustrate the contributions we discuss a special case of the problem formulation in Papers II–IV. Consider a homogeneous group of linear systems with uncoupled dynamics:

$$\dot{x}_i(t) = Ax_i(t) + B_u u_i(t) + B_{w|i} w_i(t), \quad i = 1, \ldots, \nu, \tag{2.13}$$

where the state $x_i(t) \in \mathbb{R}^n$ can be measured, $u_i(t) \in \mathbb{R}^m$ and the disturbances $w_i$ are mutually independent Gaussian white noise processes with unit intensity. The objective of each system is to optimize its own performance, which corresponds to minimizing

$$\mathcal{J}_i := \mathbf{E}\left(x_i^T(t) Q_\alpha x_i(t) + u_i(t)^T u_i(t)\right),$$

for some $Q_\alpha \geq 0$. The systems are coupled by a requirement to coordinate their inputs in order to satisfy the constraint:

$$\bar{u} = \bar{F}\bar{x}, \tag{2.14}$$

where $\bar{u} = \sum_{i=1}^{\nu} u_i$ and $\bar{x} = \sum_{i=1}^{\nu} x_i$ are the aggregate control and state trajectories, respectively. Here, the matrix $\bar{F}$ is intended as a design parameter which can be used to shape the dynamics of the aggregate system into

$$\dot{\bar{x}} = (A + B_u \bar{F})\bar{x} + \bar{B}_w w,$$

where $\bar{B}_w = \begin{bmatrix} B_{w|i} & \cdots & B_{w|\nu} \end{bmatrix}$ and $w = \begin{bmatrix} w_1^T & \cdots & w_\nu^T \end{bmatrix}^T$. The overall problem formulation is to minimize a weighted sum of the individual system costs

$$\mathcal{J} := \sum_{i=1}^{\nu} \lambda_i \mathcal{J}_i,$$

subject to (2.14) and the dynamics in (2.13). Here, each $\lambda_i > 0$ and without loss of generality we assume that the weights are are normalized so that $\sum_{i=1}^{\nu} \lambda_i^{-1} = 1$ (this assumption will simplify the expressions below).

The problem formulation above is a constrained linear-quadratic state feedback problem. It is representative of a more general class of resource allocation problems, which includes the wind farm application in Paper IV.

In principle, the constraint (2.14) can be resolved in any of the control inputs, e.g. $u_1 = \bar{F}(x_1 + \cdots + x_\nu) - (u_2 + \cdots + u_\nu)$. This would convert the problem into a standard linear-quadratic state-feedback problem with non-diagonal "A" and "$B_u$"-matrices. While this approach can be used on moderately sized problems, it does not scale as the number of subsystems $\nu$ grows large.

The task of designing a scalable and well-performing controller for arbitrary large-scale systems is notoriously difficult [Papadimitriou and Tsitsiklis, 1986]. A common approach is to design local control laws, where each subsystem is only given access to information about a limited set of other subsystems. This amounts to imposing a sparsity pattern on the structure of the controller, where nonzero elements correspond to permitted information exchange between subsystems. Once a suitable sparsity structure has been chosen, the next step is to decide on the values of the associated controller parameters. The complexity of this task may be heavily dependent on the chosen pattern. If the plant and controller have compatible sparsity patterns, the controller can be designed by means of convex optimization [Rotkowitz and Lall, 2006]. If not, then the standard approach is to either search for locally optimal solutions as in [Mårtensson and Rantzer, 2012] (an example is given in Section 2 of Paper II) or to impose additional restrictions on the closed loop behavior. Examples of such restrictions include positivity requirements [Tanaka and Langbort, 2011; Rantzer, 2012] and the existence of diagonal Lyapunov functions [Zečević and Šiljak, 2010, Chapter 2]. Both options normally lead to additional performance degradation.

***Scalable and transparent solution:*** A contribution of the research in this thesis is to reveal that the solution to the problem described above is *inherently* scalable, that is, there is no trade-off between scalability and performance. More specifically, it is shown that the solution to the coordination problem is given by

$$u_i = F_\alpha x_i + \lambda_i^{-1}(\bar{F} - F_\alpha)\bar{x}, \tag{2.15}$$

where $F_\alpha x_i$ is the optimal uncoordinated control law that the systems would apply if they were not constrained by (2.14). Moreover, the values of the individual cost functions under control law (2.15) are given by

$$\mathcal{J}_i = \mathcal{J}_{i|\text{opt}} + \lambda_i^{-2} \sum_{j=1}^{\nu} (\bar{\mathcal{J}}_j - \mathcal{J}_{j|\text{opt}}), \tag{2.16}$$

where $\mathcal{J}_{i|\text{opt}}$ and $\bar{\mathcal{J}}_i$ are the values of $\mathcal{J}_i$ under the optimal uncoordinated control law $F_\alpha x_i$ and the control law $\bar{F}x_i$, respectively.

The control law (2.15) has two important properties in terms of scalability. First, to form it, we only need to compute the local feedback gains $F_\alpha$, which amounts to solving an unconstrained problem for a single subsystem. The computational effort required to obtain the solution is thus *independent* of the number of subsystems. Second, the only global computation needed in order to execute (2.15) is to form $\bar{x}$. This only requires a

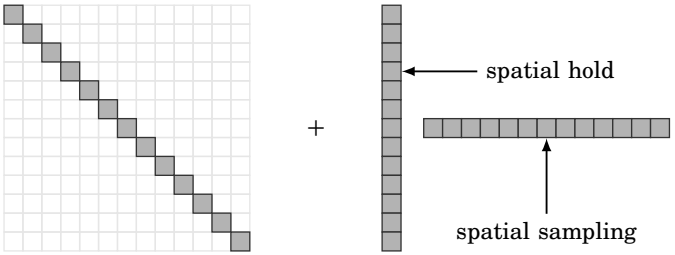


**Figure 2.2** Structure of the optimal control law (2.15). It consists of a block-diagonal (decentralized) part and a block-rank-one term. The rank-one term is responsible for coordinating the individual subsystems. This is done through a spatial sampling operation, which aggregates information from all subsystems into a single quantity, $(\bar{F}-F_\alpha)\bar{x}(t)$, and a spatial hold operation that broadcasts this condensed information back to the subsystems.

single summation, which scales well as the number of subsystems $\nu$ grows large.

A property of equal importance is the transparent and intuitive structure of the solution and the associated cost function. The optimal control law in (2.15) states that each system should behave as if it was not constrained by (2.14) and then compensate for a portion, $\lambda_i^{-1}$, of the resulting constraint violation. Expression (2.16) clearly shows the effect of constraint (2.14) on the cost of each system. Together, these two expressions provide transparency and insight into the optimal coordination policy, which are desirable features, especially in large scale applications.

**Suitable controller structure in large-scale applications** The structure of the optimal control law in (2.15) suggests an alternative to the sparsity based control design approach discussed above. As opposed to the sparse control structures, which restrict the communication capability of each system to a limited set of neighboring systems, the control law (2.15) reduces information processing by aggregating information from *all systems* into a single quantity, $(\bar{F}-F_\alpha)\bar{x}(t)$, which is then made available to each of the systems. This type of operation can be thought of as a *spatial generalized sample and hold* operation, and is a feature that is exclusive to controllers with a diagonal-plus-rank-one structure. See Figure 2.2.

An approach for designing controllers with a diagonal-plus-low-rank structure is suggested in [Zečević and Šiljak, 2005]. This structure is a generalization of the diagonal-plus-rank-one structure in that, in general, the low-rank term requires multiple averaging operations ($r$ operations for a rank-$r$ term). The proposed approach relies on the existence of cer-

tain structured Lyapunov functions and uses an LMI-design procedure to synthesize the resulting controller.

A question associated with any control structure, is in what type of application it will perform well. This knowledge is useful when deciding on a control structure during the synthesis procedure, and it might also be important in terms of deciding on a suitable communication network topology for the application. In this regard, a contribution of this thesis is to identify a class of problems for which the diagonal-plus-low-rank structure is optimal, that is, it cannot be outperformed by any other structure. This provides insight and an indication of the type of applications for which the proposed structure is well-suited.

# Bibliography


Barthelmie, R., K. Hansen, and S. Pryor (2013). "Meteorological controls on wind turbine wakes". *Proceedings of IEEE* **101**:4, pp. 1010–1019.

Biegel, B., L. Hansen, J. Stoustrup, P. Andersen, and S. Harbo (2014). "Value of flexible consumption in the electricity markets". *Energy* **66**:0, pp. 354 –362.

Burton, T., D. Sharpe, N. Jenkins, and E. Bossanyi (2001). *Wind Energy Handbook*. John Wiley & Sons, Chichester, UK.

Couture, T. D., K. Cory, C. Kreycik, and E. Williams (2010). *A Policymaker's Guide to Feed-in Tariff Policy Design*. Tech. rep. NREL/TP-6A2-44849. National Renewable Energy Laboratory.

Danish Government (2011). *Our future energy*. ISBN 978-87-7844-915-3. URL: http://www.cphcleantech.com/media/1465822/our_future_energy.pdf.

Ela, E., B. Kirby, E. Lannoye, M Milligan, D. Flynn, B. Zavadil, and M. O'Malley (2010). "Evolution of operating reserve determination in wind power integration studies". In: *Proceedings of the 2010 IEEE Power and Energy Society General Meeting*, pp. 1–8.

European Comission (2006). *A European strategy for sustainable, competitive and secure energy*. COM(2006) 105 final. URL: http://europa.eu/documents/comm/green_papers/pdf/com2006_105_en.pdf.

European Wind Energy Association (2013). *Wind in power: 2012 European statistics*. Retrieved 2014-04-20. URL: http://www.ewea.org/fileadmin/files/library/publications/statistics/Wind_in_power_annual_statistics_2012.pdf.

European Wind Energy Association (2014). *Wind in power: 2013 European statistics*. Retrieved 2014-04-20. URL: http://www.ewea.org/fileadmin/files/library/publications/statistics/EWEA_Annual_Statistics_2013.pdf.

Global Wind Energy Council (2014). *Global wind power statistics 2013*. Retrieved 2014-04-20. URL: http://www.gwec.net/wp-content/uploads/2014/02/GWEC-PRstats-2013_EN.pdf.

Glover, J. D., M. S. Sarma, and T. J. Overbye (2008). *Power System Analysis and Design*. 4th ed. Cengage Learning, Stamford, CT.

Grunnet, J., M. Soltani, T. Knudsen, M. Kragelund, and T. Bak (2010). "Aeolus toolbox for dynamic wind farm modeling, simulation and control". In: *Proceedings of the 2010 European Wind Energy Conference*, pp. 3119–3129.

Hammerum, K. (2006). *A Fatigue Approach to Wind Turbine Control*. M.Sc. Thesis IMM-Thesis-2006-105. Technical University of Denmark.

Johnson, K. and N. Thomas (2009). "Wind farm control: addressing the aerodynamic interaction among wind turbines". In: *Proceedings of the 2009 American Control Conference*, pp. 2104 –2109.

Jonkman, J., S. Butterfield, W. Musial, and G. Scott (2009). *Definition of a 5-MW Reference Wind Turbine for Offshore System Development*. Tech. rep. NREL/TP-500-38060. National Renewable Energy Laboratory, Golden, CO.

Kanoria, Y., A. Montanari, D. Tse, and B. Zhang (2011). "Distributed storage for intermittent energy sources: control design and performance limits". *ArXiv e-prints*. arXiv: 1110.4441. URL: http://adsabs.harvard.edu/abs/2011arXiv1110.4441K.

Klessmann, C., C. Nabe, and K. Burges (2008). "Pros and cons of exposing renewables to electricity market risks — a comparison of the market integration approaches in Germany, Spain, and the UK". *Energy Policy* **36**:10, pp. 3646–3661.

Krohn, S., P. Morthorst, and S. Awerbuch (2009). *The Economics of Wind Energy*. European Wind Energy Association. URL: http://www.ewea.org/fileadmin/ewea_documents/documents/00_POLICY_document/Economics_of_Wind_Energy__March_2009_.pdf.

Manwell, J., J. McGowan, and A. Rogers (2009). *Wind Energy Explained*. 2nd ed. John Wiley & Sons, Chichester, UK.

Marden, J., S. Ruben, and L. Pao (2013). "A model-free approach to wind farm control using game theoretic methods". *IEEE Transactions on Control Systems Technology* **21**:4, pp. 1207–1214.

Mårtensson, K. and A. Rantzer (2012). "A scalable method for continuous-time distributed control synthesis". In: *Proceedings of the 2012 American Control Conference*. Montreal, QC, pp. 6308–6313.

McKay, P., R. Carriveau, and D. S. Ting (2012). "Wake impacts on downstream wind turbine performance and yaw alignment". *Wind Energy* **16**:2, pp. 221–234.

Nord Pool Spot (2014). Retrieved 2014-05-02. URL: http://www.nordpoolspot.com.

Pao, L. and K. Johnson (2011). "Control of wind turbines". *IEEE Control Systems Magazine* **31**:2, pp. 42–62.

Papadimitriou, C. and J. Tsitsiklis (1986). "Intractable problems in control theory". *SIAM Journal on Control and Optimization* **24**:4, pp. 639–654.

Rantzer, A. (2012). "Distributed control of positive systems". URL: http://arxiv.org/abs/1203.0047.

Rotkowitz, M. and S. Lall (2006). "A characterization of convex problems in decentralized control". *IEEE Transactions on Automatic Control* **51**:2, pp. 274–286.

Soltani, M., T. Knudsen, M. Svenstrup, R. Wisniewski, P. Brath, R. Ortega, and K. Johnson (2013). "Estimation of rotor effective wind speed: a comparison". *IEEE Transactions on Control Systems Technology* **21**:4, pp. 1155–1167.

Tanaka, T. and C. Langbort (2011). "The bounded real lemma for internally positive systems and $H^\infty$ structured static state feedback". *IEEE Transactions on Automatic Control* **56**:9, pp. 2218–2223.

U.S. Department of Energy (2008). *20% wind energy by 2030: increasing wind energy's contribution to U.S. electricity supply*. DOE/GO-102008-2567. URL: http://www.nrel.gov/docs/fy08osti/41869.pdf.

Vigueras-Rodríguez, A., P. Sørensen, A. Viedma, M. Donovan, and E. Gómez Lázaro (2012). "Spectral coherence model for power fluctuations in a wind farm". *Journal of Wind Engineering and Industrial Aerodynamics* **102**, pp. 14 –21.

Zečević, A. and D. Šiljak (2005). "Global low-rank enhancement of decentralized control for large-scale systems". *IEEE Transactions on Automatic Control* **50**:5, pp. 740–744.

Zečević, A. and D. Šiljak (2010). *Control of Complex Systems: Structural Constraints and Uncertainty*. Springer-Verlag, New York, NY.

Zhou, K., J. C. Doyle, and K. Glover (1995). *Robust and Optimal Control*. Prentice-Hall, Englewood Cliffs, NJ.

# Paper I

# Dynamic Power Coordination for Load Reduction in Dispatchable Wind Power Plants

**Daria Madjidian  Maxim Kristalny  Anders Rantzer**

**Abstract**

In a dispatchable wind power plant, turbines are free to continuously vary their power production as long as the sum of their productions meets the total power demand. Previous research has shown that this freedom can be used to reduce structural loads by allowing turbines in the plant to coordinate their power. This paper explains the mechanisms that make power coordination useful for reducing structural loads on the turbine tower and the low speed shaft. In addition, it assesses the benefits of coordination at different operating points.

## 1. Introduction

In an attempt to accelerate investments in renewable energy, several regions around the world offer wind power plants (WPPs) feed-in tariffs in the form of guaranteed grid access and stable long term purchase agreements [Couture et al., 2010]. The effect of this extra-market treatment is that, unlike conventional generators that generate power to balance electrical load, WPPs lack an incentive to regulate their output power. Hence, additional amounts of reserve capacity need to be contracted to compensate for the inherent variability and uncertainty in the wind [California ISO, 2010]. As the cost for these additional reserves will be higher at deeper penetration levels, it is likely that WPPs will be required to contribute more to the balancing effort in the future.

Such policies are emerging. For instance, several countries have updated their grid codes so that large WPPs are now required to respond to power requests from the system operator [Elkraft Systems and Eltra, 2004; Hydro-Québec, 2005; Commission for Energy Regulation, 2004]. Moreover, in some countries, such as the United Kingdom and Spain, WPPs participate in electricity markets where they are penalized for deviations from contracted power levels [Hiroux and Saguan, 2010; Klessmann et al., 2008]. Also, several academic studies have investigated how WPPs can participate in electricity and ancillary markets. In [Kirby et al., 2010], the authors analyze price differences between electricity and regulation markets in Texas and California during 2008 and 2009. Their results show that for a significant number of hours each year, regulation prices exceed electricity prices. This means that WPPs could benefit economically from curtailing power in order to provide grid support. In [Bitar et al., 2011], the authors study optimal contract offers for a WPP participating in forward electricity markets. They show that, in order to avoid penalties on power deviations from contracted levels, the WPP often benefits from operating below maximum capacity.

Motivated by these developments, we consider a WPP, consisting of several wind turbines (WTs), scheduled to deliver a certain active power demand, which is lower than the WPP is capable of producing. This implies that there is freedom in distributing the power production among the WTs. In most work dedicated to dispatchable WPP control, this distribution is made with the sole purpose of attaining the power demand [Hansen et al., 2006; Kaneko et al., 2007; Chang-Chien et al., 2008]. However, it is also possible to use the freedom in distributing power to improve additional aspects of WPP operation. For instance, in [de Almeida et al., 2006], this freedom is used to reduce active power losses in the transformers and lines inside the WPP. Another possibility, which is the topic of this paper, is to use the freedom in power distribution to reduce the structural loads

experienced by the WTs. Instead of each WT following a fixed portion of the power demand, it can be allowed to continuously adjust its power production in response to local wind speed fluctuations. Since wind conditions are not uniform across the WPP, changes in power production that benefits one WT can be compensated for by WTs with opposite needs.

This idea, which we shall refer to as dynamic power coordination (DPC), was introduced in [Spudić et al., 2010]. There, the problem is divided into two parts. First, optimal set points are computed offline for each WT using a receding horizon strategy. Then, the WTs are coordinated on-line to meet the total power demand. DPC subject to communication constraints was studied in [Madjidian et al., 2011] and [Biegel, 2011]. Similar work was also presented in [Kristalny and Madjidian, 2011]. There, the problem is studied in a feedforward setting where only the wind speed is communicated between neighboring WTs.

The results in the references mentioned above, show that compared to situations where each WT follows a fixed portion of the power demand, DPC can result in a significant reduction in structural loads to both the tower and low speed shaft of the WTs. However, these references do not explain the mechanisms behind these load reductions. Moreover, they assume that the WTs are equipped with a pre-designed internal controller. The presence of internal controllers simplifies the coordination problem by reducing it to coordination of the power references. On the other hand, by limiting direct access to the pitch angle and the generator torque, the internal controller reduces the ability of the WT to respond to wind speed fluctuations. Hence, it limits the potential in coordinating the WTs.

In this paper, we study the benefits of DPC among WTs without an internal controller. While previous research was concerned with designing algorithms to carry out the coordination, we explain the mechanisms that makes DPC useful in terms of load reduction, and assess its benefits at different operating points. The remainder of this paper is organized as follows: In Section 2, we introduce the WT model and explain the control objectives. In Section 3, we study the benefits of allowing a WT to adjust its power production. DPC is studied in Section 4, and concluding remarks are presented in Section 5.

## 2. Modeling

### 2.1 Wind turbine model

We adopt a model of the NREL 5 MW variable speed, collective pitch controlled WT based on [Grunnet et al., 2010]. The WT was introduced in [Jonkman et al., 2009] where it is described in detail. Note that parameter values that are not provided below can be found in [SimWindFarm,

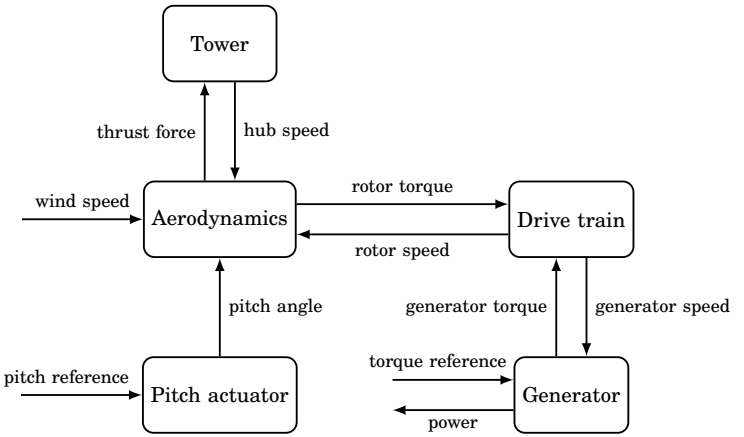


**Figure 1.** Schematic overview of a variable speed pitch controlled WT.

2014]. A schematic overview of the WT is given in Figure 1. The aerodynamics block describes the interaction with the wind,

$$m_r = \frac{\rho}{2\omega_r}\pi R^2 C_p(\lambda,\beta)v_r^3$$
$$f_t = \frac{\rho}{2}\pi R^2 C_t(\lambda,\beta)v_r^2,$$

where $m_r$ is the rotor torque, $\omega_r$ is the rotor speed, $f_t$ is the thrust force, and $v_r$ is the wind speed experienced by the rotor. The latter is given by $v_r = v - \dot{\delta}$, where $v$ is the ambient wind speed and $\delta$ is the fore-aft displacement of the WT nacelle. The parameter $\rho$ is the air density and $R$ is the rotor radius. The functions $C_p$ and $C_t$ are the power and thrust coefficient of the WT, respectively. They are static functions of the pitch angle, $\beta$, and the tip speed ratio, $\lambda = \frac{R\omega_r}{v_r}$.

The drive train connects the rotor and generator shafts via a gear box with a gear ratio of $n_g$. It is modeled as a third order system

$$J_r\dot{\omega}_r = m_r - m_{\text{sh}}$$
$$J_g\dot{\omega}_g = \frac{m_{\text{sh}}}{n_g} - m_g$$
$$\dot{\theta} = \omega_r - \frac{\omega_g}{n_g}$$

where $\omega_g$ is the generator speed, $\theta$ is the torsion of the low speed shaft and $m_{\text{sh}}$ is the restoring shaft torque:

$$m_{\text{sh}} = b_s\dot{\theta} + k_s\theta.$$

The parameters $J_r$, $J_g$, $b_s$ and $k_s$ are the rotor inertia, generator inertia, torsional damping and torsional stiffness, respectively. The drive train has a poorly damped resonant mode at $\omega_{\text{sh}} = 14$ rad/s.

The generator is modeled as a first order system with a time constant of $\tau_g = 0.1$ sec:

$$\begin{aligned} \dot{m}_g &= \frac{1}{\tau_g}(m_{g,\text{ref}} - m_g) \\ p &= m_g \omega_g, \end{aligned} \tag{1}$$

where $p$ is the electrical power, and $m_g$ and $m_{g,\text{ref}}$ are the generator torque and its reference, respectively.

The tower block describes the fore-aft displacement of the nacelle, which is modeled as a spring mass system excited by the thrust force:

$$\begin{aligned} m_t \ddot{\delta} &= f_t - f_{\text{tow}} \\ f_{\text{tow}} &= b_t \dot{\delta} + k_t \delta \end{aligned}$$

where $m_t$, $b_t$, and $k_t$ are mass, damping and stiffness parameters, respectively, and $f_{\text{tow}}$ is the restoring tower bending force. The tower has a resonance frequency of $\omega_{\text{tow}} = 2$ rad/s.

The pitch actuator is modeled as a first order system

$$\dot{\beta} = \frac{1}{0.3}(\beta_{\text{ref}} - \beta),$$

where $\beta_{\text{ref}}$ is the pitch angle reference.

## 2.2 Generalized control plant

To facilitate analysis, we consider operation around an operating point, where the WT model can be approximated by an LTI plant. The operating point is determined by the mean wind speed, $v_{\text{nom}}$, and an external demand on power production, $p_{\text{nom}}$. The choice of operating point will be explained in Section 3. Unless otherwise stated, all signals will henceforth describe the deviation from their nominal value at the operating point.

For control purposes, we use the generalized plant $P$ depicted in Figure 2. It incorporates a model of the WT, the exogenous disturbances and the regulated outputs. The inputs are the control signal and the exogenous noise

$$\begin{aligned} u &= \begin{bmatrix} \beta_{\text{ref}} & m_{g,\text{ref}} \end{bmatrix}^T \\ w &= \begin{bmatrix} w_v & w_e \end{bmatrix}^T, \end{aligned}$$

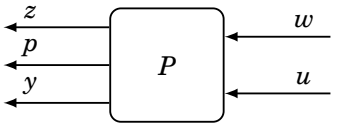


**Figure 2.** Linear turbine model.

where $w_v$ and $w_e$ are both Gaussian white noise processes with unit intensity and independent of each other. The process $w_v$ generates the wind speed fluctuations according to $v = W_v w_v$, where the filter

$$W_v(s) = \frac{0.1065}{s + 0.0143}$$

was identified from real WT data in [Kristalny et al., 2013]. The process $w_e$ generates the measurement noise. We assume that we can only measure the generator speed. The measured signal is given by

$$y = \omega_g + W_e w_e.$$

To prevent the controller from exciting unmodeled resonant modes at higher frequencies (e.g. blade bending) we set

$$W_e = 0.2\frac{s}{s + \omega_e},$$

where the corner frequency, $\omega_e = \frac{\pi}{5}$, is chosen to be ten times lower than the first edgewise blade resonance frequency [Jonkman et al., 2009]. The regulated signals are the power, $p$, and the vector

$$z = \begin{bmatrix} \omega_r & m_{\text{sh}} & f_{\text{tow}} & \tilde{\beta} & \tilde{m}_g \end{bmatrix}^T,$$

whose elements relate to relevant mechanical loads and limitations. The rotor speed, $\omega_r$, should not exceed its rated value. The tower force variation, $f_{\text{tow}}$, needs to be kept small in order to reduce fatigue damage to the tower. Similarly, to reduce fatigue damage to the gear box and low speed shaft, we penalize the shaft torque $m_{\text{sh}}$. The signals $\tilde{\beta} = W_\beta \beta_{\text{ref}}$ and $\tilde{m}_g = W_m m_{g,\text{ref}}$ are related to the pitch activity and torque activity, respectively. In order to avoid damping tower and drive train oscillations through oscillations in the pitch angle and generator torque, we set

$$W_\beta(s) = \frac{s^2}{s^2 + 0.2\omega_{\text{tow}} s + \omega_{\text{tow}}^2}$$
$$W_m(s) = \frac{s^2}{s^2 + 0.2\omega_{\text{shaft}} s + \omega_{\text{shaft}}^2}.$$

### 2.3 Wind power plant model

Wind speed variations at WTs in a WPP are correlated. However, studies show that they are correlated only at low frequencies, which are less important when controlling WT dynamics in the vicinity of an operating point [Kristalny et al., 2013]. The larger the distance between turbines, the lower the frequencies where the WTs are coupled [Vigueras-Rodríguez et al., 2012]. For the sake of simplicity, when considering several WTs around their operating points, we assume that the distance between them is large enough to neglect WT coupling.

## 3. Benefit of allowing wind turbine power variations

The purpose of this section is to investigate the potential for reducing fatigue loads by allowing WTs to vary their power production. To this end, we consider operation of a single WT under two different power tracking policies. Under Policy 1, the variation in power production is tightly constrained, whereas under Policy 2, this constraint is removed. Controllers for each of these policies are given by the solutions to Problems 1 – 2 stated below. To shorten notation, for a zero mean stationary process $x$, we let $\|x\|^2$ denote its variance: $\|x\|^2 = \mathbf{E}x^2(t)$. As a measure of tower loading, we consider the standard deviation of the tower force, $\|f_{\text{tow}}\|$. Similarly, the low speed shaft load is defined as $\|m_{\text{sh}}\|$. Let $\bar{\omega}_r$, $\bar{\beta}$, $\bar{m}_g$ and $\bar{p}$ be positive scalars.

Problem 1—Tight power tracking
Given $\eta \in [0,1]$, find a stabilizing controller, $K_1 : y \to u$, that minimizes

$$J(m_{\text{sh}}, f_{\text{tow}}) = \eta \|m_{\text{sh}}\|^2 + (1-\eta)\|f_{\text{tow}}\|^2 \tag{2}$$

and satisfies

$$\|\omega_r\| \le \bar{\omega}_r \qquad \|\tilde{\beta}\| \le \bar{\beta} \qquad \|\tilde{m}_g\| \le \bar{m}_g, \tag{3}$$

as well as

$$\|p\| \le \bar{p}. \tag{4}$$

□

The constraints in (3) constitute predefined limits on the amount of rotor speed variation, pitch activity, and generator torque activity. The constraint (4) limits the amount of variation in the WT's power production.

Problem 2—Relaxed power production
Given $\eta \in [0,1]$, find a stabilizing controller, $K_2 : y \to u$, that minimizes (2) and satisfies (3). □

Note that, as opposed to Problem 1, there is no constraint on power tracking in Problem 2.

REMARK 3.1
Problems 1 – 2 above are constrained LQG-problems. Their solution can be found by means of Lagrangian relaxation and subsequent iteration over the dual variables. For more information, we refer to [Megretsky and Treil, 1993] and [Yakubovich, 1992], where it was shown that the duality gap is zero. □

In order to set reasonable values on the bounds in (3)–(4), we introduce a standard WT controller, denoted $K_0$, from [Jonkman et al., 2009]. Above rated wind speed, the controller keeps the WT within its mechanical and electrical limits. This is achieved by varying the pitch angle to maintain rated rotor speed and adjusting the generator torque to attain rated power. Below rated wind speed, $K_0$ tries to extract maximum power. This is done by fixing the pitch angle to the angle that corresponds to the highest power capture and using the generator torque to track optimal rotor speed.

In the next two subsections, we will compare Policy 1 and Policy 2 controllers at nominal wind speeds of 15 m/s and 9 m/s. For comparison, the performance of $K_0$ at these operating points is shown in Table 1.

## 3.1 Operation at 15 m/s

In this subsection, we consider operation around $v_{\text{nom}} = 15$ m/s. We set $p_{\text{nom}} = 4$ MW, which is 1 MW less than what the WT is capable of producing at this wind speed. To attain the power production, we set nominal rotor speed to its rated value, i.e. $\omega_{\text{r,nom}} = \omega_{\text{r,rated}}$. At 15 m/s, this choice of operating point is consistent with the operating points in [Garcia and Jurado, 2008; Ma and Chowdbury, 2010; Rodríguez-amenedo et al., 2002; Grunnet et al., 2010].

The bounds in Problem 1–2 are set to $\bar{\omega}_r = 5.4 \cdot 10^{-3}$, $\bar{\beta} = 0.19$, $\bar{m}_g = 200$ and $\bar{p} = 12 \cdot 10^3$. Note that all the bounds in (3) and (4), except the bound on the generator torque activity, are set according to the performance of $K_0^{15}$. The generator torque bound, $\bar{m}_g$, is set higher because at $p_{\text{nom}} = 4$ MW, the WT operates well below its rated torque level and can allow more variation in the generator torque.

Next, we compute the solution to Problem 1 and Problem 2 for $\eta \in [0, 1]$. Figure 3 shows the complete trade off curve for Problem 1 (solid black) and the leftmost part of the trade off curve for Problem 2 (dashed blue). Figure 3 also shows the trade off curves obtained by solving Problem 1 with different values of $\bar{p}$ (gray). As $\bar{p}$ increases, these trade off curves approach the trade off curve of Problem 2 (dashed blue). Above some level of $\bar{p}$, the leftmost part of the curves coincide with the trade

**Table 1.** Performance of different controllers.

| | $\|w_r\|$ | $\|m_{\text{sh}}\|$ | $\|f_{\text{tow}}\|$ | $\|\tilde{\beta}\|$ | $\|\tilde{m}_g\|$ | $\|p\|$ |
|---|---|---|---|---|---|---|
| | mrad/sec | kNm | kN | – | – | kW |
| $K_0^9$ | 83 | 383 | 75.8 | 0 | 66 | 619 |
| $K_0^{15}$ | 5.4 | 37.66 | 33.20 | 0.19 | 46 | 12 |
| $K_1^{15}$ | 5.5 | 18.72 | 20.47 | 0.19 | 200 | 12 |
| $K_2^{15}$ | 5.4 | 147.89 | 11.68 | 0.19 | 200 | 204 |
| $K_{1,r}^{15}$ | 325.2 | 802.70 | 11.60 | 0.19 | 200 | 12 |
| $K_{2,r}^{15}$ | 55.2 | 14.55 | 11.59 | 0.19 | 200 | 175 |
| $K_1^9$ | 34.4 | 50.00 | 39.57 | 0.19 | 200 | 12 |
| $K_2^9$ | 103.3 | 10.76 | 11.41 | 0.19 | 200 | 192 |
| $K_{3,1}^9$ | 80.1 | 50.00 | 28.20 | 0.19 | 200 | 136 |

off curve of Problem 2. This implies that trade offs characterized by low shaft loads (large $\eta$) can be attained with less power variation than trade offs characterized by low tower loads (small $\eta$).

In order to understand how relaxing the power tracking requirement leads to reduced tower loading, we will compare the responses of a Policy 1 controller, denoted $K_1^{15}$, and a Policy 2 controller, denoted $K_2^{15}$, to the "Mexican hat" gust illustrated in Figure 4. Both $K_1^{15}$ and $K_2^{15}$ are designed with zero weight on the shaft load (i.e. $\eta = 0$). The performance of these controllers is shown in Table 1. Although they result in high shaft loads, they allow us to study an ideal response in terms of the tower load. The result is shown in Figure 5. Under $K_1^{15}$, the generator torque tends to decrease whenever the rotor speed increases, thereby accelerating the rotor speed deviations. This behavior is due to the bound on power variations (4) and the algebraic relation between power, generator torque and generator speed in (1). The acceleration caused by the generator torque increases the pitch effort needed to damp rotor speed variations. This behavior is not present in $K_2^{15}$ which applies a decelerating torque at the expense of larger power fluctuations. This additional damping unloads the pitch actuator in terms of rotor speed damping and enables a pitch behavior which is better suited with respect to tower loading.

To further illustrate that the possibility to reduce the tower load is linked to the rotor speed constraint, we introduce the Policy 1 controller $K_{1,r}^{15}$ and the Policy 2 controller $K_{2,r}^{15}$. They are designed with $\eta = 0$, $\bar{\omega}_r = \infty$, $\bar{\beta} = 0.19$, $\bar{m}_g = 200$ and $\bar{p} = 12 \cdot 10^3$. The difference between these controllers and $K_1^{15}$ and $K_2^{15}$ is that the constraint on rotor speed has

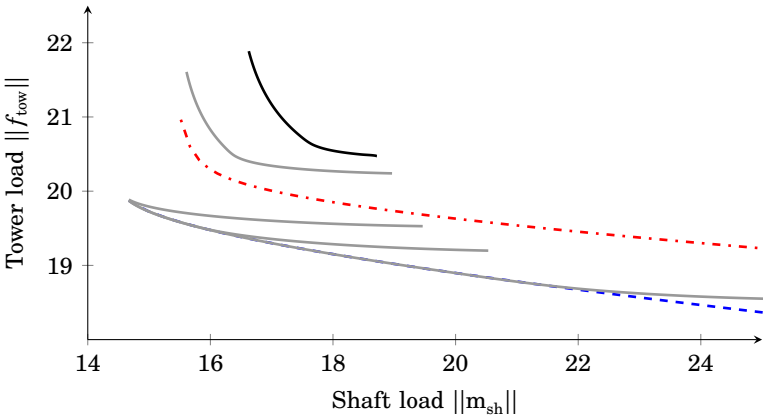


**Figure 3.** Trade offs at $v_{nom} = 15$ m/s between tower and shaft loads under Policy 1 (solid black), Policy 2 (dashed blue) and Policy 3 for $N = 2$ WTs (dash-dotted red). The gray curves are trade off curves for Problem 1 with $\bar{p} = \{15,\ 25,\ 30,\ 40\}$ kW. The increase in power fluctuations, $\|p\|$, needed to obtain a simultaneous reduction in tower and shaft loads does not exceed 40 kW.

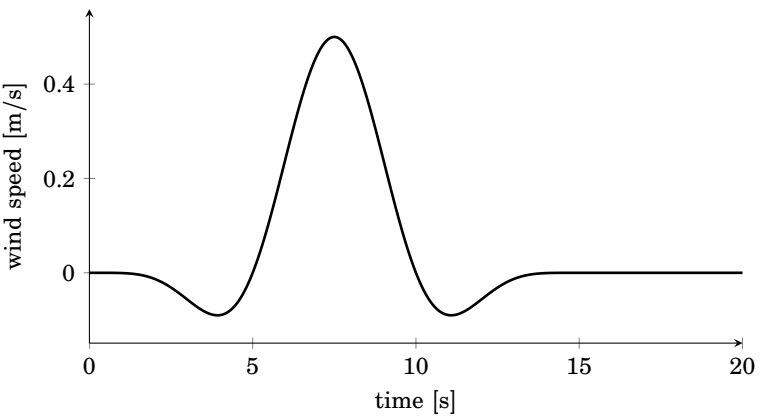


**Figure 4.** Mexican hat gust.

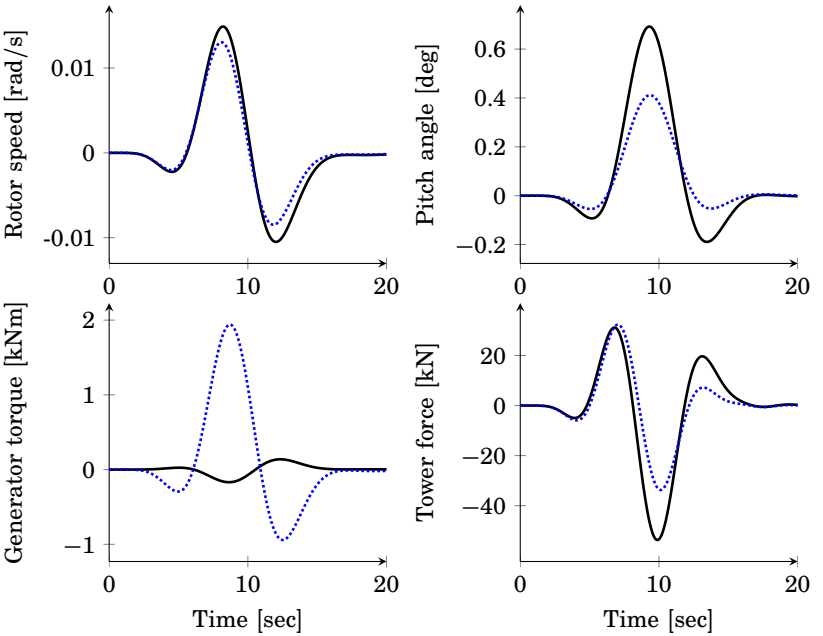


**Figure 5.** Response of $K_1^{15}$ (solid black) and $K_2^{15}$ (dashed blue) to the Mexican hat gust. All plots show deviations from nominal values. The advantage with respect to tower loading of allowing $K_2^{15}$ to adjust the power production is that it can use the generator torque to damp rotor speed variations. This additional damping unloads the pitch actuator and enables a pitch behavior that is better suited with respect to tower loading. This behavior is not present in $K_1^{15}$ which, in order to track the power demand, has a torque behavior which exacerbates the rotor speed variations.

been removed. The performances of $K_{1,r}^{15}$ and $K_{2,r}^{15}$ is shown in Table 1. The results show that if there were no need to control the rotor speed, the tower load under Policy 1 would be at level with the tower load under Policy 2. Moreover, the difference between $K_{1,r}^{15}$ and $K_{2,r}^{15}$ shows that removing the power constraint in addition to the rotor speed constraint only results in a minor additional tower load reduction.

REMARK 3.2
Unlike $K_2^{15}$ and $K_{1,r}^{15}$, $K_{2,r}^{15}$ manages to reduce both tower and shaft loads. This will be further explained in the next subsection. □

## 3.2 Operation at 9 m/s

We now consider operation around $v_{\text{nom}} = 9$ m/s and set the nominal power production to $p_{\text{nom}} = 2$ MW, which is 0.6 MW less than what the

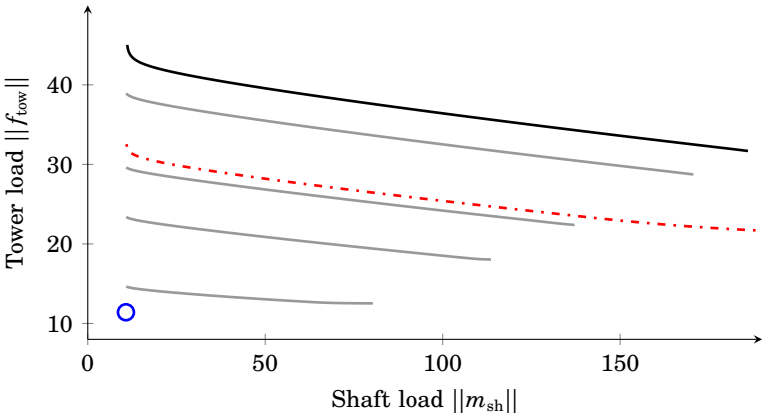


**Figure 6.** Trade offs at $v_{\text{nom}} = 9$ m/s between tower and shaft loads for a wind turbine under Policy 1 (solid black), Policy 2 (blue circle), and Policy 3 for $N = 2$ WTs (dash-dotted red). The gray curves are trade off curves for Problem 1 with $\bar{p} = \{30,\ 70,\ 100,\ 150\}$ kW. There is no trade off between reducing tower and shaft loads under Policy 2. The Policy 3 curve shows that by coordinating the power of only two WTs it is possible to track a total power demand and retain a significant portion of the load reduction under Policy 2 at the same time.

WT is capable of producing. This time the nominal power production is attained by setting the nominal rotor speed below rated rotor speed[1], $\omega_{\text{r,nom}} = \frac{\lambda^* v_{\text{nom}}}{R}$, where $\lambda^*$ is the tip-speed ratio that corresponds to the highest nominal power extraction.

As before, we begin by setting the bounds on the constraints (3) and (4): $\bar{\omega}_r = 115 \cdot 10^{-3}$, $\bar{\beta} = 0.19$, $\bar{m}_g = 200$ and $\bar{p} = 12 \cdot 10^3$. All bounds, except the bound on rotor speed variations, are equal to those used in Section 3.1. The constraint on rotor speed has been relaxed compared to Section 3.1 because at 9 m/s the WT operates well below rated rotor speed. The bound used here is set so that the rotor speed stays below its rated value 95% of the time.

Figure 6 shows the trade off curve under Policy 1 (solid black) and Policy 2 (blue circle). Under Policy 2 there is no trade off between reducing tower and shaft loads. This is because, as explained in Section 3.1, the constraint on the power variations (4) increases the control effort needed in order to limit the rotor speed variations. Because of the high bound on the allowed rotor speed variation at $v_{\text{nom}} = 9$ m/s, removing the power

[1] In general there are several pitch angle and rotor speed configurations that result in the same power production. The configuration used here is consistent with [Ma and Chowdbury, 2010; Rodríguez-amenedo et al., 2002].

tracking requirement is enough to deactivate the rotor speed constraint. Then, since the generator torque has a relatively small effect on the tower motion, the optimal Policy 2 controller, denoted $K_2^9$, can be designed in two separate steps. First, a pitch control loop is designed to minimize the tower load. Second, a generator torque loop is designed to minimize the shaft load. The performance of $K_2^9$ together with a Policy 1 controller, denoted $K_1^9$, is presented in Table 1.

Comparing Figure 6 with Figure 3, we see that both the load reductions and the power variation, $\|p\|$, needed to attain the reductions are larger at 9 m/s than at 15 m/s. This indicates that power coordination might be especially useful at low wind speeds.

REMARK 3.3
The reason for the larger load reductions at 9 m/s compared to 15 m/s is that, at low wind speeds, the constraint (4) has a larger effect on the rotor speed. Therefore, removing this effect is especially beneficial at low wind speeds. □

## 4. Coordination

In Section 3 we showed that a WT can benefit in terms of tower and shaft loading by allowing larger fluctuations around its power set point. In this section, we demonstrate that when several WTs operate in a WPP, part of this benefit can be retained while jointly tracking a total power demand. The power coordination needed in order to achieve this is referred to as power tracking Policy 3. The controller in this policy is given by the solution to Problem 3 stated below.

PROBLEM 3—COORDINATED POWER TRACKING
Consider $N$ WT plants $P_1, \ldots, P_N$. Given $\eta \in [0,1]$, find stabilizing controllers

$$K_{3,i} : \begin{bmatrix} y_1 \\ \vdots \\ y_N \end{bmatrix} \to u_i, \ i = 1, \ldots, N,$$

that satisfy (3) locally and minimize

$$\sum_{i=1}^{N} \left( \eta \left\| m_{\mathrm{sh,i}} \right\|^2 + (1-\eta) \left\| f_{\mathrm{tow,i}} \right\|^2 \right)$$

subject to the joint power constraint

$$\left\| \sum_{i=1}^{N} p_i \right\| \leq \bar{p}\sqrt{N}. \tag{5}$$

□

The bound in (5) corresponds to the joint

power variation of $N$ WTs operating under Policy 1. Indeed, since the power fluctuations from such WTs are assumed to be uncorrelated (see Section 2.3), we have

$$\left\| \sum_{i=1}^{N} p_i \right\|^2 = \sum_{i=1}^{N} \|p_i\|^2 = N\bar{p}^2.$$

Note that (loosely speaking), Problem 3 is a relaxation of Problem 1, and that Problem 2 is a relaxation of Problem 3. More specifically, let $J_{\text{Policy 1}}$ and $J_{\text{Policy 2}}$ denote the optimal cost in Problem 1 and Problem 2, respectively. Also let $J_{N,\text{Policy 3}}$ be the local cost for a WT in Problem 3. Then, provided that both the bounds on the constraints and $\eta$ in Problems 1 – 3 are identical, we have

$$J_{\text{Policy 2}} \leq J_{N,\text{Policy 3}} \leq J_{\text{Policy 1}}, \text{ for } N = 1, 2, \ldots$$

Moreover, it can be shown that as $N$ grows large, Policy 3 cost approaches Policy 2 cost. That is,

$$\lim_{N\to\infty} J_{N,\text{Policy 3}} = J_{\text{Policy 2}}.$$

In particular, this means that Problem 2 provides a tight upper bound on the improvement that can be obtained by coordinating power.

Next, we consider two WTs ($N = 2$), each operating at $v_{\text{nom}} = 9$ m/s with a nominal power production of $p_{\text{nom}} = 2$ MW. We set $\bar{\omega}_r = 115 \cdot 10^{-3}$, $\bar{\beta} = 0.19$, $\bar{m}_g = 200$ and $\bar{p} = 12 \cdot 10^3$, which is in accordance with the bounds used to design Policy 1 and Policy 2 controllers in Section 3.2. The trade off between the two loads in Problem 3 is shown in Figure 6 (red dash-dotted). It shows that by coordinating its power production with one other WT, a WT can retain a significant portion of the load reduction possible under Policy 2. The trade off curve for a WT operating at $v_{\text{nom}} = 15$ m/s and $p_{\text{nom}} = 4$ MW is constructed analogously and shown in Figure 3.

Let $K_{3,1}$ and $K_{3,2}$ denote the Policy 3 controllers designed to match the shaft load performance of the Policy 1 controller $K_1^9$. Their performance is listed in Table 1. Figure 8 shows the power responses of $K_{3,1}$ and $K_1^9$ to the turbulent wind in Figure 7. Note that the variation in total plant power is almost identical under both policies (Figure 8 left). However, because $K_{3,1}^9$ coordinates its power production with $K_{3,2}^9$, it may allow larger fluctuations in its production than $K_1^9$.

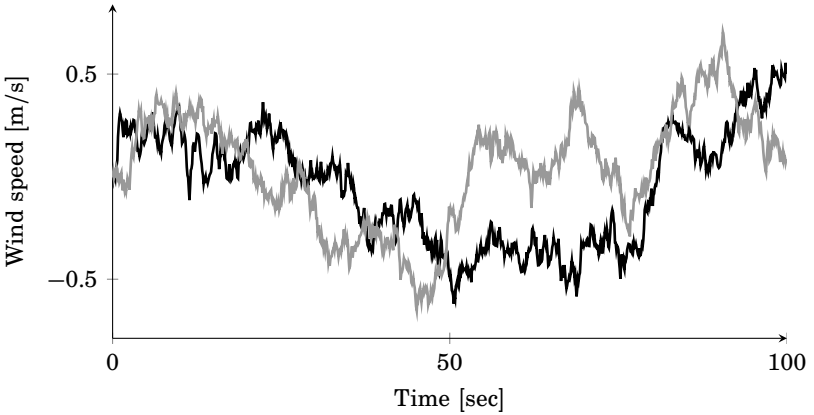


**Figure 7.** Turbulent wind speed variations at WT 1 (black) and WT 2 (gray).

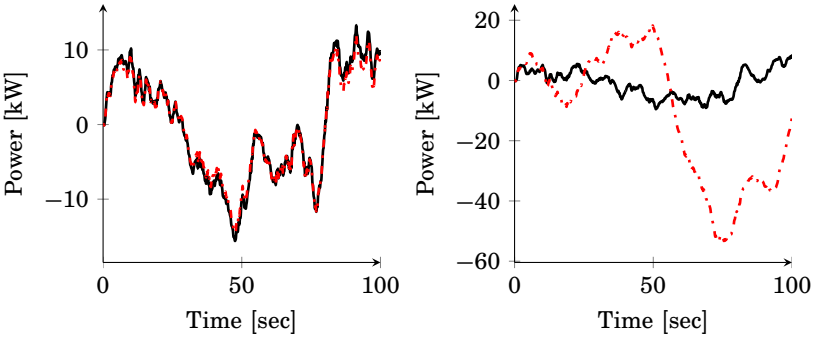


**Figure 8.** Power fluctuations in response to turbulent wind speeds in Figure 7 under Policy 1 (solid black) and Policy 3 (dash-dotted red). The left plot illustrates the total power variations of the two wind turbines (the curves overlap almost perfectly) and the right plot shows the local power variations at WT 1.

## 5. Conclusions

Dynamic power coordination (DPC) allows wind turbines (WTs) in a wind power plant to vary their individual power production as long as the sum of their production meets a total power demand. This paper provides insight into the mechanisms that make DPC useful for reducing fatigue loads on the WT tower and on the low speed shaft.

We saw that a tight constraint on a WT's power production restricts its generator torque behavior and leaves the pitch angle as the only control signal to regulate the rotor speed and the loads. Hence, a benefit of allowing the WT to vary its power is that this restriction is removed. Another benefit is that it helps to reduce rotor speed variations. This effect is especially important because the need to regulate the rotor speed variations causes trade off between reducing tower and shaft loads.

We compared the load reduction that could be obtained by allowing a WT to vary its power at two different nominal wind speeds. At 15 m/s, where the WT operated at rated rotor speed, there was a trade off between reducing tower and shaft loads. In this case, a reasonable range of trade offs could be attained at the expense of a moderate increase in power variation. At 9 m/s, where the WT operated below rated rotor speed, the situation was different. In this case, partially due to the relaxed requirements on the rotor speed control, there was no conflict between reducing tower and shaft loads. Also, the load reduction at 9 m/s was larger than at 15 m/s, but came at the expense of considerable power variations. This implies that DPC might be especially beneficial at low wind speeds.

Finally, we showed how power fluctuation at individual WTs may be compensated by coordination. In particular, we demonstrated that even coordination among two WTs may be enough to obtain substantial load reductions.

## Acknowledgments

This work was supported by the Swedish Research Council through the LCCC Linnaeus Center and by the European commission through the project AEOLUS.

## References

Biegel, B. (2011). *Distributed Control of Wind Farm*. M.Sc. Thesis. Lund University.

Bitar, E., R. Rajagopal, P. Khargonekar, K. Poolla, and P. Varaiya (2011). "Bringing wind energy to market". *IEEE Transactions on Power Systems* **27**:3, pp. 1225–1235.

California ISO (2010). *Integration of renewable resources: operational requirements and generation fleet capability at 20% rps*. Retrived 2014-05-03. URL: `https://www.caiso.com/informed/Pages/StakeholderProcesses/IntegrationRenewableResources.aspx`.

Chang-Chien, L., C. Hung, and Y. Yin (2008). "Dynamic reserve allocation for system contingency by dfig wind farms". *IEEE Transactions on Power Systems* **23**:2, pp. 729–736.

Commission for Energy Regulation (2004). *Wind Farm Transmission Grid Code Provisions – A Direction by the Commission for Energy Regulation*. Tech. rep. CER/04/237.

Couture, T. D., K. Cory, C. Kreycik, and E. Williams (2010). *A Policymaker's Guide to Feed-in Tariff Policy Design*. Tech. rep. NREL/TP-6A2-44849. National Renewable Energy Laboratory.

de Almeida, R. G., E. Castronuovo, and J. A. P. Lopes (2006). "Optimum generation control in wind parks when carrying out system operator requests". *IEEE Transactions on Power Systems* **21**:2.

Elkraft Systems and Eltra (2004). *Wind Turbines Connected to Grids with Voltages above 100 kV – Technical regulation for the properties and the regulation of wind turbines*. Tech. rep. Regulation TF 3.2.5.

Garcia, L. M. F. C. A. and F. Jurado (2008). "Comparative study on the performance of control systems for doubly fed induction generator (dfig) wind turbines operating with power regulation". *Energy* **33**, pp. 1438–1452.

Grunnet, J., M. Soltani, T. Knudsen, M. Kragelund, and T. Bak (2010). "Aeolus toolbox for dynamic wind farm modeling, simulation and control". In: *Proceedings of the 2010 European Wind Energy Conference*, pp. 3119–3129.

Hansen, A., P. Sorensen, F. Iov, and F F. Blaabjerg (2006). "Centralised power control of wind farm with doubly fed induction generators". *Renewable Energy* **31**:7, pp. 935–951.

Hiroux, C. and M. Saguan (2010). "Large-scale wind power in European electricity markets : time for revisiting support schemes and market designs?" *Energy Policy* **38**:7, pp. 3135–3145.

Hydro-Québec (2005). *Technical requirements for the connection of generation facilities to the hydro-québec transmission system – supplementary requirements for wind generation*. Retrieved 2014-05-03. URL: http://www.hydroquebec.com/transenergie/fr/commerce/pdf/Exig_compl_eolien_transport_mai03_ang.pdf.

Jonkman, J., S. Butterfield, W. Musial, and G. Scott (2009). *Definition of a 5-MW Reference Wind Turbine for Offshore System Development*. Tech. rep. NREL/TP-500-38060. National Renewable Energy Laboratory, Golden, CO.

Kaneko, T., T. Senjyu, A. Yona, M. Datta, T. Funabashi, and C. Kim (2007). "Output power coordination control for wind farm in small power system". In: *the 2007 International Conference on Intelligent Systems Applications to Power Systems*.

Kirby, B., M. Milligan, and E. Ela (2010). "Providing minute-to-minute regulation from wind plants preprint". In: *Proceedings of the 9th Annual International Workshop on Large-Scale Integration of Wind Power into Power Systems and Transmission Networks for Offshore Wind Power Plants*. Quebec, Canada.

Klessmann, C., C. Nabe, and K. Burges (2008). "Pros and cons of exposing renewables to electricity market risks — a comparison of the market integration approaches in Germany, Spain, and the UK". *Energy Policy* **36**:10, pp. 3646–3661.

Kristalny, M. and D. Madjidian (2011). "Decentralized feedforward control of wind farms: prospects and open problems". In: *Proceedings of the 50th IEEE Conference on Decision and Control and European Control Conference*. Orlando, FL, USA, pp. 3464–3469.

Kristalny, M., D. Madjidian, and T. Knudsen (2013). "On using wind speed preview to reduce wind turbine tower oscillations". *IEEE Transactions on Control Systems Technology* **21**:4, pp. 1191–1198.

Ma, H. T. and B. H. Chowdbury (2010). "Working towards frequency regulation with wind plants : combined control approaches". *IET Renewable Power Generation* **4**:4, pp. 308–316.

Madjidian, D., K. Mårtensson, and A. Rantzer (2011). "A distributed power coordination scheme for fatigue load reduction in wind farms". In: *Proceedings of the 2011 American Control Conference*. San Francisco, CA, USA, pp. 5219–5224.

Megretsky, A. and S. Treil (1993). "Power distribution inequalities in optimization and robustness of uncertain systems". *Journal of Mathematical Systems, Estimation, and Control* **3**:3, pp. 301–319.

Rodríguez-amenedo, J. L., A. Arnalte, and J. C. Burgos (2002). "Automatic generation control of a wind farm with variable speed wind turbines". *IEEE Transactions on Energy Conversion* **17**:2, pp. 279–284.

SimWindFarm (2014). *Aeolus SimWindFarm Toolbox*. Retrieved 2014-04-16. URL: `http://www.ict-aeolus.eu/SimWindFarm/index.html`.

Spudić, V., M. Jelavić, M. Baotić, and N. Perić (2010). "Hierarchical wind farm control for power/load optimization". In: *Proceedings of the Science of Making Torque from Wind*, pp. 681 –692.

Vigueras-Rodríguez, A., P. Sørensen, A. Viedma, M. Donovan, and E. Gómez Lázaro (2012). "Spectral coherence model for power fluctuations in a wind farm". *Journal of Wind Engineering and Industrial Aerodynamics* **102**, pp. 14 –21.

Yakubovich, V. (1992). "Nonconvex optimization problem: the infinite-horizon linear-quadratic control problem with quadratic constraints". *System and Control Letters* **19**:1, pp. 13–22.

# Paper II

# Distributed Control with Low-Rank Coordination

**Daria Madjidian  Leonid Mirkin**

**Abstract**

A common approach to distributed control design is to impose sparsity constraints on the controller structure. Such constraints, however, may greatly complicate the control design procedure. This paper puts forward an alternative structure, which is not sparse yet might nevertheless be well suited for distributed control purposes. The structure appears as the optimal solution to a class of coordination problems arising in multi-agent applications. The controller comprises a diagonal (decentralized) part, complemented by a rank-one coordination term. Although this term relies on information about all subsystems, its implementation only requires a simple averaging operation.

## 1. Introduction

The ability to cope with complexity is one of the contemporary challenges of control engineering. Already an established research area by the late 1970s [Mesarović et al., 1970; Singh and Titli, 1978; Šiljak, 1978], control of complex systems reinvigorated during the last decade, impelled by recent technological progress, networking and integration trends, efficiency demands, etc.

Complexity may be manifested through different attributes, one of which is the presence of a very large number of sensors and actuators. In such situations fully centralized, structureless, information processing becomes infeasible. This motivates the quest for distributed control methods, with various constraints on information exchange between subsystems and information processing in the controller. Such structural constraints are conventionally expressed in terms of sparsity patterns [Šiljak, 1978; Zečević and Šiljak, 2010; Mahajan et al., 2012], with nonzero elements corresponding to permitted coordination between subsystems. Sometimes, delay constraints on the communication between subsystems are considered [Mahajan et al., 2012].

Although a sparse structure can effectively limit the amount of information processing in the controller, it substantially complicates the control design. Many well understood problems might turn acutely opaque when sparsity constraints on the controller are added [Wistenhausen, 1968; Tsitsiklis and Athans, 1985]. Design is simplified if the plant happens to possess a compatible sparsity pattern (the quadratic invariance condition [Rotkowitz and Lall, 2006; Mahajan et al., 2012]) or if additional constraints are imposed on the closed-loop behavior (like positivity [Tanaka and Langbort, 2011; Rantzer, 2011]). But even then the computational burden grows rapidly with the problem dimension and, more importantly, structural properties of the resulting controller are rarely transparent. Revealing such properties proved to be a challenge even in seemingly simple problems, see [Lessard and Lall, 2012] and the references therein.

This paper puts forward an alternative structure. We study a class of large-scale coordination problems that happens to admit a solution of a different type: not sparse, but nevertheless scalable. Specifically, we consider a homogeneous group of autonomous agents, i.e., a group of systems having identical dynamics and identical local criteria. Coordination requirements are then introduced through a (global) linear constraint imposed on an "average" agent. This setting is motivated by certain control tasks arising in the control of wind farms. The problem admits an analytic solution endowed with two appealing properties. First, the computational burden in this setting is independent of the number of agents.

Second, the optimal feedback gain is of the form of a block-diagonal matrix perturbed by a block-rank-one component. The structures of these components are transparent. The diagonal part merely comprises the local, uncoordinated, gains. The rank-one part is then responsible for coordination via fine-tuning the local controllers on the basis of measurements of an "average" agent.

The (weighted) averaging is the only non-sparse, centralized, task that has to be performed by the controller. We argue that this task may be network-friendly. Averaging is a relatively simple numerical operation, which might be robust to sensor imperfections for large groups. It can be performed either locally, by each agent [Xiao and Boyd, 2004], or globally, by a coordinator. The averaging of measured variables of individual subsystems may be viewed as a spatial counterpart of the generalized sampling operation [Araki, 1993]. This is in contrast to the decentralized structure, which may be thought of as a form of the ideal sampling, which ignores the intersample information. Considering this analogy, it might even be useful to impose the control structure in problems where, unlike in our formulation, it does not appear as a property of the optimal solution. In fact, one such approach, also in the context of large-scale systems, was proposed in [Zečević and Šiljak, 2005], see Remark 3.5 for more details.

The paper is organized as follows. In Section 2 we consider a coordination problem arising in wind farms. This problem serves a motivation for the theoretical developments in Sections 3 (problems with hard coordination constraints) and 4 (soft constraint formulations). Both sections illustrate their developments by numerical studies of the same wind farm coordination problem. Section 3 also contains an extensive discussion on properties of the resulting controller configuration and the structure of the optimal cost. Concluding remarks are then provided in Section 5.

**Notation** The transpose of a matrix $M$ is denoted by $M'$. By $e_i$ we refer to the $i$th standard basis of a Euclidean space and by $I_n$ to the $n \times n$ identity matrix (we drop the dimension subscript when the context is clear). The notation $\otimes$ stands for the Kronecker product of matrices [Zhou et al., 1995, §2.5]. The $L^2(\mathbb{R}^+)$ norm [Zhou et al., 1995, Ch. 4] of a signal $\xi$ is denoted as $\|\xi\|_2$.

## 2. Motivation: Coordination in Wind Farms

Wind energy is an increasingly active application area for control [Pao and Johnson, 2011]. Lately, the focus has been shifting from control of a stand-alone wind turbine (WT) to coordinated control of networks of WTs,

known as wind power plants (WPP) or wind farms. Below we consider one such problem, which is used to motivate the problem studied in this paper.

## 2.1 Problem description

We consider the problem discussed in [Spudić et al., 2011; Biegel et al., 2013], where a wind farm is required to meet a certain power demand. To achieve this, the WTs need to coordinate their power production. Since there are multiple WTs in the farm, certain freedom exists in distributing the power demand among them. This freedom can be used to address local objectives of individual turbines, such as regulating rotor speed, reducing fatigue loads, preventing excessive pitch action, etc. Thus, instead of following a fixed portion of the power demand, a WT can be allowed to continuously adjust its power production in response to local wind speed fluctuations. Since wind speed fluctuations are not the same across the WPP, changes in power production that benefit one WT can be compensated for by changes at WTs with opposite needs.

For control design purposes, it is common practice to model a WT as a linear system around an operating point. It may also be natural to make two additional simplifying assumptions.

1. WTs in a WPP are often identical in their design. By assuming that they operate around the same mean wind speed and mean power production, the WTs may be considered to have equal dynamics.

2. Due to a large distance between individual turbines in WPPs, it may be assumed that wind speed variations experienced by them are uncorrelated [Vigueras-Rodríguez et al., 2012; Kristalny et al., 2013].

With these observations in mind, below we address a coordination problem among a group of $\nu$ WTs. For simplicity, we use a stripped-down[1] version of the individual WT model and performance index studied in [Kristalny et al., 2013]. The model is derived from [Grunnet et al., 2010] and describes an NREL 5-MW wind turbine [Jonkman et al., 2009], operating around a mean wind speed of 10 m/s and a nominal power production of 2 MW. Each WT is assumed to be equipped with an internal controller, which manipulates the blade pitch angle and generator torque in order to track an external power reference. At the nominal power production, the WT operates in the derated mode (below maximum power

[1] We measure the input in MW and use neither the dynamic model of the effective wind speed (its DC gain is absorbed into the model) nor dynamic weights on regulated signals (we use approximate static weights instead).

production) and is able to both increase and decrease its power production. The turbine models are given by

$$\dot{x}_i = Ax_i + B_w w_i + B_u u_i, \quad i = 1, \dots, v$$

where $\left[\begin{array}{c|c|c} A & B_w & B_u \end{array}\right]$ take the following numerical values:

$$\left[\begin{array}{ccccc|c|c} 0 & 120 & -0.92 & 0 & 0 & 0 & 0 \\ 0.0084 & -0.032 & 0 & 0 & 0 & 0.12 & -0.021 \\ 0 & 150 & -1.6 & 0 & 0 & 0 & 0 \\ 0 & 0 & 0 & 0 & 1 & 0 & 0 \\ 0.021 & 0.054 & 0 & -4 & -0.32 & 0.2 & 0 \end{array}\right].$$

Here the state vector spells out as

$$x_i = \left[\begin{array}{c} \text{pitch angle} \\ \text{rotor speed} \\ \text{internal controller state} \\ \text{nacelle fore-aft position} \\ \text{nacelle fore-aft speed} \end{array}\right]$$

and the exogenous disturbance $w_i$ is the deviation in wind speed from its nominal value, modeled as a white noise process with unit intensity. The control signal $u_i$ is the deviation in the power reference from its nominal value. The model neglects generator dynamics, which makes $u_i$ equal to the actual deviation in the power production of the WT.

Following [Kristalny et al., 2013], we assume that each turbine aims at achieving a trade-off between regulating the rotor speed, reducing fatigue loads on the tower, and preventing excessive pitch activity and power deviations. The performance of the $i$th turbine is quantified as the variance of the regulated variable $z_i = C_z x_i + D_{zu} u_i$, where

$$\left[\begin{array}{cc} C_z & D_{zu} \end{array}\right] = \left[\begin{array}{cc} \operatorname{diag}\{\sqrt{0.1}, 100, 0, 100, 0\} & 0 \\ 0 & 1 \end{array}\right].$$

In other words, for each turbine we consider the state-feedback $H^2$ problem for the closed-loop system from $w_i$ to $z_i$.

The combined power production of the WTs must satisfy a power demand to the WPP, which is assumed to be the sum of nominal WT power productions. Since $u_i$ is the deviation from nominal WT power production, this requirement can be imposed as the constraint

$$u_1 + u_2 + \cdots + u_v = 0, \tag{1}$$

which forces the wind turbines to coordinate their actions.

The resulting constrained $H^2$ problem can be converted to a standard unconstrained one by resolving (1) for any $i$, say as $u_1 = -(u_2 + \cdots + u_\nu)$. This results in an $H^2$ problem with $\nu$ subsystems and $\nu - 1$ control signals. Yet, in this approach, the cost function and the dynamics of the subsystems become coupled. This might, especially if the number of turbines in the WPP is very large, considerably complicate both the solution procedure (the curse of dimensionality) and the implementation of the resulting controllers. Therefore a *scalable* solution procedure is of interest.

## 2.2 Towards a scalable solution

As discussed in the introduction, the conventional approach in the field is to impose some form of sparsity constraints on the controller and seek a scalable optimization procedure to solve it. By limiting the information exchange between subsystems, a sparse structure can ensure that the information processing at each subsystem remains viable as the number of subsystems grows. This property is important, so it frequently preponderates over inevitable losses of performance. The problem is that imposing sparsity constraints might significantly complicate the design. Once constraint (1) is resolved, our problem only satisfies the quadratic invariance condition of [Rotkowitz and Lall, 2006] for a handful of structural constraint options (e.g., block triangular). Another choice discussed in the introduction, which is to impose positivity constraints on the closed-loop dynamics [Tanaka and Langbort, 2011], is not suitable for our problem because we work in deviations from nominal values. We thus may consider resorting to non-convex optimization procedures, relying upon a proper choice of initial values.

To provide a flavor of such an approach, we confine our attention to static state-feedback controllers, $u = Fx$, and add the constraint that $F_{ij} = 0$ whenever $|i - j| > \eta$ for a given $\eta \in \mathbb{N}$ (the addition in the spatial variable is performed modulo-$\nu$, e.g., $\nu + 1 = 1$). We then use an approach, similar to that proposed in [Biegel et al., 2013], which, in turn, makes use of the distributed gradient method of [Mårtensson and Rantzer, 2012].

Fig. 1 shows the normalized difference between the $H^2$ performances attained with and without the coordination constraint (1) (the normalized cost of coordination) as a function of $\nu$ for different degrees of sparsity $\eta$. We can see that as the sparsity restriction is relaxed, i.e., as $\eta$ increases, the performance improves. Besides, the performance of sparse controllers improves as $\nu$ increases. We can also see that the improvement is not as fast as in the non-sparse solution (shown by the solid line). However, this was expected and is not the main focus of this example.

Instead, we would like to emphasize difficulties encountered in designing the sparse controllers. Although not visible on the plot, these difficul-

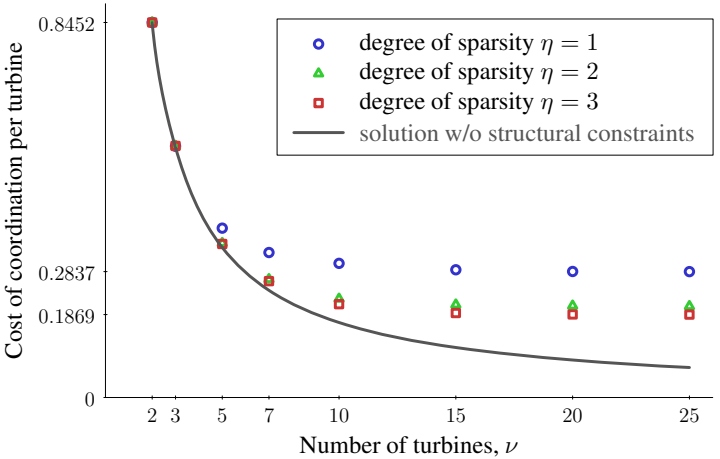


**Figure 1.** Cost of coordination per turbine under different degrees of sparsity.

ties are readily appreciable. The fact that the problem is not convex (the constraint set is not quadratically invariant under this plant) renders the whole procedure sensitive to the choice of initial values for the feedback gain. We did experience convergence to local minima, so the solutions presented in Fig. 1 are the result of multiple runs of the algorithm. And we still cannot guarantee that the results are globally optimal[2]. In addition, the optimization procedure itself is quite demanding, its computational complexity grows with the increase of $\nu$. Finally, the results of the numerical procedure are not transparent, with no indication of what effect small changes of the system parameters might have on it.

To conclude, from the distributed control viewpoint the problem appears to be a challenge. Nonetheless, in the next section we show that it has a closed-form solution, which is computationally scalable and possesses additional appealing properties from the distributed control perspective.

## 3. LQR with Coordination Constraints

Motivated by the problem considered in Section 2, in this section we study an optimization problem for non-interacting subsystems, having identical dynamics, with coordination constraints. To simplify the presentation, we

[2] In fact, they are not, as attested by the sub-optimality of the resulting cost in the case of $\eta = 3$ and $\nu = 7$, for instance.

consider an LQR version of the problem, although the extension to the $H^2$ formulation (external disturbances) is straightforward.

### 3.1 Problem statement

Consider $\nu$ independent systems

$$\Sigma_i : \dot{x}_i(t) = Ax_i(t) + Bu_i(t), \quad x_i(0) = x_{i0} \tag{2}$$

where $x_i(t) \in \mathbb{R}^n$ can be measured, $u_i(t) \in \mathbb{R}^m$, and $A \in \mathbb{R}^{n\times n}$ and $B \in \mathbb{R}^{n\times m}$ are such that the pair $(A, B)$ is stabilizable. Associate with each of these systems the performance index

$$\mathcal{J}_i = \int_0^\infty \big(x_i'(t)Q_\alpha x_i(t) + u_i'(t)u_i(t)\big)\,\mathrm{d}t \tag{3}$$

for some $n \times n$ matrix $Q_\alpha \geq 0$ such that the pair $(Q_\alpha, A)$ has no unobservable modes on the j$\omega$-axis. Minimizing $\mathcal{J}_i$ for $\Sigma_i$ would be a set of $\nu$ standard uncoupled LQR problems. We couple these problems by constraining the behavior of the *center of mass* of $\Sigma_i$, understood as the system

$$\bar{\Sigma} : \dot{\bar{x}}(t) = A\bar{x}(t) + B\bar{u}(t), \quad \bar{x}(0) = \bar{x}_0 \tag{4}$$

connecting the signals

$$\bar{u}(t) := \sum_{i=1}^{\nu} \mu_i u_i(t) \quad \text{and} \quad \bar{x}(t) := \sum_{i=1}^{\nu} \mu_i x_i(t), \tag{5}$$

where the weights $\mu_i \neq 0$ may be thought of as the masses of each subsystem. Coordination is then imposed by requiring $\bar{\Sigma}$ to evolve according to

$$\dot{\bar{x}}(t) = (A + B\bar{F})\bar{x}(t), \quad \bar{x}(0) = \bar{x}_0 \tag{6}$$

for a given gain $\bar{F} \in \mathbb{R}^{m\times n}$. This yields the following problem formulation:

$$\begin{aligned} \text{minimize} \quad & \mathcal{J} := \sum_{i=1}^{\nu} \mathcal{J}_i && \text{(7a)} \\ \text{subject to} \quad & \Sigma_i, \quad i = 1, \ldots, \nu && \text{(7b)} \\ & \bar{u} - \bar{F}\bar{x} = 0 && \text{(7c)} \end{aligned}$$

where $\bar{u}$ from (7c) substituted into (4) yields (6). In addressing (7), we implicitly restrict our attention to stabilizing controllers only. Without loss of generality, we also assume that the weights are normalized as $\sum_i \mu_i^2 = 1$.

REMARK 3.1—CONNECTIONS WITH THE MOTIVATING PROBLEM
It is readily seen that the problem considered in Section 2 is a particular case of (7) corresponding to $\bar{F} = 0$. Constraint (7c) can thus also be viewed as a constraint imposed on average trajectories. □

REMARK 3.2—MINIMIZING WEIGHTED SUM OF $\mathcal{J}_i$
The weights $\mu_i$ may be manipulated to assign importance to each subsystem. This can also be attained via replacing $\mathcal{J}$ in (7a) with the weighted sum $\mathcal{J} = \sum_i \lambda_i \mathcal{J}_i$ for some $\lambda_i > 0$. The addition of $\lambda_i$, however, does not enrich the design. It is only a matter of scaling each $x_i$ and $u_i$ by $\sqrt{\lambda_i}$ and then replacing $\mu_i$ with $\mu_i/\sqrt{\lambda_i}$ (with the normalization assumption $\sum_i \mu_i^2/\lambda_i = 1$). In the choice between '$\mu$' and '$\lambda$' scalings we picked the former because it allows negative weights. □

## 3.2 Problem solution

We start with rewriting (7) in an aggregate form using the Kronecker product notation. Introduce the unit vector

$$\mu := \begin{bmatrix} \mu_1 & \cdots & \mu_\nu \end{bmatrix}'$$

and the aggregate state and control signals $x := \sum_i e_i \otimes x_i$ and $u := \sum_i e_i \otimes u_i$, respectively. In this notation, the dynamics of the aggregate systems are

$$\dot{x}(t) = (I_\nu \otimes A)x(t) + (I_\nu \otimes B)u(t), \tag{8}$$

the cost function in (7a) is

$$\mathcal{J} = \int_0^\infty \big(x'(t)(I_\nu \otimes Q_\alpha)x(t) + u'(t)u(t)\big)\mathrm{d}t, \tag{9}$$

and the constraint (7c) reads

$$(\mu' \otimes I_m)u - (\mu' \otimes \bar{F})x = 0, \tag{10}$$

The key idea behind our solution is to apply coordinate transformations to the state and input signals that decouple constraint (7c) on the one hand, while preserving the uncoupled structure of the system and cost on the other. This can be achieved by the coordinate transformations

$$\tilde{x} := (U \otimes I_n)x \quad \text{and} \quad \tilde{u} := (U \otimes I_m)u \tag{11}$$

for some *unitary* matrix $U \in \mathbb{R}^{\nu\times\nu}$. Indeed, using the relation $(M_1 \otimes N_1)(M_2 \otimes N_2) = (M_1M_2) \otimes (N_1N_2)$, it is readily seen that both (8) and (9) remain the same, modulo the replacement of $x$ and $u$ with $\tilde{x}$ and $\tilde{u}$, respectively, while the coordination constraint changes and becomes

$$(\mu'U' \otimes I_m)\tilde{u} - (\mu'U' \otimes \bar{F})\tilde{x} = 0.$$

To achieve decoupling, we may consider the following requirements on $U$:

$$U\mu = e_1. \tag{12}$$

Because $\mu$ is assumed to be a unit vector, there is always a unitary $U$ satisfying (12). A possible choice is the matrix of transpose left singular vectors of $\mu$.

Thus, when expressed in terms of $\tilde{x}$ and $\tilde{u}$ with $U$ satisfying (12), problem (7) still has an uncoupled cost function and uncoupled dynamics. But now the constraint, which reads $(e_1' \otimes I_m)\tilde{u} - (e_1' \otimes \bar{F})\tilde{x} = 0$, is imposed only upon the first elements of $\tilde{u}$ and $\tilde{x}$, i.e., it reduces to

$$\tilde{u}_1 - \bar{F}\tilde{x}_1 = 0. \tag{13}$$

Hence, (7) splits into $\nu$ independent problems, with the $i$th problem depending only on the variables $\tilde{x}_i$ and $\tilde{u}_i$.

For $i = 2, \ldots, \nu$, we have identical unconstrained LQR problems with dynamics of the form (2) and cost functions of the form (3). Each one of these problems is then solved by the (stabilizing) control laws $\tilde{u}_i(t) = F_\alpha \tilde{x}_i(t)$, where $F_\alpha := -B'X_\alpha$ and $X_\alpha \geq 0$ is the stabilizing solution of the algebraic Riccati equation (ARE)

$$A'X_\alpha + X_\alpha A + Q_\alpha - X_\alpha B B' X_\alpha = 0. \tag{14}$$

These control laws attain the optimal performance $\tilde{x}_{i0}' X_\alpha \tilde{x}_{i0}$.

For $i = 1$, constraint (13) completely determines $\tilde{u}_1$, as $\tilde{u}_1 = \bar{F}\tilde{x}_1$, rendering the optimization irrelevant. The plant dynamics then become

$$\dot{\tilde{x}}_1(t) = (A + B\bar{F})\tilde{x}_1(t), \quad \tilde{x}_1(0) = \tilde{x}_{10}$$

and the cost function is given by

$$\int_0^\infty \tilde{x}_1'(t)(Q_\alpha + \bar{F}'\bar{F})\tilde{x}_1(t)\mathrm{d}t.$$

The dynamics of $\tilde{x}_1$ are stable iff $A + B\bar{F}$ is Hurwitz and in this case the value of its cost function is finite and equals $\tilde{x}_{10}'\bar{X}\tilde{x}_{10}$, where $\bar{X} \geq 0$ verifies the Lyapunov equation

$$(A + B\bar{F})'\bar{X} + \bar{X}(A + B\bar{F}) + Q_\alpha + \bar{F}'\bar{F} = 0. \tag{15}$$

The arguments above solve (7) in terms of the transformed variables in (11). What is left is to transform this solution back to $x$ and $u$. This is done in the following theorem, which is the main technical result of this section:

THEOREM 3.1
Let $A + B\bar{F}$ be Hurwitz and the pair $(Q_\alpha, A)$ have no unobservable pure imaginary modes. Then the ARE (14) and the Lyapunov equation (15) are solvable, with $\bar{X} \geq X_\alpha$, and the unique solution of (7) is

$$u_i(t) = F_\alpha x_i(t) + \mu_i(\bar{F} - F_\alpha)\bar{x}(t), \tag{16}$$

where $F_\alpha = -B'X_\alpha$ is the LQR gain, associated with the uncoordinated version of the problem, i.e. without (7c), and $\bar{x}$ is the state vector of the center of mass $\bar{\Sigma}$ defined by (5). The optimal performance attained by this controller is

$$\mathcal{J}_{\text{opt}} = \sum_{i=1}^{\nu} \mathcal{J}_{i,\text{opt}} + \bar{x}_0'(\bar{X} - X_\alpha)\bar{x}_0, \tag{17}$$

where $\mathcal{J}_{i,\text{opt}} = x_{i0}'X_\alpha x_{i0}$ is the optimal uncoordinated costs of $\Sigma_i$ and $\bar{x}_0$ is the initial condition of the center of mass. □

***Proof*** The solvability of the Riccati equations under the conditions of the theorem is a standard result [Zhou et al., 1995, Thm. 13.7]. The inequality $\bar{X} \geq X_\alpha$ follows by the fact that if $u_i = \bar{F}x_i$, then $\mathcal{J}_i = x_{i0}'\bar{X}x_{i0} \geq x_{i0}'X_\alpha x_{i0} = \mathcal{J}_{i,\text{opt}}$ for any $x_{i0}$. Now, the developments preceding the formulation of the theorem imply that the optimal control law for the transformed system is $\tilde{u} = \tilde{F}\tilde{x}$, where

$$\tilde{F} = (I_\nu - e_1e_1') \otimes F_\alpha + (e_1e_1') \otimes \bar{F}.$$

Then (11) implies that the optimal control law for the aggregate problem (8)–(10) is $u = Fx = (U' \otimes I_m)\tilde{F}(U \otimes I_n)x$, so, with the help of (12), we end up with the optimal gain

$$F = I_\nu \otimes F_\alpha + (\mu\mu') \otimes (\bar{F} - F_\alpha), \tag{18}$$

which yields (16). Finally,

$$\mathcal{J}_{\text{opt}} = \tilde{x}_0'((I_\nu - e_1e_1') \otimes X_\alpha + (e_1e_1' \otimes \bar{X}))\tilde{x}_0 \tag{19a}$$

$$= x_0'(I_\nu \otimes X_\alpha + (\mu\mu') \otimes (\bar{X} - X_\alpha))x_0, \tag{19b}$$

from which (17) follows immediately. □

REMARK 3.3—CONSTRAINING A PART OF $\bar{u}$
If $\bar{F} = F_\alpha$, then the Lyapunov equation (15) is solved by $\bar{X} = X_\alpha$ and (16) reduces to the decentralized control law solving the uncoordinated version of (7). In other words, the coordination constraint becomes void if it attempts to mimic the optimal unconstrained dynamics. Likewise, we

can constrain only a part of $\bar{u}$ by mimicking the optimal, with respect to (3), control trajectory of the partially constrained problem by its other part. Namely, let $E$ be a tall matrix such that $E'E = I$. It can be shown that the optimization of (7), with (7c) replaced by the partial constraint $E'\bar{u} - \bar{F}_1\bar{x} = 0$, corresponds to the original formulation with

$$\bar{F} = E\bar{F}_1 - (I - EE')B'X_2$$

where $X_2 \geq X_\alpha$ is the stabilizing solution of the ARE

$$(A+BE\bar{F}_1)'X_2+X_2(A+BE\bar{F}_1)+(Q_\alpha+\bar{F}_1'\bar{F}_1)-X_2B(I-EE')B'X_2 = 0$$

and the stabilizability of the pair $(A + BE\bar{F}_1, B(I - EE'))$ is required. Equation (15) is solved then by $\bar{X} = X_2$. □

## 3.3 Discussion

The remainder of this section is devoted to properties of the solution presented in Theorem 3.1. In particular, we discuss the structure of the optimal controller and its suitability for distributed control applications (§3.3), interpret the LQR problems in terms of the transformed variables (11) that arise as a technical step in the derivation of the solution (§3.3), quantify the effect of the coordination constraint (7c) on the performance of each subsystem (§3.3), and explore the possibility of adding tracking requirements to the behavior of the center of mass (§3.3).

***Control law: computation and structure*** An important property of the solution of Theorem 3.1 is its computational scalability. To calculate the optimal controller, we only need to solve ARE (14), which is the Riccati equation associated with the local, unconstrained, LQR. The *computational effort* to obtain the solution is thus independent of the number of subsystems $\nu$, which is an attractive property in the context of distributed control.

The low computational burden is not the only property of controller (16) that is appealing in distributed control applications. Its structure is even more intriguing. The optimal control law is a superposition of a local term, $F_\alpha x_i(t)$, and a (scaled) coordination term,

$$u_{\text{coord}}(t) := (\bar{F} - F_\alpha)\bar{x}(t). \tag{20}$$

The former is the optimal uncoordinated control law for $\Sigma_i$ and is fully decentralized. Coordination then adds a "correction" of the form $\mu_i u_{\text{coord}}$ to this local controller. This term destroys the (sparse) decentralized structure as none of the elements of the overall feedback gain (18) is zero in

general. Nonetheless, the resulting configuration might suit large-scale applications well.

The non-sparse coordination term, which may be thought of as a (block) rank-one correction to the (block) diagonal local controller (cf. (18)), depends only on the behavior of the center of mass. Thus, although this term hinges upon information about all subsystems, the only operation required in its construction is averaging. This information clustering may be thought of as a form of *spatial generalized sampling* where the information required to form the correction component, $u_{\text{coord}}$, is obtained by aggregating distributed information in a weighted average.

The information aggregation via $\bar{x}$ is clearly less demanding, from both computation and communication viewpoints, than an individual processing of each $x_i$. Hence, the control law (16), although centralized, may be feasible for distributed control. Measurements of the center of mass could, in principle, be done either globally, by a coordinator, or even locally, by each subsystem.

REMARK 3.4—AN INTERPRETATION OF THE COORDINATION POLICY
Constraint (7c) can be satisfied without information exchange if each subsystem applies $u_i = \bar{F}x_i$. The term $(\bar{F} - F_\alpha)x_i$ can then be interpreted as a desired violation of this strategy in order to improve the performance with respect to $\mathcal{J}_i$. By rewriting the coordination term (20) as

$$u_{\text{coord}}(t) = \sum_{i=1}^{\nu} \mu_i(\bar{F} - F_\alpha)x_i(t),$$

we see that exchanging information (coordination) allows the subsystems to compensate for each other's violations. □

REMARK 3.5—EARLIER APPEARANCE
The diagonal-plus-low-rank configuration was previously proposed in [Zečević and Šiljak, 2005], also in the context of control of large-scale systems. The motivation and technical tools used there, however, are quite different from those studied in this paper. The "low-rank centralized correction" to block-diagonal controllers is introduced in [Zečević and Šiljak, 2005] to enlarge the design parameter space in the context of robust control of interconnected systems. The parameters are then designed via an LMI procedure, which utilizes some of the degrees of freedom brought about by this addition. In our setup, the structure *results from* an optimization problem. Its low-rank part is responsible for coordinating otherwise uncoupled subsystems and has a clearly traceable effect on control performance (see below). □

***LQR problems in terms of*** $\tilde{x}_i$ ***and*** $\tilde{u}_i$ The transformation of state and input coordinates defined by (11) and (12) serves the purpose of decomposing the problem into one problem with a prespecified control law and and $\nu - 1$ unconstrained LQRs. These problems have meaningful interpretations.

First, a comparison of (13) and (7c) suggests that $\tilde{x}_1 = \bar{x}$ and $\tilde{u}_1 = \bar{u}$. This is indeed true, as can be seen through $\tilde{x}_1 = (e_1' \otimes I_n)\tilde{x} = ((e_1'U) \otimes I_n)x = (\mu' \otimes I_n)x = \bar{x}$, for instance. Thus, the constrained problem is concerned with the center of mass (4) and its solution results in the dynamics as in (6), as expected.

The other components of $\tilde{x}$ and $\tilde{u}$ do not possess such interpretations per se, they are not even unique. Nevertheless, the unconstrained LQR cost built on them,

$$\tilde{\mathcal{J}} := \sum_{i=2}^{\nu} \int_0^\infty \big(\tilde{x}_i'(t) Q_\alpha \tilde{x}_i(t) + \tilde{u}_i'(t)\tilde{u}_i(t)\big)\,\mathrm{d}t$$

(this is what the control law (16) actually minimizes), can be interpreted. To this end, rewrite

$$\sum_{i=2}^{\nu} \tilde{u}_i'\tilde{u}_i = \tilde{u}'((I - e_1e_1') \otimes I_m)\tilde{u} = u'((I_\nu - \mu\mu') \otimes I_m)u$$

(the last equality is obtained by (11) and (12)) and, likewise, $\sum_{i=2}^{\nu} \tilde{x}_i' Q_\alpha \tilde{x}_i = x'((I_\nu - \mu\mu') \otimes Q_\alpha)x$. It can be shown, by routine regrouping, that

$$I_\nu - \mu\mu' = \sum_{i=1}^{\nu} (e_i - \mu_i\mu)(e_i - \mu_i\mu)' \tag{21a}$$

$$= \sum_{i=1}^{\nu-1} \sum_{j=i+1}^{\nu} (\mu_j e_i - \mu_i e_j)(\mu_j e_i - \mu_i e_j)'. \tag{21b}$$

From (21a),

$$\tilde{\mathcal{J}} = \sum_{i=1}^{\nu} \Big( \Big\| Q_\alpha^{1/2}(x_i - \mu_i\bar{x}) \Big\|_2^2 + \|u_i - \mu_i\bar{u}\|_2^2 \Big).$$

In other words, $\tilde{\mathcal{J}}$ may be thought of as the cost of deviating from the normalized center of mass. The normalization becomes particularly transparent if all systems have equal masses, i.e., if $\mu_i = 1/\sqrt{\nu}$. In this case $\mu_i\bar{x} = \frac{1}{\nu}\sum_i x_i$ and $\mu_i\bar{u} = \frac{1}{\nu}\sum_i u_i$ are merely the average state and input

signals and $\tilde{\mathcal{J}}$ quantifies the cumulative deviation from the average. In the same vein, (21b) leads to

$$\tilde{\mathcal{J}} = \sum_{i=1}^{\nu-1} \sum_{j=i+1}^{\nu} \left( \left\| Q_\alpha^{1/2} (\mu_j x_i - \mu_i x_j) \right\|_2^2 + \|\mu_j u_i - \mu_i u_j\|_2^2 \right),$$

which penalizes mutual deviations of each subsystem from the others (the scaling factors $\mu_i$ and $\mu_j$ just align the subsystems to render the comparison meaningful), thus encouraging the achievement of an optimal *consensus*.

Summarizing, by solving (7) we effectively reach two goals: impose a required behavior on the center of mass and minimize discrepancy between subsystems. The optimal $\tilde{\mathcal{J}}$ can then be viewed as a measure of "gregariousness" or, perhaps, as a "herd instinct index" in the aggregate system (8). It follows from the proof of Theorem 3.1 (cf. (19a)) that

$$\begin{aligned} \tilde{\mathcal{J}}_{\text{opt}} &= \tilde{x}_0' \big( (I_\nu - e_1 e_1') \otimes X_\alpha \big) \tilde{x}_0 = x_0' \big( (I_\nu - \mu\mu') \otimes X_\alpha \big) x_0 \\ &= \sum_{i=1}^{\nu} \mathcal{J}_{i,\text{opt}} - \bar{x}_0' X_\alpha \bar{x}_0. \end{aligned} \tag{22}$$

Thus, the attainable local uncoordinated costs $\mathcal{J}_{i,\text{opt}}$ also determine the cumulative closeness of systems $\Sigma_i$ to each other. It is worth emphasizing that $\tilde{\mathcal{J}}_{\text{opt}}$ does not depend on the constraint imposed on the behavior of the center of mass. This separation is an intriguing property of the solution of (7).

***Cost of coordination per subsystem*** The last term in the right-hand side of (17) quantifies the deterioration of the (aggregate) performance $\mathcal{J}$ due to the coordination constraint (7c). Below, we look into the effect of coordination on the performance of individual subsystems.

We begin with the following result:

PROPOSITION 3.2
The value of the $i$th performance index $\mathcal{J}_i$ under the control law (16) is

$$\mathcal{J}_i = \mathcal{J}_{i,\text{opt}} + \mu_i^2 \bar{x}_0' (\bar{X} - X_\alpha) \bar{x}_0, \tag{23}$$

where $\bar{x}_0$ is the initial condition of the center of mass. □

***Proof*** The control law (16) is a superposition of the locally optimal control law and the signal $v_i = \mu_i (\bar{F} - F_\alpha) \bar{x}$. It is known (see the proof of [Zhou et al., 1995, Thm. 14.2]) that $\mathcal{J}_i = \mathcal{J}_{i,\text{opt}} + \|v_i\|_2^2$ for any $v_i$. As follows from

(6), the last term in the right-hand side above equals $\mu_i^2 \bar{x}_0' X_v \bar{x}_0$, where $X_v \geq 0$ solves the Lyapunov equation

$$(A + B\bar{F})' X_v + X_v (A + B\bar{F}) + (\bar{F} - F_\alpha)'(\bar{F} - F_\alpha) = 0.$$

Expression (23) then follows by the fact that $X_v = \bar{X} - X_\alpha$, which can be verified by straightforward algebra. □

The second term in the right-hand side of (23) is exactly the cost of coordination for the $i$th subsystem. It is a function of the other subsystems through the vector $\bar{x}_0$. The dependence of $\bar{x}_0$ on an unspecified relation between the initial states of all subsystems complicates the interpretation of the cost of coordination. If, for instance, $\bar{x}_0 = 0$, then $\mathcal{J}_i = \mathcal{J}_{i,\text{opt}}$ and the coordination in that case comes at no cost. But if every $x_{i0} = \mu_i \chi$ for some $\chi \in \mathbb{R}^n$, then $\bar{x}_0 = \chi$ and we end up with $\mathcal{J}_i = x_{i0}' \bar{X} x_{i0}$. This is what we would have if the control laws $u_i = \bar{F} x_i$ were applied to each subsystem, which would correspond to an attempt to enforce (7c) without communication between subsystems. To avoid the dependence on $\bar{x}_0$, we assume through the rest of this subsection that $\bar{x}_0$ is bounded as a function of the number of subsystems $v$. In this case the term $\bar{x}_0'(\bar{X} - X_\alpha)\bar{x}_0$ is bounded as well and the cost of coordination becomes quadratically proportional to the corresponding "mass" $\mu_i$.

Consider now what happens with the cost of coordination per subsystem when the number of subsystems $v \to \infty$. It follows from the normalization assumption $\sum_{i=1}^{v} \mu_i^2 = 1$ that at most a finite number subsystems may have $\mu_i \not\to 0$ in this case. If such subsystems do exist, they dominate (5) and we then effectively have coordination between a finite number of subsystems. It is then natural that the cost of coordination for those subsystems does not vanish as $v$ grows. If, however, all $\mu_i \to 0$ as $v \to \infty$, the situation is different. In this case the coordination constraint (7c) is, in a sense, spread among all subsystems and the cost of coordination per subsystem vanishes with the increase of $v$. For example, if we assign equal weights to each subsystem, i.e., if every $\mu_i = 1/\sqrt{v}$, then the coordination toll per subsystem decreases inversely proportional to the number of subsystems. The decrease of the coordination cost is intuitive, as the addition of more subsystems brings more opportunities for coordination.

***Tracking*** Constraint (7c) can be modified to incorporate tracking requirements on the center of mass (4). For example, we may consider the constraint

$$\bar{u} = \bar{F}\bar{x} + r$$

for an exogenous signal $r$ (e.g., it may be a function of a reference signal). This would yield the control law

$$u_i(t) = F_\alpha x_i(t) + \mu_i(\bar{F} - F_\alpha)\bar{x}(t) + \mu_i r(t),$$

instead of (16) and the following dynamics of $\bar{\Sigma}$:

$$\dot{\bar{x}}(t) = (A + B\bar{F})\,\bar{x}(t) + Br(t)$$

in lieu of (6). A group tracking animation illustrating this possibility can be seen in [Madjidian and Mirkin, 2013, Fig. 2]. $\mathcal{J}$ is then no longer relevant per se, it might even be unbounded. Still, the "measure of gregariousness" interpretation of the unconstrained part of the optimization, as discussed in §3.3, remains valid. Moreover, the value of the cost function in (22) is finite and independent of $r$, so it can quantify group tracking properties of the system.

## 3.4 Wind farm example (cont'd)

We are now in the position to return to the example studied in Section 2. To render the current LQR problem formulations compatible with that in §2.1, we assume that $x_{i0} = B_w v_i$, where $v_i$ are mutually independent random variables of unit variance. This yields $\bar{x}_0 = B_w\bar{v}$, where $\bar{v} := \sum_i \mu_i v_i$ is of unit variance as well. We then end up with (7) with $B = B_u$, $Q_\alpha = C_z'C_z$, $\bar{F} = 0$, and $\mu_i = 1/\sqrt{\nu}$ for all $i$.

By Theorem 3.1, the optimal control law is given by

$$u_i = F_\alpha x_i - F_\alpha x_\mathrm{a},$$

where $x_\mathrm{a} := \frac{1}{\nu}\sum_i x_i$ is the average state of wind turbines and the gain $F_\alpha$ is obtained by solving ARE (14). To calculate the cost of coordination depicted in Fig. 1 by the solid line, we use Proposition 3.2 to derive $\mathcal{J}_i - \mathcal{J}_{i,\mathrm{opt}} = \frac{1}{\nu}B_w'(\bar{X} - X_\alpha)B_w$, where $\bar{X}$ is the observability Gramian of $(C_z, A)$. This cost tends to zeros as $\nu \to \infty$.

With its structural properties revealed, the non-sparse solution to (7) compares favorably with the sparsity-based one considered in §2.2. Our calculations are scalable, in fact, they are independent of the number of turbines. The result is always globally optimal. The effect of the coordination constraint on the local performance of each turbine is transparent and easy to calculate as well. The price we pay is that the resulting controller is centralized. This might not be feasible in some situations where communication constraints are restrictive. Still, the only centralized information processing that is required to execute the control law is the averaging operation to calculate $F_\alpha x_\mathrm{a}$. This does not require an individual processing of the global state of the whole farm by each turbine. It thus could be feasible even for a large farm.

## 4. Alleviating the Burden of Coordination

In some situations, it might not be necessary to enforce the coordination requirement as a hard constraint. For instance, in the example in §2.1 some fluctuations in wind farm power production might be tolerated, at least at higher frequencies. Constraint (7c) can then be relaxed to improve the local performance of each subsystem. In this section, we consider an alternative problem formulation, where we seek a trade-off between improving the performance of each subsystem and coordinating their behavior.

### 4.1 Soft constraint formulation

Coordination requirements may be taken into account via soft constraints. The minimization of (7a) under constraint (7c) may be substituted with

$$\text{minimize} \quad \mathcal{J} = \sum_{i=1}^{\nu} \mathcal{J}_i + \frac{\lambda}{1-\lambda} \left\| \bar{u} - \bar{F}\bar{x} \right\|_2^2 \tag{24a}$$

$$\text{subject to} \quad \Sigma_i, \quad i = 1, \ldots, \nu \tag{24b}$$

for some $\lambda \in [0, 1]$ and no constraints imposed on the behavior of the center of mass. The case $\lambda = 1$ corresponds to the hard constraint formulation. Picking $\lambda < 1$ would mean that the coordination requirement is displaced with a coordination incentive. A satisfactory trade-off between local objectives and coordination can then be reached via tuning $\lambda$.

The arguments of §3.2 apply to (24) mutatis mutandis[3], splitting the minimization of the coupled $\mathcal{J}$ into $\nu$ uncoupled problems. As in the hard constraint case, $\nu - 1$ of them are unconstrained LQR problems in terms of $\tilde{x}_i$ and $\tilde{u}_i$, $i = 2, \ldots, \nu$. The remaining problem, the one formulated in terms of $\tilde{x}_1 = \bar{x}$ and $\tilde{u}_1 = \bar{u}$, is now the LQR problem for (4) and the performance index

$$\int_0^\infty \begin{bmatrix} \bar{x}' & \bar{u}' \end{bmatrix} \begin{bmatrix} Q_\alpha + \dfrac{\lambda}{1-\lambda}\bar{F}'\bar{F} & -\dfrac{\lambda}{1-\lambda}\bar{F}' \\ -\dfrac{\lambda}{1-\lambda}\bar{F} & \dfrac{1}{1-\lambda} I_m \end{bmatrix} \begin{bmatrix} \bar{x} \\ \bar{u} \end{bmatrix} \mathrm{d}t.$$

The resulting control law for the center of mass is:

$$\bar{u}(t) = (\lambda\bar{F} - (1-\lambda)B'X_\lambda)\,\bar{x}(t), \tag{25}$$

where $X_\lambda \geq 0$ is the stabilizing solution of the ARE

$$(A + \lambda B\bar{F})'X_\lambda + X_\lambda(A + \lambda B\bar{F}) + Q_\alpha + \lambda\bar{F}'\bar{F} - (1-\lambda)X_\lambda BB'X_\lambda = 0. \tag{26}$$

[3] Theorem 4.2 in §4.2 presents a formal proof of a more general problem.

The overall controller is then in the same "diagonal plus rank-one" form (16), modulo replacing $\bar{F}$ with $\lambda\bar{F} - (1-\lambda)B'X_\lambda$.

REMARK 4.1
The soft constraint formulation could, in principle, be viewed as a special case of (7). Indeed, the solution of Theorem 3.1 is recovered via the mere substitution $\bar{F} \to \lambda\bar{F} - (1-\lambda)B'X_\lambda$. Thus, formulation (24) brings no extra freedom to the design. Rather, we view it as a convenient means to trade off local and global goals. Moreover, the soft constraint formulation prompts extensions that are not covered by (7). One such extension will be considered in Section 4.2. □

The following proposition quantifies the trade-off between coordination and the local performance for the $i$th subsystem.

PROPOSITION 4.1
The stabilizing solution $X_\lambda$ of (26) satisfies $X_\alpha \leq X_\lambda \leq \bar{X}$ and $Y_\lambda := \frac{\mathrm{d}}{\mathrm{d}\lambda}X_\lambda \geq 0$. Furthermore, the optimal solution of (24) renders

$$\mathcal{J}_i = \mathcal{J}_{i,\mathrm{opt}} + \mu_i^2\,\bar{x}_0'(X_\lambda - \lambda(1-\lambda)Y_\lambda - X_\alpha)\bar{x}_0,$$

which never exceeds the quantity in Proposition 3.2, and

$$\sigma(\lambda) := \left\|\bar{u} - \bar{F}\bar{x}\right\|_2^2 = (1-\lambda)^2\,\bar{x}_0'Y_\lambda\bar{x}_0. \qquad \square$$

***Proof*** It can be shown, by differentiating (26) and rearranging terms, that $Y_\lambda$ satisfies the Lyapunov equation

$$A_\lambda'Y_\lambda + Y_\lambda A_\lambda + (\bar{F} + B'X_\lambda)'(\bar{F} + B'X_\lambda) = 0, \tag{27}$$

where $A_\lambda := A + B(\lambda\bar{F} - (1-\lambda)B'X_\lambda)$ is Hurwitz. This proves that $Y_\lambda \geq 0$. The first claim of the proposition then follows by the facts that $X_\alpha = X_\lambda|_{\lambda=0}$ and $\bar{X} = X_\lambda|_{\lambda=1}$.

The expression for $\mathcal{J}_i$ results from Proposition 3.2 by replacing $\bar{F} \to \lambda\bar{F} - (1-\lambda)B'X_\lambda$ (cf. Remark 4.1) and using the fact that under this choice $\bar{X} \to X_\lambda - \lambda(1-\lambda)Y_\lambda$ (can be verified by straightforward, albeit lengthy, algebra).

Finally, the control law (25) violates constraint (7c) by

$$\bar{u}(t) - \bar{F}\bar{x}(t) = -(1-\lambda)(\bar{F} + B'X_\lambda)\bar{x}(t) = -(1-\lambda)(\bar{F} + B'X_\lambda)e^{A_\lambda t}\bar{x}_0.$$

The expression for the norm of the constraint violation then follows by (27). □

Comparing the expressions for $\mathcal{J}_i$ given in Propositions 3.2 and 4.1, we can see that by relaxing the coordination constraint we reduce the cost of coordination for the $i$th subsystem by

$$\alpha_i(\lambda) := \mu_i^2 \bar{x}_0'(\bar{X} - X_\lambda + \lambda(1-\lambda)Y_\lambda)\bar{x}_0 \geq 0.$$

In fact, it can be shown that $\alpha_i(\lambda) = 0$ iff the cost of coordination in the original formulation $\mu_i^2 \bar{x}_0'(\bar{X} - X_\alpha)\bar{x}_0 = 0$ as well. In other words, whenever the coordination constraint (7c) does not come for free, formulation (24) alleviates its burden. Furthermore, it is readily seen that

$$\dot{\alpha}_i(\lambda) = \mu_i^2 \, \lambda \, \bar{x}_0' Z_\lambda \bar{x}_0 \quad \text{and} \quad \dot{\sigma}(\lambda) = (1-\lambda)\, \bar{x}_0' Z_\lambda \bar{x}_0,$$

where $Z_\lambda := (1-\lambda)\, \frac{\mathrm{d}}{\mathrm{d}\lambda} Y_\lambda - 2Y_\lambda \leq 0$ verifies

$$A_\lambda' Z_\lambda + Z_\lambda A_\lambda - 2(\bar{F} + B'X_\lambda - (1-\lambda)B'Y_\lambda)'(\bar{F} + B'X_\lambda - (1-\lambda)B'Y_\lambda) = 0$$

and is uniformly bounded as a function of $\lambda$. Hence, we have that $\lim_{\lambda \to 1} \dot{\sigma}(\lambda) = 0$, whereas, in general, $\lim_{\lambda \to 1} \dot{\alpha}_i(\lambda) \neq 0$.

Thus, we may expect that a relatively small deviation from the ideal behavior of the center of mass may result in a relatively large reduction in the cost of coordination for the subsystems. As a matter of fact, at the other end of the range, at $\lambda = 0$, the picture is mirrored. Thus, by adding a slight coordination penalty to the global cost function $\sum_i \mathcal{J}_i$ we can introduce coordination with little effect on local performances.

## 4.2 Frequency weighted soft constraints

In many situations, we might not be interested in coordinating the center of mass over all possible situation in local subsystems. For example, we can persuade coordination only in a low frequency range. This may be useful in applications where the required group behavior (e.g., power production of a wind power plant discussed in Section 2) is slower than that of individual subsystems (e.g., dynamics of a wind turbine). Such situations can be accommodated by replacing the second term in the right-hand side of (24a) with the $L^2$ norm of the signal $z_\sigma$, satisfying

$$\begin{cases} \dot{x}_\phi(t) = A_\phi x_\phi(t) + B_\phi(\bar{u}(t) - \bar{F}\bar{x}(t)), \quad x_\phi(0) = 0 \\ z_\sigma(t) = C_\phi x_\phi(t) + D_\phi(\bar{u}(t) - \bar{F}\bar{x}(t)). \end{cases}$$

Thus, $z_\sigma$ is the signal $\bar{u} - \bar{F}\bar{x}$ filtered by

$$W_\phi(s) = D_\phi + C_\phi(sI - A_\phi)^{-1}B_\phi.$$

(without loss of generality we may assume that the realization of $W_\phi$ is minimal). This leads to the following problem:

$$\text{minimize} \quad \mathcal{J} := \sum_{i=1}^{\nu} \mathcal{J}_i + \|z_\sigma\|_2^2 \tag{28a}$$

$$\text{subject to} \quad \Sigma_i, \quad i = 1, \ldots, \nu \tag{28b}$$

The weighing filter $W_\phi$ aims at shaping the coordination penalty over different frequencies. Moreover, by choosing $W_\phi(s)$ with pure imaginary poles we can enforce hard coordination constraints at some frequencies.

To formulate the solution to (28) we need the ARE

$$A_\sigma' X_\sigma + X_\sigma A_\sigma + C_\sigma' C_\sigma - (X_\sigma B_\sigma + C_\sigma' D_\sigma)(D_\sigma' D_\sigma)^{-1}(B_\sigma' X_\sigma + D_\sigma' C_\sigma) = 0, \tag{29}$$

where

$$\left[\begin{array}{c|c} A_\sigma & B_\sigma \\ \hline C_\sigma & D_\sigma \end{array}\right] := \left[\begin{array}{cc|c} A_\phi & -B_\phi \bar{F} & B_\phi \\ 0 & A & B \\ \hline C_\phi & -D_\phi \bar{F} & D_\phi \\ 0 & Q_\alpha^{1/2} & 0 \\ 0 & 0 & I \end{array}\right],$$

and the associated feedback gain

$$F_\sigma = \left[\begin{array}{cc} F_{\sigma 1} & F_{\sigma 2} \end{array}\right] := -(D_\sigma' D_\sigma)^{-1}(B_\sigma' X_\sigma + D_\sigma' C_\sigma),$$

partitioned compatibly. The following theorem is the main result of this subsection:

THEOREM 4.2
Let $A + B\bar{F}$ be Hurwitz and $(Q_\alpha, A)$ have no unobservable pure imaginary modes. Then (29) has a stabilizing solution $X_\sigma \geq 0$ such that its $(2,2)$ block, partitioned compatibly with the partition of $A_\sigma$, satisfies $\bar{X} \geq X_{\sigma 22} \geq X_\alpha$, and the control law solving (28) is

$$u_i(t) = F_\alpha x_i(t) + \mu_i(\bar{F} - F_\alpha)\bar{x}(t) + \mu_i \bar{u}_\phi(t), \tag{30}$$

where $\bar{u}_\phi := M_\phi(F_{\sigma 2} - \bar{F})\bar{x}$ and

$$M_\phi(s) := I + F_{\sigma 1}(sI - A_\phi - B_\phi F_{\sigma 1})^{-1} B_\phi. \qquad \square$$

***Proof*** To shorten the exposition, we assume through the proof that $D_\phi = 0$, the general case follows by similar steps.

Following the arguments of §3.2, we rewrite the problem in terms of the aggregate variables $x$ and $u$. The dynamics of the aggregate system are now coupled,

$$\begin{bmatrix} \dot{x}_\phi \\ \dot{x} \end{bmatrix} = \begin{bmatrix} A_\phi & \mu' \otimes (-B_\phi \bar{F}) \\ 0 & I_\nu \otimes A \end{bmatrix} \begin{bmatrix} x_\phi \\ x \end{bmatrix} + \begin{bmatrix} \mu' \otimes B_\phi \\ I_\nu \otimes B \end{bmatrix} u,$$

and the cost function is uncoupled (not if $D_\phi \neq 0$):

$$\mathcal{J} = \int_0^\infty \big(x_\phi' C_\phi' C_\phi x_\phi + x'(I_n \otimes Q_\alpha)x + u'u\big)\mathrm{d}t.$$

The dynamics of the plant can still be decoupled via transformation (11) with $U$ satisfying (12). It is readily verifiable that the transformed dynamics are now

$$\begin{bmatrix} \dot{x}_\phi \\ \dot{\tilde{x}} \end{bmatrix} = \begin{bmatrix} A_\phi & e_1' \otimes (-B_\phi \bar{F}) \\ 0 & I_\nu \otimes A \end{bmatrix} \begin{bmatrix} x_\phi \\ \tilde{x} \end{bmatrix} + \begin{bmatrix} e_1' \otimes B_\phi \\ I_\nu \otimes B \end{bmatrix} \tilde{u}$$

and the weights matrices of the criterion remain unchanged. Thus, we again end up with $\nu$ separate problems. The last $\nu - 1$ of them are exactly the same problems in terms of $\tilde{x}_i$ and $\tilde{u}_i$ for $i = 2, \ldots, \nu$ as in the case studied in Section 3. The first one is the LQR problem for the plant

$$\dot{x}_\sigma = A_\sigma x_\sigma + B_\sigma \tilde{u}_1, \quad \text{where } x_\sigma := \begin{bmatrix} x_\phi \\ \tilde{x}_1 \end{bmatrix}$$

and the cost function $\tilde{\mathcal{J}}_1 = \|C_\sigma x_\sigma + D_\sigma \tilde{u}_1\|_2^2$. This problem is well defined. Indeed, *(i)* the pair $(A_\sigma, B_\sigma)$ is stabilizable by the controllability of $(A_\phi, B_\phi)$ and the first assumption of the theorem ($A_\sigma + B_\sigma \begin{bmatrix} F_\phi & \bar{F} \end{bmatrix}$ is Hurwitz iff $A_\phi + B_\phi F_\phi$ is Hurwitz); *(ii)* the observability of $(C_\sigma, A_\sigma)$ and the second assumption guarantee that the realization $D_\sigma + C_\sigma(sI - A_\sigma)^{-1}B_\sigma$ has no imaginary axis invariant zeros. The optimal solution of the LQR above is then the static state feedback

$$\tilde{u}_1 = F_\sigma x_\sigma = F_{\sigma 1} x_\phi + F_{\sigma 2} \tilde{x}_1,$$

where $F_\sigma$ is generated by the stabilizing solution of (29). Because $\tilde{x}_1 = \bar{x}$, $\tilde{u}_1 = \bar{u}$, and $x_\phi = (sI - A_\phi)^{-1}B_\phi(\bar{u} - \bar{F}\bar{x})$, the state feedback above can be expressed as follows:

$$\tilde{u}_1 = \big(\bar{F} + M_\phi(s)(F_{\sigma 2} - \bar{F})\big)\tilde{x}_1.$$

The control law (30) in the original coordinates follows then by repeating the steps of the proof of Theorem 3.1. □

Comparing (30) and (16), the effect of replacing the hard constraint (7c) with filtered soft constraints amounts to adding the signal $\bar{u}_\phi$ to the control law. Because the zeros of $M_\phi(s)$ are exactly the poles of $W_\phi(s)$, the spectrum of $\bar{u}_\phi$ vanishes at the frequencies where the weight goes to infinity (the imaginary poles of $W_\phi(s)$), recovering the hard constraint case. This shows that we can indeed enforce hard coordination constraints at certain frequencies via weighs with j$\omega$ poles.

The expressions for the coordination mismatch and the local costs of coordination are not as transparent as those analyzed in the previous subsection. Namely,

$$\mathcal{J}_i = \mathcal{J}_{i,\mathrm{opt}} + \mu_i^2 \bar{x}_0' X_{v22} \bar{x}_0,$$

where $X_{v22} \leq \bar{X} - X_\alpha$ is the $(2,2)$-subblock of $X_v$ solving

$$(A_\sigma + B_\sigma F_\sigma)' X_v + X_v (A_\sigma + B_\sigma F_\sigma) + (F_\sigma - F_\alpha E_2')'(F_\sigma - F_\alpha E_2') = 0.$$

These formulae can be derived in line with the proof of Proposition 3.2, see [Madjidian and Mirkin, 2013] for details.

## 4.3 Wind farm example (cont'd)

From a load balancing perspective, it is the slow variations in power mismatch that are troublesome, whereas the fast ones are considered relatively benign. To account for this, we consider an alternative formulation, where the power tracking requirement is relaxed at high frequencies. This is achieved via the formulation (28) with $B = B_u$, $Q_\alpha = C_z' C_z$, $\bar{F} = 0$, $\mu_i = 1/\sqrt{\nu}$, and

$$W_\phi(s) = \frac{\sqrt{\lambda/(1-\lambda)}}{s} \tag{31}$$

for $\lambda \in [0,1]$. The integrator in $W_\phi$ guarantees zero net DC-power deviation. Indeed, by Theorem 4.2 the solution is

$$u_i = F_\alpha x_i - F_\alpha x_\mathrm{a} + u_\mathrm{a},$$

where $x_\mathrm{a}$ is the average state (as in §3.4), $u_\mathrm{a} = M_\phi F_{\sigma 2} x_\mathrm{a}$, and the filter

$$M_\phi(s) = \frac{s}{s + \omega_\sigma}$$

where $\omega_\sigma = -F_{\sigma 1}$. The high-pass form of $M_\phi$ ensures that the spectrum of $u_\mathrm{a}$ vanishes at the zero frequency. Since $u_\mathrm{a}$ corresponds to the contribution of an average WT to the net power deviation, zero net power deviation is enforced at DC.

The solid line in Fig. 2 shows the trade-off between the cost of coordination per an individual turbine and $\|u_\mathrm{a}\|_2^2$. The results show that a small relaxation of the power tracking requirement results in a relatively

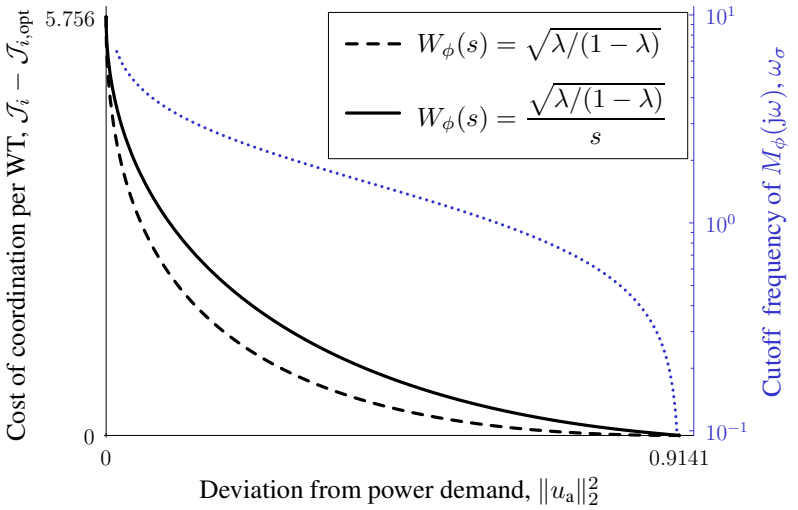


**Figure 2.** Trade-off curves for local and coordination performances with $W_\phi = \sqrt{\lambda/(1-\lambda)}$ (dashed line) and $W_\phi = \sqrt{\lambda/(1-\lambda)}/s$ (solid line). The dotted blue line shows the cutoff frequency $\omega_\sigma$ of the filter $M_\phi$.

large improvement in individual WT performance. For comparison, we also present the trade-off curve for the formulation considered in §4.1 (the dashed line). This formulation corresponds to the static $W_\phi = \sqrt{\lambda/(1-\lambda)}$ in (28). We can see that the use of the static $W_\phi$ yields better coordination performance $\|u_a\|_2$ for every level of deterioration of the local performances. This, however, may be expected, because the weight (31) effectively imposes hard constraints at the zero frequency for every $\lambda \neq 0$.

The dotted blue curve in Fig. 2 presents the cutoff frequency $\omega_\sigma$ of $M_\phi(j\omega)$. As the individual turbine performance improves, $\omega_\sigma$ decreases, which implies that less of the slow variations are removed from the net power deviation.

## 5. Concluding Remarks

In this paper we have studied a class of LQR problems, where autonomous agents with identical dynamics seek to reduce their own costs while coordinating their center of mass (average behavior). We have shown that the solution to these problems has two important *scalable* properties. First, the problem decomposes into two independent LQR problems: one for a single uncoordinated agent and one for the center of mass, whose dynamics has the same dimension as those of individual agents. Hence, the

computational effort required to obtain the solution is independent of the number of agents (since all agents are assumed to be identical, only one unconstrained LQR problems needs to be solved). Second, the structure of the resulting controller is transparent, comprising a (block) diagonal decentralized part and a (block) rank-one coordination term. The coordination term relies on information about all subsystems, but only requires a simple averaging operation. This renders the structure well suited for implementation in distributed control applications.

We have also revealed several other properties of the optimal solution. In particular, the cost of coordination incurred by each subsystem has been quantified and shown to vanish as the number of subsystems grows; the coordination problem has been interpreted in terms of a consensus-like cost function; the cost of the cumulative deviation of subsystems from the center of mass has shown to be independent of the behavior of the center of mass itself. We have also considered imposing coordination via soft constraints and quantified the trade-off between local and coordination performances in this case.

Although we have studied only the specific LQR problem, the diagonal-plus-low-rank structure may show up in a wider spectrum of applications. Relatively straightforward extensions include problems with $r$ coordination constraints (would result in a diagonal-plus-rank-$r$ configuration) and output-feedback $H^2$ formulations (adding local estimators). Other directions may be less trivial. For instance, it may be important to account for additional constraints on the information exchange between agents, like delays or a sampled-data structure. Another possible direction that might require a substantial alternation of the solution procedure is to consider coordination among heterogeneous agents. Furthermore, it is interesting to investigate the possibility of reducing information processing / complexity by imposing the diagonal-plus-low-rank structure in problems, where it does not arise as an outcome of the unconstrained optimization procedue.

Finally, up to this point we managed to discuss distributed control without mentioning the word “graph.”

## Acknowledgments

This work was supported by the Swedish Research Council through the LCCC Linnaeus Center and by the European commission through the project AEOLUS.

## References

Araki, M. (1993). "Recent developments in digital control theory". In: *Proceedings of the 12th IFAC World Congress*, pp. 251–260.

Biegel, B., D. Madjidian, V. Spudić, A. Rantzer, and J. Stoustrup (2013). "Distributed low-complexity controller for wind power plant in derated operation". In: *Proceedings of the 2013 IEEE Multi-Conference on Systems and Control*. Hyderabad, India, pp. 146–151.

Grunnet, J., M. Soltani, T. Knudsen, M. Kragelund, and T. Bak (2010). "Aeolus toolbox for dynamic wind farm modeling, simulation and control". In: *Proceedings of the 2010 European Wind Energy Conference*, pp. 3119–3129.

Jonkman, J., S. Butterfield, W. Musial, and G. Scott (2009). *Definition of a 5-MW Reference Wind Turbine for Offshore System Development*. Tech. rep. NREL/TP-500-38060. National Renewable Energy Laboratory, Golden, CO.

Kristalny, M., D. Madjidian, and T. Knudsen (2013). "On using wind speed preview to reduce wind turbine tower oscillations". *IEEE Transactions on Control Systems Technology* **21**:4, pp. 1191–1198.

Lessard, L. and S. Lall (2012). "Optimal controller synthesis for the decentralized two-player problem with output feedback". In: *Proceedings of the 2012 American Control Conference*. Montréal, Canada, pp. 6314–6321.

Madjidian, D. and L. Mirkin (2013). "Distributed control with low-rank coordination". URL: `http://arxiv.org/abs/1310.1025`.

Mahajan, A., N. C. Martins, M. C. Rotkowitz, and S. Yüksel (2012). "Information structures in optimal decentralized control". In: *Proceedings of the 51st IEEE Conference on Decision and Control*. Maui, HW, pp. 1291–1306.

Mårtensson, K. and A. Rantzer (2012). "A scalable method for continuous-time distributed control synthesis". In: *Proceedings of the 2012 American Control Conference*. Montreal, QC, pp. 6308–6313.

Mesarović, M. D., D. Macko, and Y. Takahara (1970). *Theory of Hierarchical, Multilevel Systems*. Academic Press, NY.

Pao, L. and K. Johnson (2011). "Control of wind turbines". *IEEE Control Systems Magazine* **31**:2, pp. 42–62.

Rantzer, A. (2011). "Distributed control of positive systems". In: *Proceedings of the 50th IEEE Conference on Decision and Control*. Orlando, FL, pp. 6608–6611.

Rotkowitz, M. and S. Lall (2006). "A characterization of convex problems in decentralized control". *IEEE Transactions on Automatic Control* **51**:2, pp. 274–286.

Šiljak, D. D. (1978). *Large-Scale Dynamic Systems: Stability and Structure*. North-Holland, NY.

Singh, M. G. and A. Titli, (Eds.) (1978). *Systems: Decomposition, Optimization and Control*. Pergamon Press, Oxford, UK.

Spudić, V., M. Jelavić, and M. Baotić (2011). "Wind turbine power references in coordinated control of wind farms". *Automatika – Journal of Control, Measurements, Electronics, Computing and Communications.* **52**:2, pp. 82–94.

Tanaka, T. and C. Langbort (2011). "The bounded real lemma for internally positive systems and $H^\infty$ structured static state feedback". *IEEE Transactions on Automatic Control* **56**:9, pp. 2218–2223.

Tsitsiklis, J. N. and M. Athans (1985). "On the complexity of decentralized decision making and detection problems". *IEEE Transactions on Automatic Control* **30**:5, pp. 440–446.

Vigueras-Rodríguez, A., P. Sørensen, A. Viedma, M. Donovan, and E. Gómez Lázaro (2012). "Spectral coherence model for power fluctuations in a wind farm". *Journal of Wind Engineering and Industrial Aerodynamics* **102**, pp. 14 –21.

Wistenhausen, H. S. (1968). "A counterexample in stochastic optimum control". *SIAM Journal on Control* **6**:1, pp. 131–147.

Xiao, L. and S. Boyd (2004). "Fast linear iterations for distributed averaging". *System and Control Letters* **53**:1, pp. 65–78.

Zečević, A. and D. Šiljak (2005). "Global low-rank enhancement of decentralized control for large-scale systems". *IEEE Transactions on Automatic Control* **50**:5, pp. 740–744.

Zečević, A. and D. Šiljak (2010). *Control of Complex Systems: Structural Constraints and Uncertainty*. Springer-Verlag, New York, NY.

Zhou, K., J. C. Doyle, and K. Glover (1995). *Robust and Optimal Control*. Prentice-Hall, Englewood Cliffs, NJ.

# Paper III

# Optimal Coordination of Homogeneous Agents Subject to Delayed Information Exchange

**Daria Madjidian  Leonid Mirkin**

**Abstract**

We consider a class of large scale linear-quadratic coordination problems where the information exchange is subject to a time-delay. We show that several previously known properties of the optimal solution to the delay-free problem extend to this case. In particular, the optimal control law comprises a diagonal (decentralized) term complemented by a rank-one coordination term, which can be implemented by a simple averaging operation. Moreover, the computational effort required to obtain the controller is independent of the number of subsystems.

Submitted to the *2014 IEEE Conference on Decision and Control*.

## 1. Introduction

Control of large scale systems has been an established area of research for more than half a century and has received renewed attention over the last two decades. These systems are characterized by a very large number of interconnected subsystems, each with their own sensors and actuators. In such situations, fully centralized, structureless information processing becomes infeasible.

A common approach to limiting the amount of information processing in the controller, is to impose a sparsity pattern on the controller structure, where nonzero elements correspond to permitted information exchange between subsystems [Šiljak, 1978; Shah and Parrilo, 2013; Mahajan et al., 2012]. However, the design of these type of structured controllers is generally a notoriously difficult problem [Wistenhausen, 1968; Tsitsiklis and Athans, 1985]. In the control community, considerable effort has been devoted to understanding the nature of these difficulties and devise tools to address them. See [Rotkowitz and Lall, 2006; Rantzer, 2012; Zečević and Šiljak, 2010] and references therein.

Although sparse information structures appear naturally in several applications, e.g. control of electrical power systems and vehicle platoons [Andreasson et al., 13; Lin et al., 2012], alternative control structures might be better suited for other applications. One example of a non-sparse, yet scalable controller is the diagonal-plus-low rank configuration proposed in [Zečević and Šiljak, 2005]. This type of controller comprises a block-diagonal term, which is completely decentralized, complemented by a low-rank component that can be implemented by a few averaging operations ($r$ averaging operations for a rank-$r$ term). Recently, we showed that this type of control structure appears naturally (i.e. without being imposed) as the optimal solution to a class of large-scale linear-quadratic coordination problems [Madjidian and Mirkin, 2014]. More specifically, we studied a homogeneous group of autonomous agents that are coupled through a constraint on their average state. It was shown that the optimal *centralized* solution has the diagonal-plus-rank-one form shown in Figure 1. Although the rank-one term depends on information from all systems, the only centralized computation required to implement it is a single averaging operation, which scales well as the number of agents grows large. We also showed that the solution has an additional attractive property in terms of large scale applications: the computational effort required to obtain the solution is independent of the number of agents.

A potential limitation of the solution derived in [Madjidian and Mirkin, 2014] is that it assumes immediate information exchange between the agents. This might not be feasible in some applications due to communication constraints. In this paper, we show that the properties of the

optimal control law discussed above for the delay-free case, extend to the case with delayed information exchange. Moreover, we derive analytic expressions that quantify the performance deterioration due to the delay. An important implication of our result is that it adds insight into the class of diagonal plus low-rank controllers by enlarging the class of known problems for which they are optimal.

**Notation** The transpose of a matrix $M$ is denoted by $M'$. By $e_i$ we refer to the $i$th standard basis of a Euclidean space and by $I_n$ to the $n \times n$ identity matrix (we drop the dimension subscript when the context is clear). The $L^2(\mathrm{j}\mathbb{R})$ norm [Zhou et al., 1995, Ch. 4] of a system $G$ is denoted $\|G\|_2$. The notation $\otimes$ stands for the Kronecker product of matrices:

$$A \otimes B := \begin{bmatrix} a_{11}B & \cdots & a_{1m}B \\ \vdots & \ddots & \vdots \\ a_{p1}B & \cdots & a_{pm}B \end{bmatrix}.$$

## 2. Preliminaries

In this section we review the main results of [Madjidian and Mirkin, 2014], where we considered a coordination problem among $\nu$ uncoupled homogeneous systems

$$\Sigma_i : \dot{x}_i(t) = Ax_i(t) + B_u u_i(t), \quad x_i(0) = x_{i0}$$

where $x_i(t) \in \mathbb{R}^n$ can be measured and $u_i(t) \in \mathbb{R}^m$. Associated with each system is the cost function

$$\mathcal{J}_i = \int_0^\infty \big(x_i'(t)Q_\alpha x_i(t) + u_i'(t)u_i(t)\big)\,\mathrm{d}t.$$

The systems $\Sigma_i$ are coupled through a constraint on the dynamics of their *center of mass*, which is defined as the system

$$\bar{\Sigma} : \dot{\bar{x}}(t) = A\bar{x}(t) + B_u\bar{u}(t), \quad \bar{x}(0) = \bar{x}_0$$

where

$$\bar{u}(t) := \sum_{i=1}^{\nu} \mu_i u_i(t) \quad \text{and} \quad \bar{x}(t) := \sum_{i=1}^{\nu} \mu_i x_i(t), \tag{1}$$

and where the weights $\mu_i \neq 0$ may be thought of as the masses of each subsystem. The coupling constraint is given by

$$\bar{u} - \bar{F}\bar{x} = 0,$$

where $\bar{F}$ can be though of as a feedback gain that shapes the dynamics of the center of mass $\bar{\Sigma}$ into

$$\dot{\bar{x}}(t) = (A + B_u \bar{F})\bar{x}(t), \quad \bar{x}(0) = \bar{x}_0.$$

The problem formulation in [Madjidian and Mirkin, 2014] is

$$\begin{aligned} \text{minimize} \quad & \mathcal{J} := \sum_{i=1}^{\nu} \mathcal{J}_i && \text{(2a)} \\ \text{subject to} \quad & \Sigma_i \text{ in (4)}, \quad i = 1, \dots, \nu && \text{(2b)} \\ & \bar{u} - \bar{F}\bar{x} = 0 && \text{(2c)} \end{aligned}$$

This is a constrained LQR problem, which can, in principle, be reduced to a standard, unconstrained, LQR via resolving (2c) in one of $u_i$'s. Although this approach can be used on moderately sized problems, it does not scale as the number of subsystems $\nu$ grows large. Instead, in [Madjidian and Mirkin, 2014] we applied certain coordinate transformations that split problem (2) into a set of $\nu$ uncoupled problems. Using this approach, it was shown that the optimal control law has the following simple form:

$$u_i(t) = F_\alpha x_i(t) + \mu_i(\bar{F} - F_\alpha)\bar{x}(t), \quad i = 1, \dots, \nu, \tag{3}$$

where $F_\alpha$ corresponds to the optimal LQR gain associated with the local, unconstrained, problem with the plant $\Sigma_i$ and the cost function $\mathcal{J}_i$.

The control law (3) has two attractive scalability properties. First, the computational effort required to obtain it is independent of the number of subsystems $\nu$. This is because only one local unconstrained LQR problem needs to be solved in order to obtain $F_\alpha$. Second, the only global information required by each subsystem is the state of the center of mass, $\bar{x}$. Computing this quantity only requires a single averaging operation, which is far less demanding, from both computation and communication viewpoints, than full centralized information processing. This last property is common to all controllers with the block-diagonal-plus-rank-one structure, presented in Figure 1.

Despite its appealing properties, a potential limitation of the control law (3) is that each system requires immediate access to $\bar{x}$. This might not be possible in several applications because communication networks are often subject to restrictions. In this paper, we revisit the coordination problem (2) with the additional constraint that the information exchange between the subsystems is subject to a time-delay. This type of restriction is a typical characteristic of communication networks.

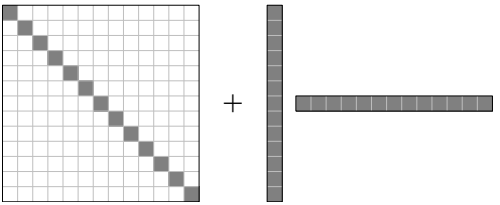

**Figure 1.** Overall optimal controller corresponding to (3)

## 3. Problem Formulation

Instead of the LQR-formulation in [Madjidian and Mirkin, 2014] (nonzero initial conditions, no disturbances) we consider systems with exogenous disturbances and zero initial conditions. That is

$$\Sigma_i : \dot{x}_i(t) = Ax_i(t) + B_{w|i}w_i(t) + B_u u_i(t) \tag{4}$$

for $i = 1, \dots, \nu$, where the state $x_i(t) \in \mathbb{R}^n$ can be measured, the control input $u_i(t) \in \mathbb{R}^m$ and the disturbance $w_i(t) \in \mathbb{R}^{p_i}$. The objective of each subsystem is now expressed in terms of the regulated output

$$z_i(t) := C_z x_i(t) + D_{zu} u_i(t). \tag{5}$$

Combining (4) and (5) for all $i = 1, \dots, \nu$, the local problems can be expressed in the standard framework [Zhou et al., 1995, §14.8.1] depicted in Figure 2(a), where $w$, $z$, $u$, and $x$ are the aggregate disturbance, regulated output, control input, and measured state vector, respectively (e.g., $x := \begin{bmatrix} x_1' & \cdots & x_\nu' \end{bmatrix}'$.

As in Section 2, the coupling between the systems will be due to coordination constraint (2c), where the signals $\bar{u}$ and $\bar{x}$ are defined in (1). The constraint spells out as

$$\bar{v}(t) := \bar{u}(t) - \bar{F}\bar{x}(t) = (\mu \otimes I_m)u - (\mu' \otimes \bar{F})x = 0, \tag{6}$$

where

$$\mu := \begin{bmatrix} \mu_1 & \cdots & \mu_\nu \end{bmatrix}.$$

The addition of (6) is illustrated by Figure 2(b), where the generalized plant is given by

$$G = \begin{bmatrix} G_{zw} & G_{zu} \\ G_{\bar{v}w} & G_{\bar{v}u} \\ G_{xw} & G_{xu} \end{bmatrix} = \left[\begin{array}{c|cc} I_\nu \otimes A & B_w & I_\nu \otimes B_u \\ \hline I_\nu \otimes C_z & 0 & I_\nu \otimes D_{zu} \\ -\mu' \otimes \bar{F} & 0 & \mu' \otimes I_m \\ I_{\nu n} & 0 & 0 \end{array}\right],$$

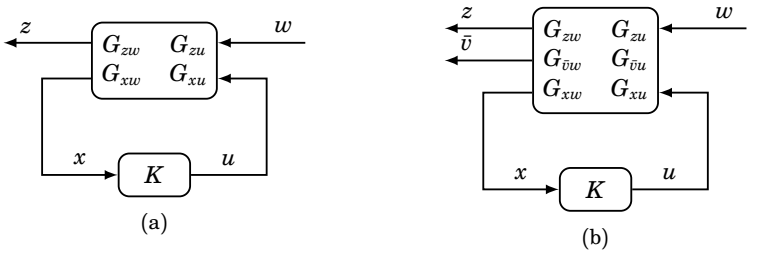


**Figure 2.** Standard state-feedback framework for local uncoordinated problems (a) and the overall coordination problem (b).

and where $B_w = \mathrm{diag}(B_{w|i}, \ldots, B_{w|v})$. The problem studied in [Madjidian and Mirkin, 2014] corresponds to minimizing the $H^2$-norm of the closed-loop system from $w$ to $z$ in Figure 2(b) under constraint (2c), which corresponds to the closed-loop system from $w$ to $\bar{v}$ being zero. In this paper we impose the additional restriction that the information exchange between subsystems is subject to a delay. This can be incorporated by requiring the controller $K$ to be of the form

$$K(s) = \begin{bmatrix} K_{11}(s) & e^{-sh}K_{12}(s) & \cdots & e^{-sh}K_{1v}(s) \\ e^{-sh}K_{21}(s) & K_{22}(s) & \cdots & e^{-sh}K_{2v}(s) \\ \vdots & \vdots & \ddots & \vdots \\ e^{-sh}K_{v1}(s) & e^{-sh}K_{v2}(s) & \cdots & K_{vv}(s) \end{bmatrix} \tag{7}$$

for some causal $K_{ij}$ and $h \geq 0$. This structure implies that the information exchange between any two subsystems is delayed by at least $h$ time units.

The problem formulation is as follows:

$$\begin{aligned} &\text{minimize} && \|T_{zw}\|_2 && \text{(8a)} \\ &\text{subject to} && T_{\bar{v}w} = 0 && \text{(8b)} \\ & && K \text{ is of the form (7)} && \text{(8c)} \end{aligned}$$

where $T_{zw}$ and $T_{\bar{v}w}$ are the closed-loop transfer functions in Figure 2(b) from $w$ to $z$ and from $w$ to $\bar{v}$, respectively. In this formulation, the objective (8a) corresponds to minimizing the sum of the local objectives for the systems in (4), and constraint (8b) is a reformulation of (2c).

Hereafter we will assume that

$\mathcal{A}_1$: $(A, B_u)$ is stabilizable,

$$\mathcal{A}_2\text{:} \begin{bmatrix} A - \mathrm{j}\omega I & B_u \\ C_z & D_{zu} \end{bmatrix} \text{ has full column rank } \forall \omega \in \mathbb{R},$$

$\mathcal{A}_3$: $D_{zu}'D_{zu} = I$,

$\mathcal{A}_4$: $\mu'\mu = 1$ and all entries in $\mu$ are non-zero,

$\mathcal{A}_5$: the matrix $\bar{A} := A + B_u\bar{F}$ is Hurwitz.

Assumptions $\mathcal{A}_{1,2}$ are necessary for the well-posedness of the unconstrained local problems and assumption $\mathcal{A}_5$ is necessary for the stabilizability of the overall system. The normalization assumptions in $\mathcal{A}_{3,4}$ are made to simplify the exposition and can be relaxed. Also, if $\mu_i = 0$ then the $i$th system is not a part of the coordination problem and can therefore be excluded from the analysis.

## 4. Problem Solution

To formulate the solution, we need the following algebraic Riccati equation:

$$A'X_\alpha + X_\alpha A + C_z'C_z - (X_\alpha B_u + C_z'D_{zu})(B_u'X_\alpha + D_{zu}'C_z) = 0 \qquad (9)$$

The main result of this paper, whose proof is presented in §4.2, is formulated below.

THEOREM 4.1
Suppose assumptions $\mathcal{A}_{1\text{-}5}$ are satisfied. Then ARE (9) has a unique stabilizing solution $X_\alpha \geq 0$, and the unique solution to (8) is given by

$$u_i(t) = \bar{F}x_i(t) + (F_\alpha - \bar{F})x_{h|i}(t) + \mu_i(\bar{F} - F_\alpha)e^{\bar{A}h}\bar{x}(t-h), \qquad (10)$$

where $F_\alpha = -B_u'X_\alpha - D_{zu}'C_z$ is the optimal feedback gain associated with the local uncoupled $H^2$ problems (i.e. without (8b) and (8c)), the signal $x_{h|i}$ is given by

$$x_{h|i}(t) := e^{\bar{A}h}x_i(t-h) + \int_{t-h}^{t} e^{\bar{A}(t-\theta)}B_u\big(u_i(\theta) - \bar{F}x_i(\theta)\big)\mathrm{d}\theta \qquad (11)$$

and $\bar{x}$, defined in (1), is the state of the center of mass. □

### 4.1 Discussion

In this subsection, we discuss some properties of the optimal control law in Theorem 4.1.

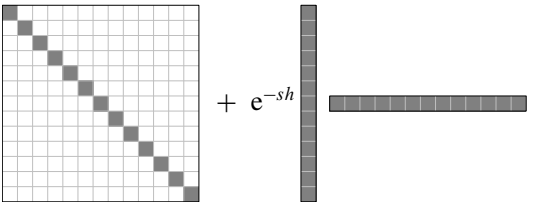


**Figure 3.** Overall optimal controller corresponding to (10)

***Computational scalability and structure*** An important consequence of Theorem 4.1 is that the two scalability properties of the solution to (2) discussed in Section 2 extend to the case with delayed information exchange. First, as in the case of $h = 0$, we only need to solve ARE (9) to form the optimal control law (10). The computational effort is thus independent of the number of subsystems $\nu$. Second, the optimal control law in Theorem 4.1 comprises three terms, where the the first two are completely decentralized. As for the last term, the only global computation needed to form it is a single (scaled) averaging operation

$$\bar{x}(t-h) = \sum_{i=1}^{\nu} \mu_i x_i(t-h).$$

The structure of the overall controller is shown in Fig. 3. This structure is identical to that presented in Fig. 1, except for the delay $e^{-sh}$ in the rank-one coordination term.

***Interpretation*** It is useful to view the control law (10) in terms of the signals

$$v_i := u_i - \bar{F}x_i, \quad i = 1, \ldots, \nu.$$

If $v_i = 0$ for every $i = 1, \ldots, \nu$, then $u_i = \bar{F}x_i$ and constraint (8b) would be satisfied without any need to exchange information between the subsystems. The signals $v_i$ thus correspond to additional degrees of freedom in the control that are brought about by the possibility to exchange information with other subsystems.

The control law (10) has an intuitive interpretation. To see it, first note that in terms of $v_i$ we can restate (11) as:

$$x_{h|i}(t) = e^{\bar{A}h}x_i(t-h) + \int_{t-h}^{t} e^{\bar{A}(t-\theta)}B_u v_i(\theta)\mathrm{d}\theta.$$

This is the minimum variance prediction of $x_i(t)$ based on $x_i(\tau)$, $\tau \leq t-h$.

Next, note that, in terms of the $v_i$, constraint (8b) reads $\bar{v} = \sum_i \mu_i v_i = 0$. Without loss of generality, we can express

$$v_i(t) = v_{i|\mathrm{loc}}(t) + v_{i|\mathrm{coor}}(t),$$

where the $v_{i|\mathrm{loc}}$ depend only on local information and the $v_{i|\mathrm{coor}}$ are coordination terms that satisfy

$$\sum \mu_i (v_{i|\mathrm{loc}} + v_{i|\mathrm{coor}}) = 0,$$

It follows that, unless $v_{i|\mathrm{coor}} + v_{i|\mathrm{loc}} = 0$, in which case there is no need for information exchange among systems, $v_{i|\mathrm{loc}}$ must be based on information that is available to other subsystems. With this condition in mind, the control law in (10) can be thought of as an approximation of the optimal delay-free strategy. Recall that the delay-free strategy is given by

$$v_{i|\mathrm{loc}}(t) = (F_\alpha - \bar{F})x_i(t), \quad v_{i|\mathrm{coor}}(t) = -\mu_i \sum_{j=1}^{\nu} \mu_j v_{j|\mathrm{loc}}(t)$$

(cf. with expression (3)). Hence, (10) is identical to the delay-free strategy, modulo replacing $v_{i|\mathrm{loc}} = (F_\alpha - \bar{F})x_i$, which is not available to any other subsystem, by its prediction $v_{i|\mathrm{loc}} = (F_\alpha - \bar{F})x_{h|i}$, which is based on information available to all subsystems.

***Implementation*** Because of the delay constraints (7), the optimal control law (10) contains the distributed-delay prediction term $x_{h|i}$ defined by (11). Such terms are an intrinsic part of many optimal control strategies, see [Kleinman, 1969; Tadmor, 2000; Meinsma and Zwart, 2000; Mirkin and Raskin, 2003; Mirkin, 2006], which study problems with a single delay, and the references therein. Although such terms may be safely implemented [Tam and Moore, 1974; Mirkin, 2004; Partington and Mäkilä, 2005], their implementation may be numerically involved. However, since matrix $\bar{A} = A + B_u\bar{F}$ is stable, the implementaion of the predictive term in (11) can be facilitated. This is because the decomposition

$$\int_0^h e^{-(sI-\bar{A})\theta}\,\mathrm{d}\theta = (sI - \bar{A})^{-1} - (sI - \bar{A})^{-1}e^{\bar{A}h}e^{-sh}$$

only has stable pole-zero cancellations (all eigenvalues of $\bar{A}$ are canceled). Consequently, without harming the internal stability of the system, we can express (10) as $u_i = \bar{F}x_i + v_i$, where $v_i$ is given by

$$\begin{aligned}
\dot{\chi}_i(t) &= \bar{A}\chi_i(t) + B_u v_i(t) - e^{\bar{A}h}B_u v_i(t-h) \\
v_i(t) &= (F_\alpha - \bar{F})\left(\chi_i(t) + e^{\bar{A}h}(x_i(t-h) - \mu_i\bar{x}(t-h)\right)
\end{aligned}$$

Straighforward algebra yields

$$\dot{\chi}_i(t) = (A + B_u F_\alpha)\chi_i(t) + \xi_i(t-h)$$
$$u_i(t) = \bar{F}x_i(t) + (F_\alpha - \bar{F})\left(\chi_i(t) + e^{\bar{A}h}\zeta_i(t-h)\right)$$

where

$$\xi_i := e^{\bar{A}h}B_u(\bar{F}x_i - u_i) + B_u(F_\alpha - \bar{F})e^{\bar{A}h}(x_i - \mu_i\bar{x})$$
$$\zeta_i := x_i - \mu_i\bar{x}.$$

The dynamic components involved in this representation are one stable system of order $n$ and a couple of delay lines. These components admit standard implementations.

## 4.2 Proof of Theorem 4.1

It is well-known [Zhou et al., 1995, Corr. 13.10] that $\mathcal{A}_{\mathbf{1\text{-}3}}$ guarantee the existence of a unique and stabilizing solution $X_\alpha \geq 0$ to (9).

In solving (8), the first step is to reduce it to a constrained $H^2$ problem in which the delay structure in (7) is replaced by a single delay element that applies to all measurement channels uniformly. This is done in the following lemma:

LEMMA 4.2
A controller $K$ satisfies (8b) and (8c) if and only if it is of the form

$$K(s) = I_\nu \otimes \bar{F} + e^{-sh}K_h(s)$$

where $K_h$ is a causal system that satisfies

$$(\mu' \otimes I_m)K_h = 0. \tag{12}$$

□

***Proof*** From the definition of $\bar{v}$ in (6) we see that the transfer function in (8b) is given by

$$T_{\bar{v}w} = (\mu' \otimes I_m)(K - (I_\nu \otimes \bar{F}))T_{xw},$$

where $T_{xw} = (I - G_{xu}K)^{-1}G_{xw}$. Provided that $B_{w|i}$ in (4) has full column-rank for each $i = 1, \ldots, \nu$ , which merely implies non-redundancy with respect to the disturbances $w_i$, then $T_{xw}$ has full normal column rank [Zhou et al., 1995, Ch. 3.11]. This implies that (8b) is equivalent to

$$(\mu' \otimes I_m)(K - (I_\nu \otimes \bar{F})) = 0, \tag{13}$$

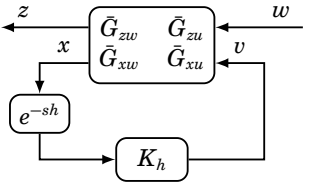


**Figure 4.** $H^2$ problem with uniformly delayed measurement channels.

from which the *if* part of the statement follows immediately. For the reverse implication, note that, if $K$ is of the form (7), then the $j$th block-column of (13) reads

$$\mu_j K_{jj}(s) + e^{-sh} \sum_{i \neq j} \mu_i K_{ij}(s) - \mu_j \bar{F} = 0$$

This condition holds if and only if

$$K_{jj}(s) = \bar{F} + e^{-sh} \tilde{K}_{jj}(s)$$

for some $\tilde{K}_{jj}$ that satisfies $\mu_j \tilde{K}_{jj} + \sum_{i \neq j} \mu_i K_{ij} = 0$. The result follows by repeating these arguments for every $j$. □

We now substitute $K$ with the right-hand side of the expression in Lemma 4.2. This is equivalent to the substitution $u_i = \bar{F} x_i + v_i$ for some signal $v_i$. This step eliminates constraint (8c) and transforms (8) into the $H^2$ problem depicted in Figure 4, where $K_h$ is now subject to (12), and the generalized plant is given by

$$\begin{bmatrix} \bar{G}_{zw} & \bar{G}_{zu} \\ \bar{G}_{xw} & \bar{G}_{xu} \end{bmatrix} = \left[\begin{array}{c|cc} I_\nu \otimes \bar{A} & B_w & I_\nu \otimes B_u \\ \hline I_\nu \otimes \bar{C}_z & 0 & I_\nu \otimes D_{zu} \\ I_{\nu n} & 0 & 0 \end{array}\right] \tag{14}$$

where $\bar{A} = A + B_u \bar{F}$ and $\bar{C}_z := C_z + D_{zu} \bar{F}$.

With the delay applied uniformly to all measurement channels, the problem in Figure 4 subject to (12) can be solved using the approach in [Madjidian and Mirkin, 2014]. Due to space considerations, we only provide an outline of the steps in the approach. For details we refer to [Madjidian and Mirkin, 2014, §3.B].

1) The first step is to decouple the local problems. To this end, let $U$ be a *unitary* matrix such that $U\mu = e_1$ (this is the singular value decomposition of $\mu$ so $U$ exists) and set

$$\tilde{x} := (U \otimes I)x, \quad \tilde{v} := (U \otimes I)v \quad \text{and} \quad \tilde{z} := (U \otimes I)z. \tag{15}$$

This coordinate transformation decouples the problem into $\nu-1$ decoupled delayed $H^2$ problems and one problem with the predefined control law $\tilde{v}_1 = 0$. Note that, the disturbances in these problems will be coupled, but due to availability of state feedback, this does not affect the solution.

2) The solution to the delayed problems is provided in [Mirkin and Raskin, 2003]:

$$\tilde{v}_i(t) = F\left(e^{\bar{A}h}\tilde{x}_i(t-h) + \int_{t-h}^{t} e^{\bar{A}(t-\theta)}B_u\tilde{v}_i(\theta)\mathrm{d}\theta\right),$$

where it can be shown that $F = F_\alpha - \bar{F}$. The overall control law in the transformed coordinates is then $\tilde{v}(t) = ((I_\nu - e_1e_1') \otimes F)\tilde{x}_h(t)$, where

$$\tilde{x}_h(t) := e^{(I_\nu\otimes\bar{A})h}\tilde{x}(t-h) + \int_{t-h}^{t} e^{(I_\nu\otimes\bar{A})(t-\theta)}(I_\nu\otimes B_u)\tilde{v}(\theta)\mathrm{d}\theta.$$

3) The last step is to return to the original coordinates. Set $x_h := \begin{bmatrix} x_{h|1}' & \cdots & x_{h|\nu}' \end{bmatrix}'$, where $x_{h|i}$ is defined in (11) and use the relations in (15) to obtain

$$\begin{aligned} v(t) &= \big((I_\nu - \mu\mu')\otimes F\big)x_h(t) \\ &= (I_\nu\otimes F)x_h(t) - \Big(\mu\otimes Fe^{\bar{A}h}\Big)\Big(\mu\otimes I\Big)x(t-h) \\ &\qquad - \int_{t-h}^{t}\Big(\mu\otimes Fe^{\bar{A}(t-\theta)}B_u\Big)\Big(\mu'\otimes I\Big)v(\theta)\mathrm{d}\theta \\ &= (I_\nu\otimes F)x_h(t) - (\mu\otimes F)e^{\bar{A}h}\bar{x}(t-h), \end{aligned} \tag{16}$$

where the last equality follows from the fact that, by construction, $(\mu'\otimes I)v = \bar{v} = 0$. Inserting $F = F_\alpha - \bar{F}$ into (16) and recalling that $u = (I_\nu\otimes\bar{F})x + v$ yields (10).

## 5. Cost of coordination per subsystem

In this section we study the performance of each system in (4) under the optimal control law (10). In particular, we investigate the influence of the delay time $h$ and the number of subsystems $\nu$ on local performance.

Let $T_{zw|i}$ denote the closed-loop system from the aggregate disturbance $w$ to the local regulated signal $z_i$ defined in (5). The (squared) cost associated with the $i$th system is then given by

$$\mathcal{J}_i := \left\|T_{zw|i}\right\|_2^2.$$

Before giving an expression for $\mathcal{J}_i$, we define two quantities. By $\mathcal{J}_{i|\text{opt}} := \text{tr}(B'_{w|i} X_\alpha B_{w|i})$ we refer to the the optimal uncoordinated cost of the subsystem, i.e. the cost attained under the control law $u_i = F_\alpha x_i$, and by $\bar{\mathcal{J}}_i := \text{tr}(B'_{w|i} \bar{X} B_{w|i})$, where $\bar{X}$ is the solution to the Lyapunov equation

$$\bar{A}'\bar{X} + \bar{X}\bar{A} + (C_z + D_{zu}\bar{F})'(C_z + D_{zu}\bar{F}) = 0, \tag{17}$$

we refer to the cost attained with $u_i = \bar{F}x_i$. Note that this is the only control law that satisfies (8b) in case the systems are not able to communicate.

PROPOSITION 5.1
Let $\bar{X}$ be the solution to Lyapunov equation (17), $X_\alpha$ the stabilizing solution to ARE (9) and set

$$X_h := (\bar{X} - X_\alpha) - e^{\bar{A}'h}(\bar{X} - X_\alpha)e^{\bar{A}h}. \tag{18}$$

Then $\bar{X} - X_\alpha \geq 0$, $X_h \geq 0$ and the cost associated with the $i$th subsystem under control law (10) is

$$\mathcal{J}_i = \mathcal{J}_{i|\text{opt}} + \mathcal{J}_{i|h} + \mu_i^2 \sum_{j=1}^{\nu} \mu_j^2 (\bar{\mathcal{J}}_j - \mathcal{J}_{j|\text{opt}}), \tag{19}$$

where

$$\mathcal{J}_{i|h} := \text{tr}\left(B'_{w|i} X_h B_{w|i}\right) - \mu_i^2 \sum_{j=1}^{\nu} \mu_j^2 \,\text{tr}\left(B'_{w|j} X_h B_{w|j}\right) \tag{20}$$

satisfies $\sum_{i=1}^{\nu} \mathcal{J}_{i|h} \geq 0$. □

***Proof*** The proof is given in the Appendix. □

The first and the last terms in (19) are independent of $h$, while the term, $\mathcal{J}_{i|h}$, vanishes when $h = 0$ and thus quantifies the performance deterioration due to the delay. Henceforth, we refer to the quantity $\mathcal{J}_i - \mathcal{J}_{i|\text{opt}}$ as the *cost of coordination*. This is the cost incurred by a subsystem due to satisfying constraint (8b).

We start by studying the cost of coordination when $h = 0$. In this case we have $\sum_{i=1}^{\nu}(\mathcal{J}_i - \mathcal{J}_{i|\text{opt}}) = \sum_{j=1}^{\nu} \mu_j^2 (\bar{\mathcal{J}}_j - \mathcal{J}_{j|\text{opt}})$ which implies that total cost of coordination for all subsystems under delay-free communication equals the (weighted) average coordination cost for a subsystem in isolation (recall that by assumption $\mathcal{A}_4$, $\sum_{i=1}^{\nu} \mu_i^2 = 1$.). Each subsystem incurs a portion, $\mu_i^2 \leq 1$, of the total cost. In particular, if $\mu_i = \mu_j$ and $B_{w|i} = B_{w|j}$, for all $i, j = 1, \ldots, \nu$, then $\mathcal{J}_i - \mathcal{J}_{i|\text{opt}} = \frac{1}{\nu}(\bar{\mathcal{J}}_i - \mathcal{J}_{i|\text{opt}})$, which

means that the cost of coordination is reduced by a factor of $\nu$ due to (delay-free) information exchange between the systems.

Next, we consider $h \geq 0$ and study what happens with the cost of coordination when the number of subsystems $\nu \to \infty$. To simplify the analysis, we assume that $\mu_i = \mu_j$ and $B_{w|i} = B_{w|j}$ for all $i, j = 1, \ldots, \nu$. The expression in (19) then reduces to

$$\mathcal{J}_i = \mathcal{J}_{i|\text{opt}} + \frac{1}{\nu}(\bar{\mathcal{J}}_j - \mathcal{J}_{j|\text{opt}}) + \mathcal{J}_{i|h},$$

where

$$\mathcal{J}_{i|h} = (1 - \frac{1}{\nu}) \operatorname{tr}(B'_{w|i} X_h B_{w|i}). \tag{21}$$

The cost of coordination can then be restated as

$$\mathcal{J}_i - \mathcal{J}_{i|\text{opt}} = \operatorname{tr}(B'_{w|i} X_h B_{w|i}) + \frac{1}{\nu} \operatorname{tr}\left( B'_{w|i} e^{\bar{A}'h} (\bar{X} - X_\alpha) e^{\bar{A}h} B_{w|i} \right),$$

which decreases as $\nu$ increases. In particular,

$$\mathcal{J}_i - \mathcal{J}_{i|\text{opt}} = \frac{1}{\nu}(\bar{\mathcal{J}}_i - \mathcal{J}_{i|\text{opt}}) + \mathcal{J}_{i|h} \to \mathcal{J}_{i|h} \quad \text{as} \quad \nu \to \infty.$$

When $h = 0$, $\mathcal{J}_{i|h} = 0$, and the cost of coordination per subsystem vanishes. However, if $h > 0$ this is not the case. In fact, from (21) we see that $\mathcal{J}_{i|h}$ *increases* as $\nu \to \infty$. Thus, although the cost of coordination decreases as the number of subsystems increses, the performance deterioration due to the delay becomes more noticeable.

## 6. Conclusions

We study a large-scale coordination problem, where a homogeneous group of autonomous agents are coupled through a constraint on their average state. In order to satisfy the coordination requirement, the agents must coordinate their actions over a delayed communication channel.

It was shown that several useful properties of the solution to the delay-free case, which was derived in [Madjidian and Mirkin, 2014], extend to the case with delayed information exchange. In particular, the optimal control law is decomposed into a diagonal term complemented by a delayed rank-one component. While the first term is completely decentralized, the latter can be implemented by a single averaging operation. Moreover, to form the solution, we only need to solve an optimal control problem for a stand-alone agent. This means that the computational effort required to obtain the solution is independent of the number of agents.

It is interesting to note that a delay on the information exchange does not add any dynamics to the rank-one term. The only complexity brought about by the delay is the introduction of a Smith predictor in the control law for each agent.

In the last part of the paper, we derived an analytic expression for the performance of each agent under the optimal control law. It was shown that in the delay-free case, the cost of satisfying the coordination constraint vanishes as the number of systems grows large. This is no longer true in the presence of a delay. In this case, the performance still improves as the number of agents increases, but the performance deterioration due to the delay becomes more noticeable.

## Acknowledgments

This work was supported by the Swedish Research Council through the LCCC Linnaeus Center and by the European commission through the project AEOLUS.

## References

Andreasson, M., D. Dimarogonas, K. Johansson, and H. Sandberg (13). "Distributed vs. centralized power systems frequency control". In: *Proceedings of the 2013 European Control Conference*, pp. 3524–3529.

Kleinman, D. L. (1969). "Optimal control of linear systems with time-delay and observation noise". *IEEE Transactions on Automatic Control* **14**:5, pp. 524–527.

Lin, F., M Fardad, and M. Jovanovic (2012). "Optimal control of vehicular formations with nearest neighbor interactions". *IEEE Transactions on Automatic Control* **57**:9, pp. 2203–2218.

Madjidian, D. and L. Mirkin (2014). "Distributed control with low-rank coordination". *IEEE Transactions on Control of Network Systems* **1**:1, pp. 53–63.

Mahajan, A., N. C. Martins, M. C. Rotkowitz, and S. Yüksel (2012). "Information structures in optimal decentralized control". In: *Proceedings of the 51st IEEE Conference on Decision and Control*. Maui, HW, pp. 1291–1306.

Meinsma, G. and H. Zwart (2000). "On $\mathcal{H}_\infty$ control for dead-time systems". *IEEE Transactions on Automatic Control* **45**:2, pp. 272–285.

Mirkin, L. (2004). "On the approximation of distributed-delay control laws". *System and Control Letters* **55**:5, pp. 331–342.

Mirkin, L. (2006). "On the dead-time compensation from $L^1$ perspectives". *IEEE Transactions on Automatic Control* **51**:6, pp. 1069–1073.

Mirkin, L. and N. Raskin (2003). "Every stabilizing dead-time controller has an observer-predictor-based structure". *Automatica* **39**:10, pp. 1747–1754.

Partington, J. R. and P. M. Mäkilä (2005). "Rational approximation of distributed-delay controllers". **78**:16, pp. 1295–1301.

Rantzer, A. (2012). "Distributed control of positive systems". URL: `http://arxiv.org/abs/1203.0047`.

Rotkowitz, M. and S. Lall (2006). "A characterization of convex problems in decentralized control". *IEEE Transactions on Automatic Control* **51**:2, pp. 274–286.

Shah, P. and P. A. Parrilo (2013). "$\mathcal{H}_2$-optimal decentralized control over posets: a state-space solution for state-feedback". *IEEE Transactions on Automatic Control* **58**:12, pp. 3084–3096.

Šiljak, D. D. (1978). *Large-Scale Dynamic Systems: Stability and Structure*. North-Holland, NY.

Tadmor, G. (2000). "The standard $H_\infty$ problem in systems with a single input delay". *IEEE Transactions on Automatic Control* **45**:3, pp. 382–397.

Tam, P. K. S. and J. B. Moore (1974). "Stable realization of fixed-lag smoothing equations for continuous-time signals". *IEEE Transactions on Automatic Control* **19**:1, pp. 84–87.

Tsitsiklis, J. and M. Athans (1985). "On the complexity of decentralized decision making and detection problems". *IEEE Transactions on Automatic Control* **30**:5, pp. 440–446.

Wistenhausen, H. S. (1968). "A counterexample in stochastic optimum control". *SIAM Journal on Control* **6**:1, pp. 131–147.

Zečević, A. and D. Šiljak (2005). "Global low-rank enhancement of decentralized control for large-scale systems". *IEEE Transactions on Automatic Control* **50**:5, pp. 740–744.

Zečević, A. and D. Šiljak (2010). *Control of Complex Systems: Structural Constraints and Uncertainty*. Springer-Verlag, New York, NY.

Zhou, K., J. C. Doyle, and K. Glover (1995). *Robust and Optimal Control*. Prentice-Hall, Englewood Cliffs, NJ.

## Appendix: Proof of Proposition 5.1

The fact that $\bar{X} - X_\alpha \geq 0$ follows from the definition of $\mathcal{J}_{i|\text{opt}}$ and $\bar{\mathcal{J}}$. The claim $X_h \geq 0$ is due to assumption $\mathcal{A}_\mathbf{5}$, which implies that $e^{\bar{A}h}$ is a contraction, and $\sum \mathcal{J}_{i|h} \geq 0$ follows from

$$\sum_{i=1}^{\nu} \text{tr}\left(B'_{w|i} X_h B_{w|i}\right) - \sum_{i=1}^{\nu} \mathcal{J}_{i|h} = \sum_{j=1}^{\nu} \mu_j^2 \left(B'_{w|j} X_h B_{w|j}\right) \leq \sum_{i=1}^{\nu} \text{tr}\left(B'_{w|i} X_h B_{w|i}\right),$$

where we have used $\sum \mu_i^2 = 1$ in both steps.

With $\eta(t) := \mu_i(\bar{F} - F_\alpha)e^{\bar{A}h}\bar{x}(t)$, the control law (10) reads

$$u_i(t) = \bar{F}x_i(t) + (F_\alpha - \bar{F})x_{h|i}(t) + \eta(t-h). \tag{22}$$

Under (22) we can express the regulated signals in (5) as

$$z_i(s) = T(s)w(s) + H(s)\eta(s),$$

for some transfer functions $T$ and $H$. If $T_{\eta w}$ is the transfer function from $w$ to $\eta$, we can write

$$\mathcal{J}_i = \|T + HT_{\eta w}\|_2^2.$$

Now, by Leibnitz's rule, $x_{h|i}$ in (11) satisfies

$$\dot{x}_{h|i}(t) = \bar{A}x_{h|i}(t) + B_u(u_i(t) - \bar{F}x_i(t)) + e^{\bar{A}h}B_{w|i}w_i(t-h).$$

Inserting (22) into the state equations for $\zeta_i := x_i - x_{h|i}$, $x_{h|i}$ as well as the equation for $z_i$ in (5) gives

$$\begin{aligned}
\dot{\zeta}_i(t) &= \bar{A}\zeta_i(t) + B_{w|i}w_i(t) - e^{\bar{A}h}B_{w|i}w_i(t-h) \\
\dot{x}_{h|i}(t) &= A_\alpha x_{h|i}(t) + B_u\eta(t-h) + e^{\bar{A}h}B_{w|i}w_i(t-h) \\
z_i(t) &= C_{\bar{F}}\zeta_i(t) + C_{F_\alpha}x_{h|i}(t) + D_z\eta(t-h),
\end{aligned}$$

where $A_\alpha := A + B_uF_\alpha$, $C_{\bar{F}} := C_z + D_z\bar{F}$ and $C_{F_\alpha} := C_z + D_zF_\alpha$. It follows that the impulse response of $T$ is $\tau = \tau_o + \tau_c$, where

$$\tau_o(t) = \begin{cases} C_{\bar{F}}e^{\bar{A}t}B_{w|i}, & t \in [0,h) \\ 0 & t \in [h,\infty) \end{cases}$$

$$\tau_c(t) = \begin{cases} 0, & t \in [0,h) \\ C_{F_\alpha}e^{A_\alpha t}e^{\bar{A}h}B_{w|i} & t \in [h,\infty) \end{cases}$$

Since, $\tau_o$ and $\tau_c$ have disjoint support, they are orthogonal to each other. Hence, by Parseval's theorem, $T = T_o + T_c$ where $T_o \perp T_c$. Since the impulse response of $H$ has support on $[h, \infty)$, we also conclude that $T_o \perp H$. Hence,

$$\mathcal{J}_i = \|T_o\|_2^2 + \|T_c + HT_{\eta w}\|_2^2 .$$

Next, we factor $T_c(s) = G_c(s)e^{-sh}$ and $H(s) = U(s)e^{-sh}$, where $G_c(s) = C_{F_\alpha}(sI - A_\alpha)^{-1}B_{w|i}$ and $U(s) = C_{F_\alpha}(sI - A_\alpha)^{-1}B_u + D_{zu}$. By [Zhou et al., 1995, Lemma 14.3], $U^\sim G_c \in (H^2)^\perp$ and $U^\sim U = I$, so

$$H^\sim T_c = U^\sim G_c \in (H^2)^\perp \quad \text{and} \quad H^\sim H = U^\sim U^\sim = I.$$

These properties, together with the fact that

$$T_{\eta w}(s) = \mu_i(\bar{F} - F_\alpha)e^{\bar{A}h}(sI - \bar{A})^{-1}\bar{B}_w \in H^2, \tag{23}$$

where $\bar{B}_w := \begin{bmatrix}\mu_1 B_{w|1} & \cdots & \mu_\nu B_{w|\nu}\end{bmatrix}$, yield

$$\mathcal{J}_i = \|T_o\|_2^2 + \|T_c\|_2^2 + \|T_{\eta w}\|_2^2 .$$

The first two terms are given by

$$\begin{aligned}\|T_o\|_2^2 &= \int_0^h \operatorname{tr}\left((C_{\bar{F}}e^{\bar{A}t}B_{w|i})'(C_{\bar{F}}e^{\bar{A}t}B_{w|i})\right)\mathrm{d}t \\ &= \operatorname{tr}\left(B'_{w|i}(\bar{X} - e^{\bar{A}'h}\bar{X}\,e^{\bar{A}h})B_{w|i}\right) \\ \|T_c\|_2^2 &= \|G_c\|_2^2 = \operatorname{tr}\left(B'_{w|i}e^{\bar{A}'h}X_\alpha e^{\bar{A}h}B_{w|i}\right),\end{aligned}$$

which together with $\mathcal{J}_{i|\text{opt}} = \operatorname{tr}(B'_{w|i}X_\alpha B_{w|i})$ result in

$$\mathcal{J}_i = \mathcal{J}_{i|\text{opt}} + \operatorname{tr}(B'_{w|i}X_h B_{w|i}) + \|T_{\eta w}\|_2^2 \tag{24}$$

As for the last term, it follows from (23) that

$$\|T_{\eta w}\|_2^2 = \mu_i^2 \operatorname{tr}(\bar{B}'_w X_\eta \bar{B}_w) = \mu_i^2 \sum_{j=1}^{\nu} \mu_j^2 \operatorname{tr}\left(B'_{w|j}X_\eta B_{w|j}\right),$$

where $X_\eta$ is the solution to the Lyapunov equation

$$\bar{A}'X_\eta + X_\eta\bar{A} + e^{\bar{A}'h}(\bar{F} - F_\alpha)'(\bar{F} - F_\alpha)e^{\bar{A}h} = 0.$$

It is then straightforward to verify that $X_\eta = e^{\bar{A}'h}(\bar{X} - X_\alpha)e^{\bar{A}h} = (\bar{X} - X_\alpha - X_h)$, which implies that

$$\|T_{\eta w}\|_2^2 = \mu_i^2 \sum_{j=1}^{\nu} \mu_j^2 \operatorname{tr}\left(B'_{w|j}(\bar{X} - X_\alpha)B_{w|j}\right) - \mu_i^2 \sum_{j=1}^{\nu} \mu_j^2 \operatorname{tr}\left(B'_{w|j}X_h B_{w|j}\right).$$

Inserting this expression into (24) completes the proof.

# Paper IV

# Distributed Control of Dispatchable Wind Power Plants

**Daria Madjidian**

**Abstract**

When a wind farm is required to meet a power set-point, its wind turbines are free to continuously vary their power production as long as the sum of their productions meets the power demand. This flexibility can be used to reduce structural loads by allowing turbines in the wind farm to coordinate their power production. Here, we present a simple, yet effective, coordination policy which minimizes the total aggregated fatigue load to the turbines, while satisfying the power demand. An appealing property is that its computational complexity is independent of the number of wind turbines in the farm, which means that it can be applied to any wind farm size. Furthermore, it allows wind turbines to be added or removed from operation without the need for any control redesign. The efficiency of the policy is illustrated in a simulation study based on real wind farm data.

Manuscript prepared for submission.

## 1. Introduction

In order to reduce emissions, many regions have set goals on renewable energy production. In particular, Europe aims to produce 20% of its electricity from renewable sources by 2020 [European Comission, 2006], the United States is looking into 20% wind power penetration by 2030 [U.S. Department of Energy, 2008], and Denmark aims to have all of its electricity supplied by renewables in 2050 [Danish Government, 2011]. Wind energy is widely considered as a clean source of energy and is expected to be a key components in achieving these goals.

As wind power penetration increases, a fundamental question arises of how to absorb the variability in the wind. One solution is to let wind power plants behave as dispatchable units that regulate their power production according to the balancing needs of the electrical power system. Such policies are already in place in Spain and the United Kingdom, where large wind power providers bear full responsibility for forecasting and balancing their own production [Klessmann et al., 2008].

Operating a large wind farm as a dispatchable power plant presents a new set of challenges and opportunities. In particular, when a wind farm tracks a power set-point, there is flexibility in distributing the total power production among its wind turbines, which can be used to improve additional aspects of wind power plant operation. For instance, in [de Almeida et al., 2006], it was used to reduce active power losses in the transformers and lines inside the wind farm. Another possibility, which is the topic of this paper, is to reduce the structural loads on the wind turbines. Instead of each turbine following a fixed portion of the power demand, it can be allowed to adjust its power production in response to local wind speed fluctuations. Since wind conditions are not uniform across the wind farm, wind turbines can coordinate their power production so that changes that benefits one turbine are compensated for by units with opposite needs.

A challenge in coordinating the production of a large number of wind turbines is that the associated control design problem might become very complex. In [Biegel et al., 2013], this was addressed by designing local control laws, where each wind turbine is only allowed to communicate with a limited number of neighboring units. In [Spudić and Baotić, 2013], a model predictive control approach was used to coordinate the turbines. The method exploits the structure of the problem in order to speed up the computation time by several orders of magnitude.

Here, the approach is based on the following observation: wind turbines in wind farms are often identical in their design and operate around similar wind conditions. The control design problem can then be formulated as a coordination problem among homogeneous agents, which was

studied in [Madjidian and Mirkin, 2014]. The optimal controller for this problem has several appealing properties in the context of wind farm control. In particular, the computational effort required to obtain it is independent of the number of turbines, and the only centralized operation required to implement it is a single averaging operation. This means that the control law can be applied to very large wind farms. Furthermore, wind turbines can be added or removed from operation without any control redesign.

The rest of the paper is organized as follows. In Section 2 we describe the wind turbine and wind farm models and in Section 3 we formulate the control design problem. The optimal controller and its properties are discussed in Section 4. To illustrate the behavior of the controller, Section 5 provides a simulation study based on real wind farm data. Conclusions are provided in Section 6.

## 2. Modeling

### 2.1 Wind turbine model

We adopt a non-linear model of the NREL 5-MW wind turbine from [Grunnet et al., 2010]. A schematic overview of the model is depicted in Figure 1. The main non-linearities in the model are in the aerodynamics block, which is implemented as a static model based on the power and thrust coefficients, and in the generator model. The drive-train and tower models are linear and contain poorly damped resonant modes. The pitch actuator is modeled as a first-order linear servo system with an internal loop delay. The wind turbine controller manipulates the generator torque and the blade pitch angle in order to meet a prescribed power demand. It has three main modes of operation, usually called “operating regions”. See Figure 2. The first two modes are identical to those of the standard NREL base-line controller described in [Jonkman et al., 2009], whereas the third mode has been modified to allow the turbine to track a power set-point. The controller operates in the third (derated) mode if the power demand is lower than the power that can be captured by the turbine, in which case excess wind power is curtailed in order to satisfy demand. This is achieved by modifying the pitch angle to keep the rotor speed close to its rated value, and adjusting the generator torque to maintain the power set-point. In this paper, we assume that the power set-point can be attained, which means that the controller operates in Region 3.

The full non-linear model will be used for simulation in Section 5. For control design, we use the simplified linear model in [Spudić et al., 2011] to approximate the wind turbine dynamics around an operating point. The linear model is illustrated in Figure 3, where $P$ represents the wind

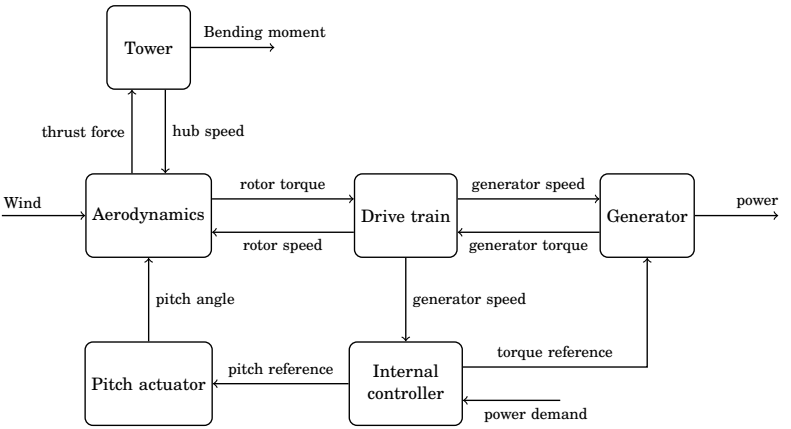


**Figure 1.** Schematic overview of the NREL wind turbine model

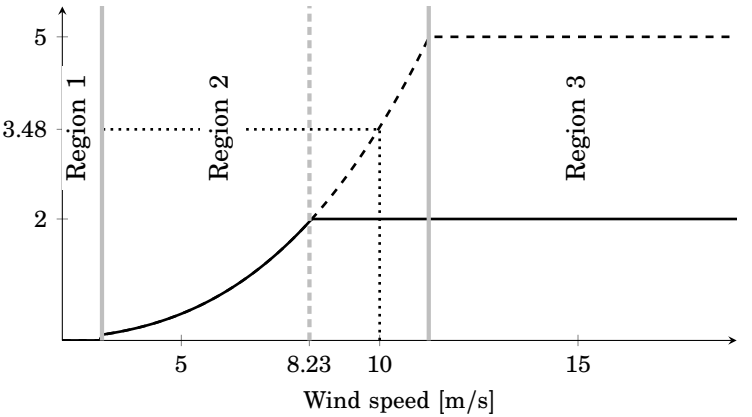


**Figure 2.** Power curve of the NREL 5-MW wind turbine. The dashed curve illustrates standard operation. The solid curve shows the power production when the power reference to the turbine is 2 MW, in which case the turbine spills 1.48 MW of the available power in order to satisfy the demand. The solid gray lines indicate transitions between operating regions. The effect of a power reference below rated power is to shift the transition point between Region 2 and Region 3 to the left as indicated by the dashed gray line. The wind turbine can only meet the 2 MW power demand if the wind speed is above 8.23 m/s.

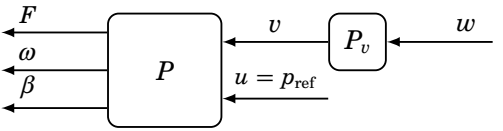


**Figure 3.** Linear model of the NREL 5 MW wind turbine. The plant $P$ describes the wind turbine and $P_v$ accounts for the spectral density of the wind speed fluctuations. The signal $v$ represents the wind speed fluctuations, $u$ is the deviation of the power reference from its nominal value, and $w$ is white noise that generates $v$. The outputs $F$, $\omega$ and $\beta$ are the deviations in thrust force, rotor speed and pitch angle from their nominal values, respectively. The model neglects generator dynamics, which makes $u$ the actual power production of the turbine.

turbine and $P_v$ accounts for the spectral density of the wind speed fluctuations. The inputs to the wind turbine, $v$ and $p_{\text{ref}}$, are the deviations in the wind speed and the power reference from their mean values, respectively. To illustrate that $p_{\text{ref}}$ is the control input to the turbine, it is also denoted by $u$. It is important to note that the linear model neglects electrical generator dynamics, which means that $u$ equals the actual power production of the turbine. The outputs $F$, $\omega$ and $\beta$ are the deviations in thrust force, rotor speed and pitch angle from their nominal values, respectively. The wind speed is modeled as $v = P_v w$, where $w$ is Gaussian white noise with unit intensity and the filter

$$P_v(s) = \frac{7.4476}{(1/0.0143)s + 1},$$

was identified from real wind turbine measurements in [Kristalny et al., 2013].

## 2.2 Wind farm model

We consider a wind farm with $\nu$ wind turbines, and use the subscript $i$ to refer to $i$th turbine in the wind farm. For instance, $\beta_i$ denotes the pitch angle deviations at the $i$th wind turbine. We make two simplifying assumptions:

- The operating point is the same for all wind turbines. The operating point is determined by the mean wind speed and the nominal power production, which are set to 10 m/s and 2 MW, respectively. Since all wind turbines are identical in their design, the assumption implies that they have identical dynamics.
- The wind speed variations experienced by different turbines are uncorrelated. This is motivated by practical studies [Vigueras-

Rodríguez et al., 2012; Kristalny et al., 2013] that show that due to the large distances between turbines, the wind speed variations are only correlated at very low frequencies. This assumption is only made to simplify the control design and is not used in the simulations in Section 5.

Based on these assumptions, the wind turbines in the wind farm can be described by

$$\frac{d}{dt}x_i(t) = Ax_i(t) + B_u u_i(t) + B_w w_i(t), \quad i = 1, \ldots, \nu, \tag{1}$$

where $w_i$ and $w_j$ are independent for $i \neq j$. The state vector is given by $x_i = \begin{bmatrix}\beta_i & \omega_i & q_i & v_i\end{bmatrix}^T$, where $q_i$ is a filtered rotor speed measurement that is used by the internal wind turbine controller. At the operating point defined above, the state space matrices take the following values

$$A = \begin{bmatrix} 0 & 1.2 \cdot 10^2 & -9.2 \cdot 10^{-1} & 0 \\ -8.4 \cdot 10^{-3} & -3.2 \cdot 10^{-2} & 0 & 1.6 \cdot 10^{-2} \\ 0 & 1.5 \cdot 10^2 & -1.6 & 0 \\ 0 & 0 & 0 & 1.43 \cdot 10^{-2} \end{bmatrix}$$

$$B = \begin{bmatrix} 0 \\ -2.1 \cdot 10^{-8} \\ 0 \\ 0 \end{bmatrix} \qquad B_w = \begin{bmatrix} 0 \\ 0 \\ 0 \\ 0.11 \end{bmatrix}.$$

## 3. Formulation of the optimal control problem

As explained above, we consider a wind farm with $\nu$ wind turbines, where each turbine operates at a mean wind speed of 10 m/s and a nominal power production of 2 MW. The power set-point to the wind farm is the sum of the nominal wind turbine production, i.e. $2\nu$ MW.

The aim of the wind farm controller is to use the flexibility in distributing the power among the wind turbines to reduce structural loads. Here, we limit our attention to fatigue loads on the tower of the turbines. The standard method for evaluating fatigue, which is used during the simulations in Section 5, is based on counting stress cycles [Manwell et al., 2009]. However, this fatigue measure cannot be directly addressed in a control design framework based on a linear model. Therefore, we will design a control law that reduces the variance of the thrust force. The idea is that, since the tower motion is mainly driven by the thrust force, a reduction in thrust should lead to less excitation and hence, lower fatigue loading.

We define the cost function for the $i$th turbine as

$$\mathcal{J}_i = \mathbf{E}\left(z_i^T(t) z_i(t)\right).$$

where

$$\begin{aligned} z_i(t) &= \begin{bmatrix} F_i(t) \\ k_u u_i(t) \end{bmatrix} = \begin{bmatrix} -5.8 \cdot 10^4 & -1.5 \cdot 10^5 & 0 & 7.4 \cdot 10^4 \\ 0 & 0 & 0 & 0 \end{bmatrix} x_i(t) + \begin{bmatrix} 0 \\ k_u \end{bmatrix} u_i(t) \\ &= C_z x_i(t) + D_z u_i(t). \end{aligned}$$

Note that, we have included $u_i$ in the cost function in order to keep the power variations at each turbine at a reasonable level. Here, the parameter $k_u > 0$ is a weight that can be used to tune the level of power fluctuations that can be accepted at a turbine.

For each wind turbine, we assume that we have access to noisy measurements of the pitch angle and the rotor speed

$$y_i = \begin{bmatrix} \beta_i + k_\beta e_i^\beta \\ \omega_i + k_\omega e_i^\omega \end{bmatrix} = \begin{bmatrix} 1 & 0 & 0 & 0 \\ 0 & 1 & 0 & 0 \end{bmatrix} x_i + \begin{bmatrix} k_\beta & 0 \\ 0 & k_e \end{bmatrix} \begin{bmatrix} e_i^\beta \\ e_i^\omega \end{bmatrix} = C_y x_i + D_y \begin{bmatrix} e_i^\beta \\ e_i^\omega \end{bmatrix} \quad (2)$$

where $e_i^\beta$ and $e_i^\omega$ are mutually independent Gaussian white noise processes with unit intensities, and $k_\beta > 0$ and $k_\omega > 0$ are design parameters that can be used to account for different signal-to-noise ratios. It is also possible to include the internal controller state, $q_i$, in the measurement, but since this is only a filtered rotor speed measurement, it does not contain any additional information.

If the wind turbines were able to freely vary their power production, each of their control laws could be obtained by solving the following decentralized optimal control problem

$$\begin{aligned} &\text{minimize} && \mathcal{J}_i && (3a) \\ &\text{subject to} && (1) \text{ and } (2). && (3b) \end{aligned}$$

This is a standard linear quadratic Gaussian control problem and its solution is well-known [Zhou et al., 1995]. It is based on the following algebraic Riccati equations

$$A^T X + XA + C_z^T C_z - (XB_u + C_z^T D_z) R_u^{-1} (B_u^T X + D_z^T C_z) = 0 \quad (4)$$

$$AY + YA^T + B_w B_w^T - (YC_y^T + D_y B_w^T) R_w^{-1} (C_y Y + B_w D_y^T) = 0, \quad (5)$$

where $R_u = D_z^T D_z$ and $R_w = D_y D_y^T$. Their solutions, $X \geq 0$ and $Y \geq 0$, are said to be stabilizing if

$$F = -R_u^{-1}(B^T X + D_z C_z) \quad (6)$$

$$L = -(YC_y^T + B_w D_y^T) R_w^{-1} \quad (7)$$

are such that the matrices $A + BF$ and $A + LC$ are stable. The solution to (3) is then given by the observer-based control law

$$\frac{d}{dt}\chi_i(t) = (A + BF)\chi_i + L(C\chi_i - Ly_i) \tag{8a}$$

$$u_i^{\text{loc}}(t) = F\chi_i(t), \tag{8b}$$

and the value of the cost function attained under this control law is $\mathcal{J}_i = \mathcal{J}_{\text{opt}}$, where

$$\mathcal{J}_{\text{opt}} = \text{tr}(B_w^T X B_w) + \text{tr}(R_u F Y F^T).$$

Since the wind farm is required to meet a certain power demand, the wind turbines cannot apply (8) directly. Instead, they must coordinate their power production to ensure that the set-point is met. Since $u_i$ is the power deviation from the nominal production of each turbine, the power demand is satisfied if $\sum_{i=1}^{\nu} u_i = 0$. The overall control problem is defined as

$$\text{minimize} \quad \mathcal{J} = \sum_{i=1}^{\nu} \mathcal{J}_i \tag{9a}$$

$$\text{subject to} \quad (1) \text{ and } (2) \tag{9b}$$

$$\text{and} \quad \sum_{i=1}^{\nu} u_i = 0. \tag{9c}$$

## 4. Optimal control law

It can be shown[1] that the optimal solution to (9) is given by

$$u_i(t) = u_i^{\text{loc}}(t) - \frac{1}{\nu}\sum_{j=1}^{\nu} u_j^{\text{loc}}(t), \quad i = 1, \ldots, \nu, \tag{10}$$

where $u_i^{\text{loc}}$, defined by (8), is the optimal control law for the local problem (3) This means that the optimal control policy with respect to (9a) is for each wind turbine to behave without concern for the power set-point of the wind farm, and then compensate for a portion, $\frac{1}{\nu}$, of the resulting deviation. The structure of the control law is illustrated in Figure 4 for

[1] A state-feedback version of (9) was solved in [Madjidian and Mirkin, 2014]. The solution can be extended to the output-feedback case by using the separation principle [Zhou et al., 1995, Section 14.9].

a wind farm with two turbines. The turbines have their own local controllers, which compute $u_1^{\text{loc}}(t)$ and $u_2^{\text{loc}}(t)$ based on measurements $y_1$ and $y_2$, respectively. If these local control signals were applied to the wind turbines directly, they would result in a deviation, $u_1^{\text{loc}}(t) + u_2^{\text{loc}}(t)$, from the power-set point of the wind farm. This is remedied by a coordinator, which computes correction terms,

$$\frac{1}{2}(u_1^{\text{loc}}(t) + u_2^{\text{loc}}(t)),$$

to the decentralized control signals.

If the controller is implemented as suggested in Figure 4, the local control laws will be independent of the number of turbines in the farm. Adding or removing wind turbines from operation is then simply a matter of keeping track of $\nu$, which is the responsibility of the coordinator. Similarly, the wind farm coordinator does not need to know the details of the local loops. New turbines can thus be added in a plug-and-play fashion without any control redesign.

Another appealing property of the optimal control law is that it scales well as the the number of turbines grows large. In order to obtain (10), we only need to compute the local feedback and observer gains $F$ and $L$ in (8), which amounts to solving problem (3) for a single turbine. The computational effort required to obtain the solution is thus independent of the number of wind turbines in the wind farm. Moreover, the only operation required in addition to the local control laws, is a single averaging operation to form the correction terms, which can easily be performed for a very large number of turbines.

It can also be shown that the value of the cost functions under (10) is

$$\mathcal{J}_i = \mathcal{J}_{\text{opt}} + \frac{1}{\nu}(\bar{\mathcal{J}} - \mathcal{J}_{\text{opt}}), \tag{11}$$

where $\mathcal{J}_{\text{opt}}$ is the cost attained under control law (8) and $\bar{\mathcal{J}} := \text{tr}(B_w^T \bar{X} B_w)$, where $\bar{X}$ is the solution to the Lyapunov equation

$$A^T \bar{X} + \bar{X} A + C_z^T C_z = 0. \tag{12}$$

The term, $\bar{\mathcal{J}}$, is the cost that would be obtained by a wind turbine if it did not deviate from its nominal power production, i.e. if $u_i = 0$. The second term in (11) quantifies the performance degradation associated with satisfying the power demand to the wind farm. Note that, by coordinating the power production among the wind turbines, the degradation is reduced by a factor $\nu$ compared to if each turbine would maintain its nominal power production. In particular, $\mathcal{J}_i \to \mathcal{J}_{\text{opt}}$ as the number of turbines $\nu \to \infty$, which means that, in large wind farms, there is practically no trade-off between satisfying the power demand and reducing fatigue loads.

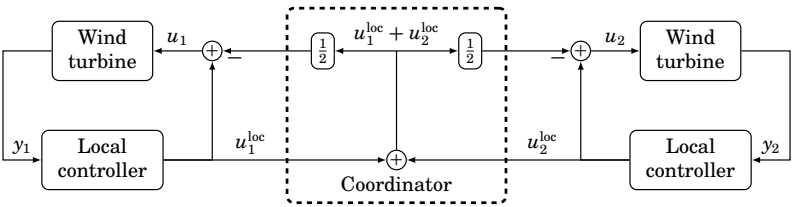


**Figure 4.** Structure of the optimal control law for a wind farm with two wind turbines. Each turbine has its own local controller, defined by (8), which communicates $u_i^{\text{loc}}$ to a wind farm coordinator. The coordinator aggregates all local control signals and returns a correction term, $-\frac{1}{v}\sum u_j^{\text{loc}}$.

Remark 4.1
In (10), the same correction term is applied all of the wind turbines. A natural extension of this control law is to introduce a different correction allocation. This is done by replacing (10) with

$$u_i(t) = u_i^{\text{loc}}(t) - \beta_i \sum_{j=1}^{v} u_j^{\text{loc}}(t), \quad i = 1, \ldots, v, \tag{13}$$

where $\beta_i > 0$ and $\sum_{i=1}^{v} \beta_i = 1$. It can be shown that (13) is the optimal control law with respect to minimizing $\sum_{i=1}^{v} \beta_i^{-1} \mathcal{J}_i$, and that the cost attained by this control law is

$$\mathcal{J}_i = \mathcal{J}_{\text{opt}} + \beta_i^2 v(\bar{\mathcal{J}} - \mathcal{J}_{\text{opt}}).$$

Control law (13) provides a method to trade off the fatigue reduction between the turbines. A low value on $\beta_i$ reflects a high priority on load reduction for the $i$th turbine. Note that, the only additional complexity brought about by (13) is that, instead of the single parameter, $v$, the coordinator needs to manage $v$ parameters $\beta_1, \ldots, \beta_v$. □

## 5. Simulation example

In this section we simulate[2] a wind farm with five NREL 5 MW wind turbines. Recall that each wind turbine operates around a mean wind speed of 10 m/s and a nominal power production of 2 MW, which is 1.48 MW below its nominal power production ability. See Figure 2. The power demand to the wind farm is 10 MW.

[2] The simulations are performed in Simulink®, where we use the wind turbine model implementation in [SimWindFarm, 2014].

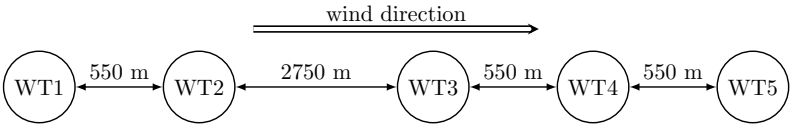


**Figure 5.** Position of the wind turbines in relation to the wind direction during the data collection. For each turbine, nine wind speed sequences of ten minutes were estimated. Since the estimated wind speeds are based on data collected from neighboring wind turbines, they account for possible correlation effects, which were neglected during the control design.

In order to provide realistic simulations, the wind speed variations are estimated from real wind farm data. The data was collected from a commercial wind farm consisting of Vestas V90 3 MW wind turbines. During the data collection the turbines operated in Region 2 where they produce maximum power. In this mode of operation, the power production is approximately a cubic function of the wind speed. The wind speed at a wind turbine was estimated as $v = (p/k)^{\frac{1}{3}}$, were $p$ is the power production of the turbine and the coefficient $k$ was obtained by using the Vestas V90 power curve in [Vestas V90, 2014]. The wind direction during the data collection is illustrated in Figure 5. It is parallel to the row of turbines, which implies that the estimated wind speeds account for possible correlation effects, which were neglected in the control design. A total of nine different ten minute effective wind speed sequences were estimated for each wind turbine. Figure 6 shows one of these sequences together with the measured nacelle wind speed.

For each wind speed sequence, we simulated the response of the wind farm under the control law (10). Based on a trial and error approach, the weights were chosen as

$$k_u = 10^{-5} \quad k_\beta = 1.5 \quad \text{and} \quad k_e = 10^{-4}.$$

For comparison, we also simulated the case where the turbines do not deviate from their nominal power references, i.e. $u_i = 0$, $i = 1,\dots,5$. After each simulation, the accumulated fatigue to each of the wind turbine towers was computed as follows.

1. Use the rain-flow counting algorithm in [Hammerum, 2006] to extract equivalent stress cycles, $s_1,\dots,s_r$, from the history of the fore-aft tower bending moment.

2. The fatigue caused by a stress cycle number $l$ is computed based on the S/N-curve as $s_l^k$, where we use $k = 4$, which is typical for steel

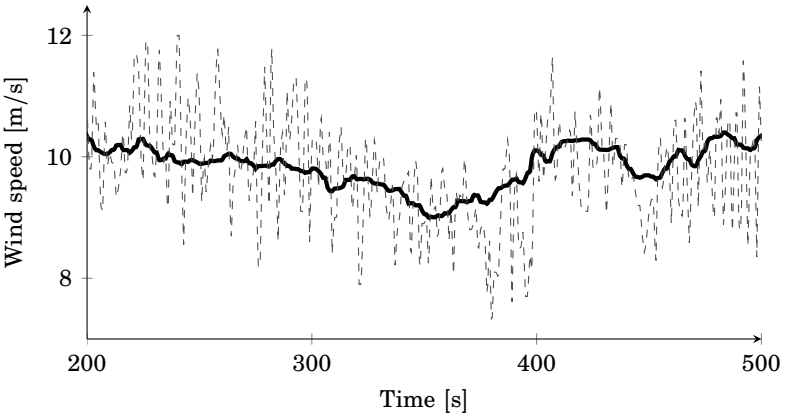


**Figure 6.** Estimated wind speed (solid black) and measured nacelle wind speed (dashed gray) at one of the turbines in the wind farm

structures [Manwell et al., 2009]. The total fatigue is then calculated according to Palmgren-Miner's rule as $\sum_{l=1}^{r} s_l^k$.

Table 1 summarizes the outcome from the nine different simulations. On average, the accumulated fatigue damage was 35% lower when using the control law (10), compared to the case when the turbines maintained their nominal power production. Figure 7 shows the increase in accumulated fatigue during one of the simulations.

The response of one of the wind turbines to one of the wind speed sequences is shown is Figure 8. An illustrative period starts after approximately 300s, when the wind speed suddenly drops. To avoid exciting the tower bending dynamics, the local wind turbine controller tries to lower the power production, which is indicated by the drop in $u_3^{\text{loc}}$. The actual power production of the turbine, after applying the correction from the coordinator (see Figure 4), is shown by the blue curve. The effect of reducing the power production of the turbine is that a large peak in tower bending moment is avoided.

In Figure 8, the desired power adjustments of the wind turbine $u_3^{\text{loc}}$ are in the same direction as the wind speed variations. This is a consistent phenomenon across all simulations and can be explained as follows. A drop in wind speed reduces the aerodynamic torque and has a decelerating effect on the rotor speed. In order to maintain rated speed, the internal wind turbine controller decreases the pitch angle, which in turn excites the tower bending dynamics. The benefit of reducing the power reference is that it helps the speed regulation by forcing the internal controller to

**Table 1.** Reduction in accumulated fatigue damage (%) when using control law (10).

| Sequence | 1 | 2 | 3 | 4 | 5 | 6 | 7 | 8 | 9 |
|---|---|---|---|---|---|---|---|---|---|
| Turbine 1 | 52 | 40 | 38 | 23 | 62 | 37 | 30 | 18 | 13 |
| Turbine 2 | 45 | 36 | 46 | 43 | 61 | 46 | 57 | 61 | 52 |
| Turbine 3 | 25 | 32 | 35 | 20 | 27 | 32 | 42 | 37 | 36 |
| Turbine 4 | 46 | 15 | 24 | 19 | 25 | 25 | 18 | 35 | 50 |
| Turbine 5 | 29 | 29 | 46 | 17 | 37 | 46 | 22 | 22 | 27 |
| Mean | 39 | 30 | 38 | 25 | 43 | 37 | 33 | 35 | 36 |

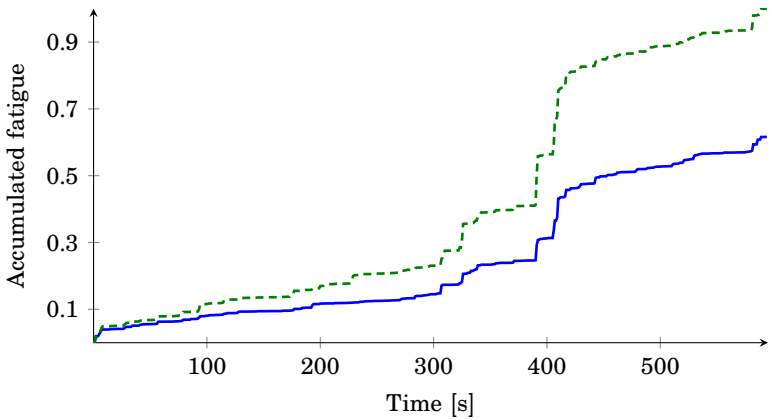


**Figure 7.** Normalized average accumulated fatigue for the five turbines during one of the simulations. With wind farm controller (solid blue) and when each wind turbine maintains a production of 2 MW (dashed green).

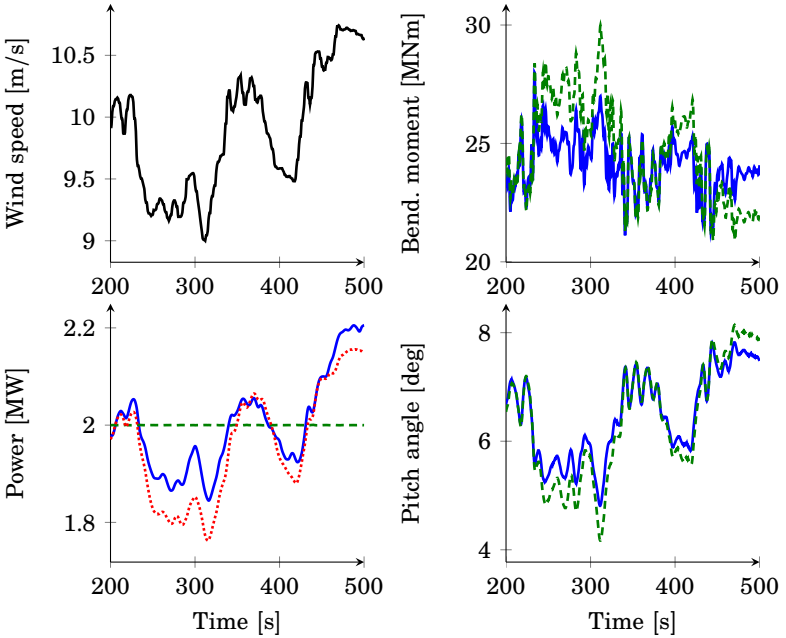


**Figure 8.** Response of wind turbine 3 to the wind speed in the upper left plot. With wind farm controller (solid blue) and when each turbine maintains a production of 2 MW (dashed green). The red dotted curve shows the desired power production $u_3^{\text{loc}}$. At time 300 s, the wind speed drops. To maintain the rated rotor speed, the internal wind turbine controller is required to reduce the pitch angle, which in turn excites the tower bending dynamics. In the case when the turbines maintain their nominal power productions, this leads to a large peak in tower bending moment. By allowing the turbine to reduce its power, the wind farm controller (10) manages to reduce the peak. The benefit of reducing the power reference is that it forces the internal controller to reduce the generator torque. This helps the speed regulation loop, which in turn reduces the required amount of pitch and consequently, leads to less excitation of the tower dynamics.

reduce the generator torque. This reduces the required amount of pitch activity and leads to less tower bending. For a more extensive discussion on the mechanisms behind the load reduction, see [Madjidian et al., 2013].

Figure 9 shows the power production for all five wind turbines from one of the simulations.The actual power production follows the local control signals, $u_i^{\text{loc}}$, relatively well, which is a consistent phenomenon across all the simulations. The lower left plot shows the total power production in the wind farm. The production when using (10) is inseparable from the

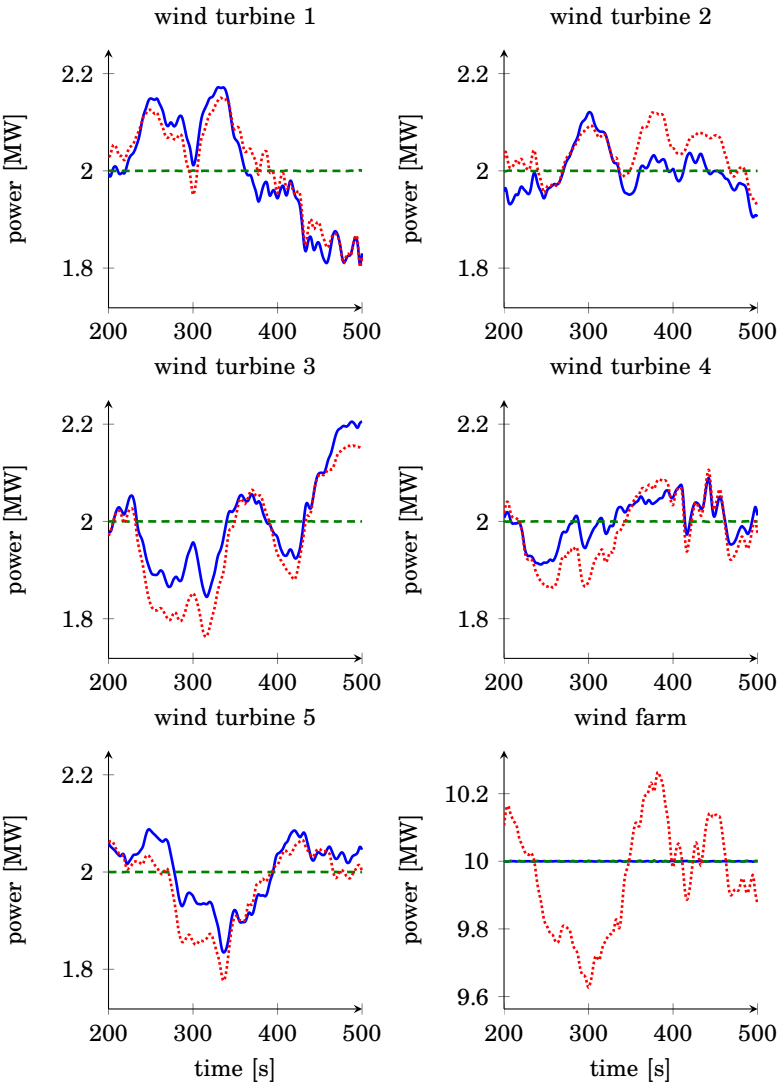


**Figure 9.** The first five plots show the power production for the wind turbines in one of the simulations. With the wind farm controller (10) (solid blue) and when each turbine maintains a production of 2 MW (dashed green). The dotted red curve shows the local control signals $u_i^{\text{loc}}$. The lower right plot, shows the total power production of the turbines. Note that the total power production under (10) is practically inseparable from the reference case. The red curve shows the sum of the desired power references $\sum_{i=1}^{5} u_i^{\text{loc}}$.

case when the wind turbines maintain their nominal power reference.

## 6. Conclusions

We consider controlling a wind farm that is required to meet a power set-point. The goal is to reduce the fatigue loads to the tower of the wind turbines, while satisfying the power demand. Our approach relies on two assumptions: that wind turbines are identical in their design and operating points, and that the wind speed variations that they experience are uncorrelated. Based on these assumptions, the control design problem can be formulated as an optimal coordination problem among homogeneous agents, which was solved in [Madjidian and Mirkin, 2014].

The resulting wind farm controller has an intuitive structure. Each wind turbine has a control law, which is divided into two parts. The first is a decentralized control law that tries to minimize the loads without concern for the power set-point, and the second is a correction term that compensates for deviations from the set-point. The correction term is simply the average of the decentralized terms and is the same for all wind turbines.

The structure of the controller has important implications. First, it can be applied regardless of the number of wind turbines in the wind farm. This is because in order to form the control law, it is only necessary to solve an optimization problem for a stand-alone wind turbine. Also, the only centralized operation required to implement the control law is a single averaging operation to form the correction terms, which can easily be performed for any realistically sized wind farm. Second, since the local control loops do not depend on the number of units in the wind farm, wind turbines can be added or removed from operation in a plug and play manner without the need to redesign the controller. Third, it is possible to give an expression for how the load reduction improves as the number of turbines increases, which further adds to the transparency of the control law. In particular, for wind turbines operating in large wind farms, there is practically no trade-off between satisfying the power-set point and reducing fatigue loads.

The control law was evaluated in a simulation study based on wind speeds that were estimated from real wind farm data. It should be noted that, since the wind speeds were estimated using data collected from neighboring wind turbines, they account for possible correlation effects which were neglected during the control design. The proposed control law resulted in an average fatigue load reduction of 35% compared to if each wind turbine had maintained their nominal power reference.

## Acknowledgements

This work was supported by the Swedish Research Council through the LCCC Linnaeus Center and by the European commission through the project AEOLUS.

## References

Biegel, B., D. Madjidian, V. Spudić, A. Rantzer, and J. Stoustrup (2013). "Distributed low-complexity controller for wind power plant in derated operation". In: *Proceedings of the 2013 IEEE Multi-Conference on Systems and Control*. Hyderabad, India, pp. 146–151.

Danish Government (2011). *Our future energy*. ISBN 978-87-7844-915-3. URL: http://www.cphcleantech.com/media/1465822/our_future_energy.pdf.

de Almeida, R. G., E. Castronuovo, and J. A. P. Lopes (2006). "Optimum generation control in wind parks when carrying out system operator requests". *IEEE Transactions on Power Systems* **21**:2.

European Comission (2006). *A European strategy for sustainable, competitive and secure energy*. COM(2006) 105 final. URL: http://europa.eu/documents/comm/green_papers/pdf/com2006_105_en.pdf.

Grunnet, J., M. Soltani, T. Knudsen, M. Kragelund, and T. Bak (2010). "Aeolus toolbox for dynamic wind farm modeling, simulation and control". In: *Proceedings of the 2010 European Wind Energy Conference*, pp. 3119–3129.

Hammerum, K. (2006). *A Fatigue Approach to Wind Turbine Control*. M.Sc. Thesis IMM-Thesis-2006-105. Technical University of Denmark.

Jonkman, J., S. Butterfield, W. Musial, and G. Scott (2009). *Definition of a 5-MW Reference Wind Turbine for Offshore System Development*. Tech. rep. NREL/TP-500-38060. National Renewable Energy Laboratory, Golden, CO.

Klessmann, C., C. Nabe, and K. Burges (2008). "Pros and cons of exposing renewables to electricity market risks — a comparison of the market integration approaches in Germany, Spain, and the UK". *Energy Policy* **36**:10, pp. 3646–3661.

Kristalny, M., D. Madjidian, and T. Knudsen (2013). "On using wind speed preview to reduce wind turbine tower oscillations". *IEEE Transactions on Control Systems Technology* **21**:4, pp. 1191–1198.

Madjidian, D. and L. Mirkin (2014). "Distributed control with low-rank coordination". *IEEE Transactions on Control of Network Systems* **1**:1, pp. 53–63.

Madjidian, D., M. Kristalny, and A. Rantzer (2013). "Dynamic power coordination for load reduction in dispatchable wind power plants". In: *Proceedings of the 2013 European Control Conference*. Zürich, Switzerland, pp. 3554–3559.

Manwell, J., J. McGowan, and A. Rogers (2009). *Wind Energy Explained*. 2nd ed. John Wiley & Sons, Chichester, UK.

SimWindFarm (2014). *Aeolus SimWindFarm Toolbox*. Retrieved 2014-04-16. URL: http://www.ict-aeolus.eu/SimWindFarm/index.html.

Spudić, V. and M. Baotić (2013). "Fast coordinated model predictive control of large-scale distributed systems with single coupling constraint". In: *Proceedings of the 2013 European Control Conference*, pp. 2783–2788.

Spudić, V., M. Jelavić, and M. Baotić (2011). "Wind turbine power references in coordinated control of wind farms". *Automatika – Journal of Control, Measurements, Electronics, Computing and Communications.* **52**:2, pp. 82–94.

U.S. Department of Energy (2008). *20% wind energy by 2030: increasing wind energy's contribution to U.S. electricity supply*. DOE/GO-102008-2567. URL: http://www.nrel.gov/docs/fy08osti/41869.pdf.

Vestas V90 (2014). *Vestas V90 brochure*. Retrieved 2014-04-19. URL: http://vestas.com/en/products_and_services/turbines/v90-3_0_mw.

Vigueras-Rodríguez, A., P. Sørensen, A. Viedma, M. Donovan, and E. Gómez Lázaro (2012). "Spectral coherence model for power fluctuations in a wind farm". *Journal of Wind Engineering and Industrial Aerodynamics* **102**, pp. 14 –21.

Zhou, K., J. C. Doyle, and K. Glover (1995). *Robust and Optimal Control*. Prentice-Hall, Englewood Cliffs, NJ.

# Paper V

# A Stationary Turbine Interaction Model for Control of Wind Farms

**Daria Madjidian  Anders Rantzer**

**Abstract**

Turbines operating in wind farms are coupled by the wind flow. This coupling results in limited power production and increased fatigue loads on turbines operating in the wake of other turbines. To operate wind farms cost effectively, it is important to understand and address these effects. In this paper, we derive a stationary model for turbine interaction. The model has a simple intuitive structure, and the parameters a clear interpretation. Moreover, the effect of upwind turbines on a downwind turbine can be completely determined through information from its closest neighbor. This makes the model well suited for distributed control. In an example, we increase total power production in a farm, by coordinating the individual power production of the turbines. The example points to an interesting model property: decreasing power in an upwind turbine causes downwind turbines to pose less of an obsticle for the wind, provided that they maintain their level of power capture.

# 1. Introduction

While economy of scale makes it attractive to position turbines close to each other in wind farms, such a placement causes problems. When a turbine extracts power from the wind, it disturbs the wind flow behind it. This creates a coupling with turbines operating in its wake. The wind in a wind turbine wake is characterized by a mean wind speed deficit and an increased turbulence level. Consequently, upwind turbines limit power production and increase fatigue loads on downwind turbines.

In order to operate wind farms cost effectively in terms of power production and maintenance costs, it is important to understand and address the issue of aerodynamic coupling. Thus far, this problem has received little attention from a control perspective (see [Pao and Johnson, 2009]). The reason for this is mainly due to the difficulty in obtaining wind farm wake models suitable for control design.

## 1.1 Previous Work

Existing wake models are usually not developed for control purposes. Since wake modeling is a large research field, a full investigation is beyond our scope. Therefore, only a partial overview is provided below.

A survey made by [Crespo et al., 1999], classifies existing wake models into three subclasses: field models, kinematic models, and roughness element models.

Field models describe the wind speed at every point in the flow field, which makes them computationally expensive. Kinematic models provide simpler expressions than field models. They usually begin with the modeling of a single wake, by using conservation of momentum. Merged wakes are then most often described by superimposing the individual wakes on the ambient flow field. Opinions on how this should be done vary, and not all kinematic models are able to handle large wind farms ([Crespo et al., 1999]). The ones that can, are sometimes based on assumptions that make them unsuitable for control purposes. For instance, [Jensen, 1983], and [Frandsen et al., 2006], both assume fixed and uniform values on thrust coefficients. However, a change in power reference at a turbine, means that the value of the thrust coefficient also changes.

Roughness element models describe the response of the ambient wind flow to a sudden change in roughness. These models are further divided into infinite cluster models, and finite cluster models.

Infinite cluster models (e.g. [Frandsen, 1992]) aggregate the effect of all turbines, and describe the entire wind farm as one roughness element. This results in an overall (“average”) wind profile for the farm, but the individual effect of turbines is lost.

A survey by [Bossayani et al., 1980] compares different roughness element models, and explains how infinite cluster models are modified to finite cluster models. As opposed to modeling the farm as a single roughness element, the finite cluster models describe the wind speed at each row of turbines perpendicular to the incoming wind direction. In order to handle wind farms of any size, all models in the survey introduce a rate of replenishment, describing the influx of momentum (or power) from the free flow.

### 1.2 Contributions and Outline

Here, we take a new approach to deriving a stationary wind farm control model for turbines arranged in a row. The turbine interaction (wake) part captures both wind speed deficits and increased turbulence levels. The assumption is that each upwind turbine adds to deficits and turbulence levels at all turbines further downwind. The result is a turbine interaction model, that maps thrust coefficients, wind speeds, and turbulence levels at upwind turbines, to wind speeds and turbulence levels at downwind turbines. The structure of the model is intuitive, and the parameters have a clear interpretation. The model also reflects the spatially distributed structure of a wind farm, in the sense that the effect on a turbine from all other turbines can be completely determined through information from its closest upwind neighbor. This makes the model a good candidate for distributed control, which is especially important as the number of turbines in wind farms increases.

A wind farm model consists of three parts: a model for the ambient wind entering the farm, turbine models, and a model describing the aerodynamic interaction between the turbines. The interaction model constitutes the main part of this paper and is presented in Section 2. Section 3 begins by describing the ambient wind and the turbines. It then links these models with the interaction model to form a complete model of the farm. In Section 4, we present an example where we increase total power production by coordinating the power production of the turbines. Finally, we point to an interesting result: by decreasing power production in an upwind turbine, all downwind turbines can reduce their thrust while maintaining the same power capture.

## 2. Wind Turbine Interaction

The basic mechanisms behind turbine interaction are explained in [Burton et al., 2001]. Each turbine extracting power produces a wake, characterized by a mean wind speed deficit and an increased turbulence level. Since the thrust coefficient determines the momentum extracted from the

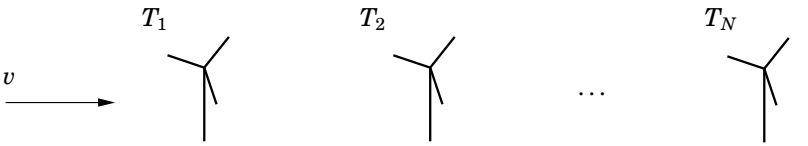


**Figure 1.** Row of turbines

flow, it is directly linked to the mean speed deficit. The wind speed gradient between the wake and the free stream results in additional shear generated turbulence. Therefore, the thrust coefficient is also directly related to the added wake turbulence. The shear generated turbulence transfers momentum from the free flow to the wake and causes the wake to expand. Therefore, as the wake travels downstream, it gradually becomes wider but shallower until the flow has fully recovered far downstream. It should also be noted that in addition to shear generated turbulence, the turbine also generates turbulence directly. This extra component is caused by the vortices shed by the blades, and from having placed an object (the turbine) in the wind field. However, this type of turbulence decays quickly, and (due the the long distances between turbines in farms) does not add significantly to turbulence levels at downwind turbines.

Our goal is to develop a model of turbine interaction, with the additional property that the wind speed at a turbine can be determined from information available at its closest neighbors. We tailor our model to a farm consisting of a row of $N$ equidistant turbines, where the mean values of the thrust coefficients are between 0 and 1. We do not consider wake meandering, and therefore assume that the wind direction is parallel to the row of turbines at all times. The setup is shown in Figure 1.

To capture the structure of aerodynamic coupling between turbines, we need a model where upwind turbines add to the wind speed deficits and turbulence levels of downwind turbines. Based on the discussion above, the deficit and turbulence that a turbine adds at another turbine depend on the thrust coefficient of the upwind turbine and the distance between the two turbines. A large thrust coefficient implies that more momentum is extracted from the flow. Therefore, both deficit and added turbulence should increase when the thrust coefficient increases. Since ambient wind flow strives to reduce wake effects, the deficit and added turbulence should decrease with the distance between turbines.

We also impose additional standard requirements on the model (see [Frandsen et al., 2006] and [Frandsen, 2007]).

i Mean wind speeds at all turbines must positive, and not above ambient

mean wind speed. In addition, in an infinitely long row of turbines, where all turbines extract maximum amount of power, there exists an asymptotic wind speed.

ii Turbulence levels at all turbines must be bounded from below by ambient turbulence intensity, and bounded from above.

We now present the interaction model. Let $v$ be the ambient mean wind speed, and denote the thrust coefficient of turbine $n$ as $C_{T_n}$. A model for the deficit experienced by turbine 2 in the row is given by:

$$v_2 = (1 - k_1 C_{T_1})v$$

where $k_1 > 0$ is a distance parameter. The larger the distance between the turbines, the smaller $k_1$ will be.

Turbine 2 and 3 will be in the wake of the turbine 1. Suppose for a moment, that turbine 2 is switched off, which implies $C_{T_2} = 0$. The deficit at the third turbine can then be modeled as:

$$v_3 = (1 - k_2 C_{T_1})v$$

where $k_2 \in (0, k_1)$. This implies $v_3 > v_2$, and the first turbine therefore shapes the wind field around the second and third turbine non-uniformly. To take this into account when merging the wakes of turbine 1 and turbine 2, we add their effects:

$$v_3 = (1 - k_1 C_{T_2} - k_2 C_{T_1})v$$

Similarly, the deficit at turbine number $n + 1$ can be expressed as:

$$v_{n+1} = (1 - k_1 C_{T_n} - \ldots - k_n C_{T_1})v \tag{1}$$

where $0 < k_n < \ldots < k_1$. The model implies that upwind turbines, $1, \ldots, n$, subtract wind from a downwind turbine, $n + 1$, according to their thrust coefficients and their distance to turbine $n + 1$.

As stated earlier, we want a model where the wind speed at a turbine can be determined from information available at its closest upwind neighbor. This can be achieved if the deficit decays exponentially with distance. For the time being we will assume that this is the case, and relax the assumption later on. Let $k = k_1$, and $k_i = k^i,\ i = 2, \ldots$, and define

$$z_n = \sum_{i=1}^{n} k^i C_{T_{(n+1-i)}}$$

Then, (1) can be written recursively:

$$\begin{aligned} v_{n+1} &= (1 - z_n)v = (1 - kC_{T_n} - kz_{n-1})v \\ &= (1 - kC_{T_n})v - kv + k(1 - z_{n-1})v \\ &= (1 - kC_{T_n})v - k(v - v_n) \end{aligned} \tag{2}$$

The first term on the right hand side describes the deficit caused by the closest neighbor $n$, whereas the second term describes the total deficit caused by other upwind turbines.

By defining the relative mean deficit at turbine $n$ as:

$$\delta_n = \frac{v - v_n}{v} \tag{3}$$

we can express (2) as:

$$\delta_{n+1} = k\delta_n + kC_{T_n}$$

This gives a new interpretation. The wind speed deficit at a turbine depends on the deficit at the previous turbine, and the direct effect of the previous turbine.

We can also rewrite (2) as

$$v_{n+1} = v_n + \underbrace{(1 - k)(v - v_n)}_{\text{recovery}} \underbrace{-kvC_{T_n}}_{\text{effect of neighbor}} \tag{4}$$

which states that the wind speed at a turbine depends on the wind speed at the previous turbine, a deficit dependent recovery term, and the direct effect of the previous turbine.

The wind speed at turbine $n$, will be described as a mean wind speed with turbulent fluctuations, $w_n(t)$, superimposed:

$$v_n + w_n(t)$$

where $w_n$ is a zero mean stationary process, with variance $\sigma_n^2$. Again, assuming an exponential decay in added wake turbulence, with the same distance parameter $k$, we can model the dependence of $\sigma_{n+1}$ on upwind turbines as:

$$\begin{aligned} \sigma_{n+1} &= (1 + kC_{T_n} + \cdots + k^n C_{T_1})\sigma \\ &= \sigma + k\sigma C_{T_n} + \frac{k\sigma}{v}(v - v_n) \end{aligned} \tag{5}$$

where $\sigma^2$ is the variance of the incoming ambient wind speed. Equation (5) states that the added turbulence at a turbine depends on the deficit at the previous turbine, and the direct effect of the previous turbine.

Even though the assumption on exponential decay is arbitrary, (4) and (5) still give an idea of how to obtain a parametrized stationary turbine interaction model. To allow more flexibility, we separate the terms by introducing one distance parameter for each:

$$v_{n+1} = v_n + k'(v - v_n) - kvC_{T_n} \tag{6}$$

$$\sigma_{n+1} = \sigma + \frac{c'\sigma}{v}(v - v_n) + c\sigma C_{T_n} \tag{7}$$

where $k'$, $k$, $c'$, and $c$ are all positive.

REMARK 2.1
By using (3), (6) can be expressed as a first order system:

$$\delta_{n+1} = (1 - k')\delta_n + kC_{T_n} \tag{8}$$

The speed of recovery corresponds to the pole of the system: $1 - k'$. □

Expressions (6) and (7) give an intuitive map from thrust coefficients, distance, ambient mean wind speed, and ambient wind speed variation to mean wind speeds and wind speed variations at the turbines. Deficit and added turbulence both increase with thrust coefficients and decrease with distance. The speed of recovery can be tuned through $k'$ and $c'$, and the effect of the nearest upwind neighbor can be tuned through $k$, and $c$.

By using requirements i) and ii) stated earlier in this section, we can provide some bounds on $k$ and $k'$.

Requirement i) states that $v_n \leq v$, for $C_{T_n} \in [0,1]$, $n = 1,\ldots,N$, and any $N \in \mathbb{N}$. Since $v_n = (1 - \delta_n)v$, the requirement translates to $\delta_n \geq 0$. From (8) we note that this is satisfied *if and only if* $k' \leq 1$.

Let $C_{T_n} = 1$, $n = 1,\ldots,N$. Then $v_n > 0$ is satisfied if and only if $\delta_n < 1$. If $k' \in (0,1]$, from (8) we see that $\exists \bar{\delta} > 0$, such that $\delta_n < \bar{\delta}$, $n = 1,\ldots$, and $\lim_{n\to\infty} \delta_n = \bar{\delta}$. $\bar{\delta}$ satisfies

$$\bar{\delta} = (1 - k')\bar{\delta} + k \Rightarrow \bar{\delta} = \frac{k}{k'}$$

The asymptotic wind speed is given by $\bar{v} = (1 - \bar{\delta})v$. We have that, $\bar{v} > 0$, *if and only if*

$$0 < k < k' \leq 1 \tag{9}$$

Since $c'$ and $c$ are positive, (9) also implies $\sigma_n \geq \sigma$, and that there is $\bar{\sigma} > 0$ such that $\sigma_n < \bar{\sigma}$ for $n = 1,\ldots,N$, and any $N \in \mathbb{N}$.

This shows that requirement i) and ii) are satisfied if and only if (9) holds.

REMARK 2.2
The model can be made more general. First, the equidistance assumption is not necessary. Different distances can be handled, by introducing $k_{i,j}$ to model the coupling between turbines $i$ and $j$, and assuming that the deficit decay satisfies

$$k_{i,j} = \prod_{l=0}^{j-1} k_{(i+l,i+l+1)}, \quad \text{for } j > i$$

Also, the term $C_{T_i}$ in (1), can be replaced by a more general expression $f_i(C_{T_i})$, where $f_i$ is monotonically increasing and

$$f_i : \quad [0,1] \to [0,1]$$

Similarly, when modeling turbulence levels, we can introduce $g_i(C_{T_i})$, where $g_i$ is monotonically increasing and

$$g_i : \quad [0,1] \to \mathbb{R}_+$$

Proceeding the same way as above results in:

$$v_{n+1} = v_n + k'_{n,n+1}(v - v_n) - k_{n,n+1} v f_n(C_{T_n})$$
$$\sigma_{n+1} = \sigma + \frac{c'_{n,n+1}\sigma}{v}(v - v_n) + c_{n,n+1}\sigma g_n(C_{T_n})$$

where $k'_{n,n+1}$, $k_{n,n+1}$, $c'_{n,n+1}$, and $c_{n,n+1}$ are all positive. □

## 3. Wind Farm Model

It is common practice to model the wind speed at a turbine as a mean wind speed, $v$, with fluctuations, $w$, superimposed. The fluctuations have zero mean when averaged over a period of about 10 minutes ([Burton et al., 2001]). This makes it natural to model incoming wind speed at a turbine as:

$$v + w(t)$$

where $v$ denotes the 10 minute wind speed, and $w$ is a stationary Gaussian process with zero mean, and variance $\sigma^2$. The standard deviation $\sigma$ is usually defined implicitly through the *turbulence intensity* $T_i$, and the relation is:

$$T_i = \frac{\sigma}{v}$$

In order for a turbine to extract power, it needs to interact with the wind. The total wind power passing through the area swept by the turbine rotor is given by:

$$P_{\text{wind}} = \frac{1}{2}\rho\pi R^2 v^3$$

where $\rho$ is the density of the air, and $R$ is the rotor radius. The power, $P$, extracted by the turbine, depends on the pitch angle $\beta$, and tip speed ratio $\lambda$:

$$P = C_P(\lambda, \beta)P_{\text{wind}}$$

$C_P$ is the *power coefficient* of the turbine, and determines the portion of total wind power that is extracted. The tip speed ratio is defined as:

$$\lambda = \frac{R\omega_r}{v}$$

where $\omega_r$ is the angular velocity of the rotor.

We define the *available power*, $P_a$ at the turbine as the maximum amount of power that the turbine can extract:

$$P_a = \min(C_{P,\max}P_{\text{wind}}, P_{\max}) \tag{10}$$

where $C_{P,\max}$ is the peak of the $C_P$ curve, and $P_{\max}$ is the rated extracted power for the turbine.

There will also be a thrust force $F_T$ on the rotor:

$$F_T = \frac{1}{2}\rho\pi R^2 C_T(\lambda, \beta)v^2$$

$C_T$ is called the *thrust coefficient*, and depends on tip speed ratio and pitch angle. As discussed in Section 2, the thrust coefficient is directly linked to the wind speed deficit and added turbulence that the turbine induces downwind.

Each turbine has a control variable, $u$, which can be generator torque and/or pitch angle for an uncontrolled turbine, or e.g. power reference for a power controlled turbine (see Section 4). By manipulation of $u$, tip speed ratio and pitch angle can be controlled. Assuming that the mapping

$$(u, v) \to (\lambda, \beta)$$

is well defined, we can define

$$c_P(u, v) = C_P(\lambda(u, v), \beta(u, v))$$
$$c_T(u, v) = C_T(\lambda(u, v), \beta(u, v))$$

Given ambient mean wind speed $v$, and ambient turbulence intensity $T_i$, the model for turbine $n + 1$ along the row is given by:

$$\begin{aligned}
P_{n+1} &= \frac{1}{2}\rho\pi R^2 c_P(u_{n+1}, v_{n+1})v_{n+1}^3 \\
y_{n+1} &= f(u_{n+1}, v_{n+1}, \sigma_{n+1}) \\
v_{n+1} &= v_n + k'(v - v_n) - kvc_T(u_n, v_n), \quad v_1 = v \\
\sigma_{n+1} &= \sigma + \frac{c'\sigma}{v}(v - v_n) + c\sigma c_T(u_n, v_n), \quad \sigma_1 = T_i v
\end{aligned}$$

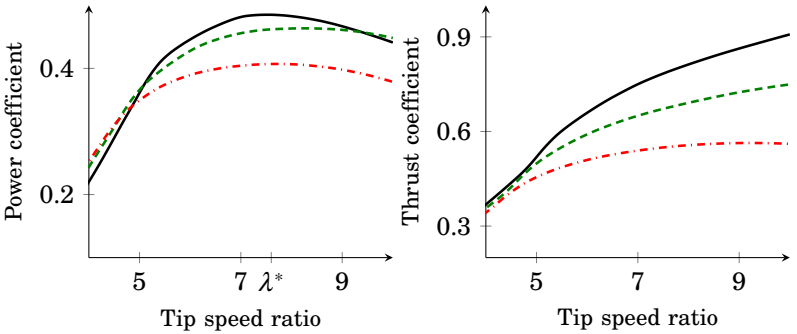


**Figure 2.** Power and thrust coefficient for the NREL 5 MW turbine. Solid: $\beta = 0^o$, dashed: $\beta = 2^o$, dash-dotted: $\beta = 4^o$. $\lambda^* = 7.6$, $\beta^* = 0^o$

where $y_n$ represents outputs of interest for turbine $n$ (e.g. a measure of fatigue loading), and $c_P$ and $c_T$ are the power and thrust coefficients as a function of control action $u_n$, and mean wind speed $v_n$.

## 4. Examples

### 4.1 NREL turbines

The wind farm in the examples below will consist of NREL 5 MW turbine models. The turbines are variable speed and pitch controlled, and described in detail in [Jonkman et al., 2009], and [Grunnet et al., 2010]. The generator has an efficiency of $\mu = 0.944$ which implies $P_{\max} = 5/\mu = 5.30$ MW. Power and thrust coefficients are shown in Figure 2.

We assume that each turbine is equipped with a standard controller that manipulates generator torque and pitch angle. The controller has three regions of operation, illustrated by Figure 3. In region 1, the wind speed is too low to produce power. In region 2, the controller tries to extract maximum power. This is done by fixing the pitch angle to the optimal angle for power capture, $\beta^*$. $\beta^*$ is the value that results in the highest value of the power coefficient (see Figure 2). The controller then varies generator torque to track the optimal tip speed ratio, $\lambda^*$. In region 3, the controller strives to maintain a power reference, $u$. This is achieved by keeping the rotational speed close to $\omega_r = \min(\frac{\lambda^* v}{R}, \omega_{r,\text{rated}})$ by varying the pitch angle, where $\omega_{r,\text{rated}}$ is the rated rotor speed. The generator torque is used to produce the desired power.

On farm level, the control input to a turbine is the power reference $u$.

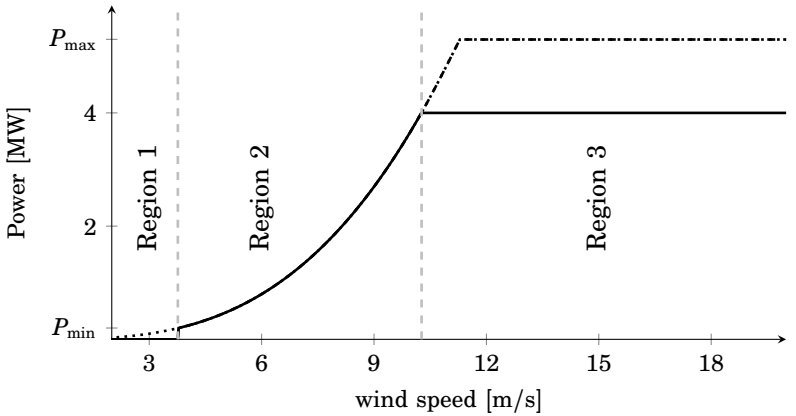


**Figure 3.** Power capture curve for the NREL 5 MW turbine. $u = 4$ MW (solid), maximum power capture (dashed), power available in the wind, $C_{\mathrm{P,max}} P_{\mathrm{wind}}$ (dotted). The gray dotted lines show the operating regions for the controller.

A turbine will only respond to farm control if

$$P_{\min} \leq u \leq P_a$$

where $P_{\min}$ is the lowest level of power production a turbine can sustain, and the available power $P_a$ is given by (10). This corresponds to operation in region 3.

Figures 4 and 5 show the power and thrust coefficients as function of power reference and wind speed. The high valued flat part of the curves correspond to operation in region 2. The slanting part of the curves correspond to operation in region 3.

## 4.2 Wind field parameters

Let incoming mean wind speed be 11 m/s, and ambient turbulence intensity 0.1. The coupling parameters are set to $k' = c' = 0.35$, $k = 0.1$, and $c = 0.92$. This means that if all turbines would operate in region 2, the second turbine would experience a mean wind speed deficit of 8%. The asymptotic mean wind speed deficit far downwind would be 22%. If we define the turbulence intensity at turbine $n$, as

$$T_{\mathrm{i,n}} = \frac{\sigma_n}{v}$$

the second turbine would experience a turbulence intensity of 0.17. The asymptotic turbulence intensity far downwind would be 0.3.

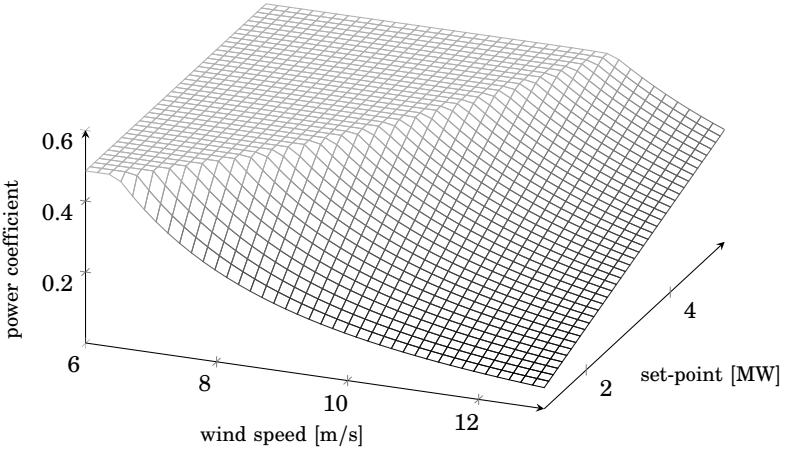


**Figure 4.** Power coefficient for the NREL 5 MW turbine as function of wind speed and power reference.

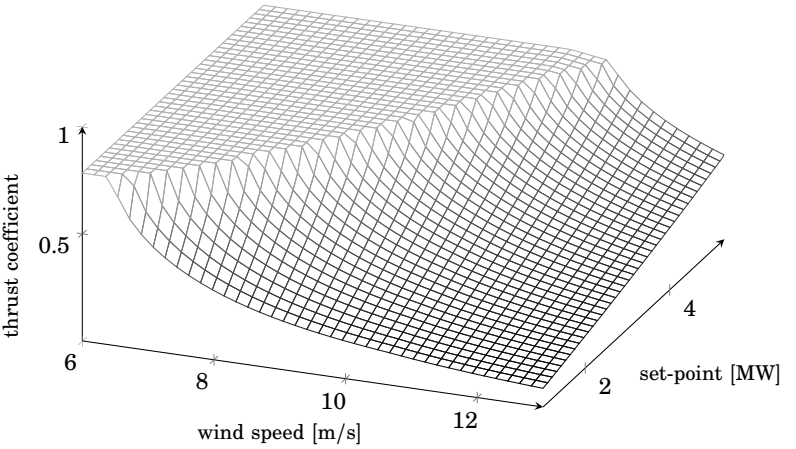


**Figure 5.** Thrust coefficient for the NREL 5 MW turbine as function of wind speed and power reference.

**Table 1.** Power extracted in each turbine (MW)

| $i$ | $P_i$ | $P_{\mathrm{a,i}}$ | $P_i/P_{\mathrm{a,i}}$ | $P^0_{\mathrm{a,i}}$ | $P_i - P^0_{\mathrm{a,i}}$ | $\sigma_i/\sigma^0_i$ |
|---|---|---|---|---|---|---|
| 1 | 4.76 | 4.92 | 0.97 | 4.92 | -0.16 | 1.00 |
| 2 | 3.72 | 3.97 | 0.94 | 3.87 | -0.15 | 0.96 |
| 3 | 3.21 | 3.47 | 0.93 | 3.26 | -0.048 | 0.93 |
| 4 | 2.95 | 3.18 | 0.93 | 2.90 | 0.047 | 0.92 |
| 5 | 2.78 | 3.00 | 0.93 | 2.68 | 0.10 | 0.92 |
| 6 | 2.68 | 2.89 | 0.93 | 2.54 | 0.13 | 0.92 |
| 7 | 2.67 | 2.82 | 0.95 | 2.46 | 0.21 | 0.92 |
| 8 | 2.66 | 2.75 | 0.97 | 2.40 | 0.26 | 0.93 |
| 9 | 2.64 | 2.67 | 0.99 | 2.37 | 0.27 | 0.95 |
| 10 | 2.58 | 2.58 | 1.00 | 2.34 | 0.23 | 0.97 |
| $\sum$ | **30.64** | **32.11** | – | **29.74** | **0.90** | – |

## 4.3 Examples

Consider a wind farm with $N$ turbines, where each turbine tries to capture as much power as possible. We will now try to increase the total power capture in the farm by limiting power capture at some of the turbines. The idea is that by decreasing power capture at upwind turbines, their thrust coefficients also decrease. This in turn, increases available power at turbines further downwind.

We proceed as follows: let each turbine capture as much power as possible, i.e. $u_i = P_{\mathrm{rated}},\ i = 1, \ldots, N$, and set $n = 1$.

1. Grid over $u_n$ to find

$$u_n^* = \arg\max_{u_n} \sum_{i=1}^{N} P_i$$

2. Set $u_n = u_n^*$, and $n = n + 1$. Go to step 1.

Table 1 shows the result for a farm with $N = 10$ turbines. $P_i$ is the power captured by turbine $i$, $P_{a,i}$ is the available power at turbine $i$, and $\sigma_i$ is the wind speed standard deviation at turbine $i$. $P^0_{a,i}$ and $\sigma^0_i$ denote the captured power and wind speed standard deviation at turbine $i$ when each turbine extracts maximum power. Limiting some of the upwind turbines, resulted in a total power capture increase of 3.0%. The turbulence levels at all turbines except turbine 1 also decreased.

Figure 6 shows the power increase when running the same algorithm for different values of $N$. Although, the power distribution might not be

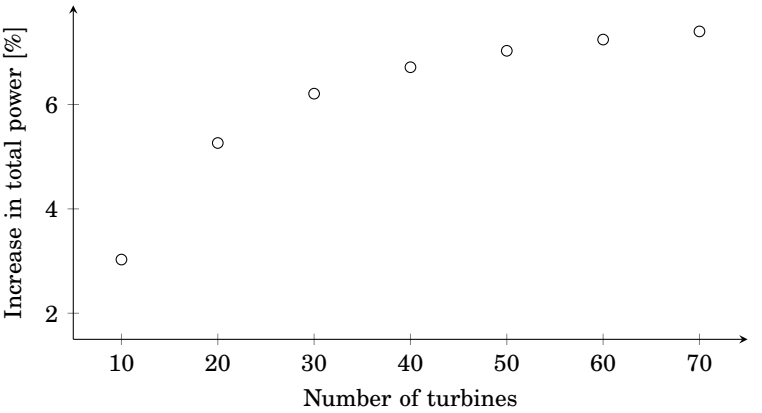


**Figure 6.** Relative gain in total captured power for different number of turbines.

optimal, the result indicates that for larger farms, the relative gain of coordinating turbines could be larger. A reason for this is that limiting power capture in turbine 1 increases the available power in turbines 2 through $N$. A larger $N$ implies more turbines that can increase their power capture.

Another reason is illustrated by the following example. Consider a farm with three turbines, where all turbines individually extract as much power as possible. Fix the power references of the turbines to the current available power. Then decrease the power capture of turbine 1 by 0.5 MW. The resulting increase in available power at turbine 3, $P_{a,3}$, is 0.26 MW. Next, shut down turbine 2 ($u_2 = 0$) and repeat the same experiment. The available power increase at turbine 3 is then 0.14 MW. Thus, turbine 2 contributes to the available power increase at the last turbine without decreasing its power capture. The reason is that the change at turbine 1 increases available power at turbines 2-3. In the first experiment turbine 2 already has a power setpoint it needs to maintain. To do this, the turbine needs to decrease the portion of wind power it captures (i.e. reduce $C_P$). This leads to a simultaneous decrease in thrust coefficient, which further increase in available power at turbines 3. The model suggests that, a negative step in power production at an upwind turbine, also causes all turbines further downwind that maintain their level of power production, to pose less of an obstacle for the wind. Having many turbines in a farm, can therefore increase the impact of decreasing power in a single turbine.

Based on the results in Figure 7, we observe that the model suggests that a power decrease at an upwind turbine can have two effects. The first is that it causes all turbines further downwind, that maintain their level

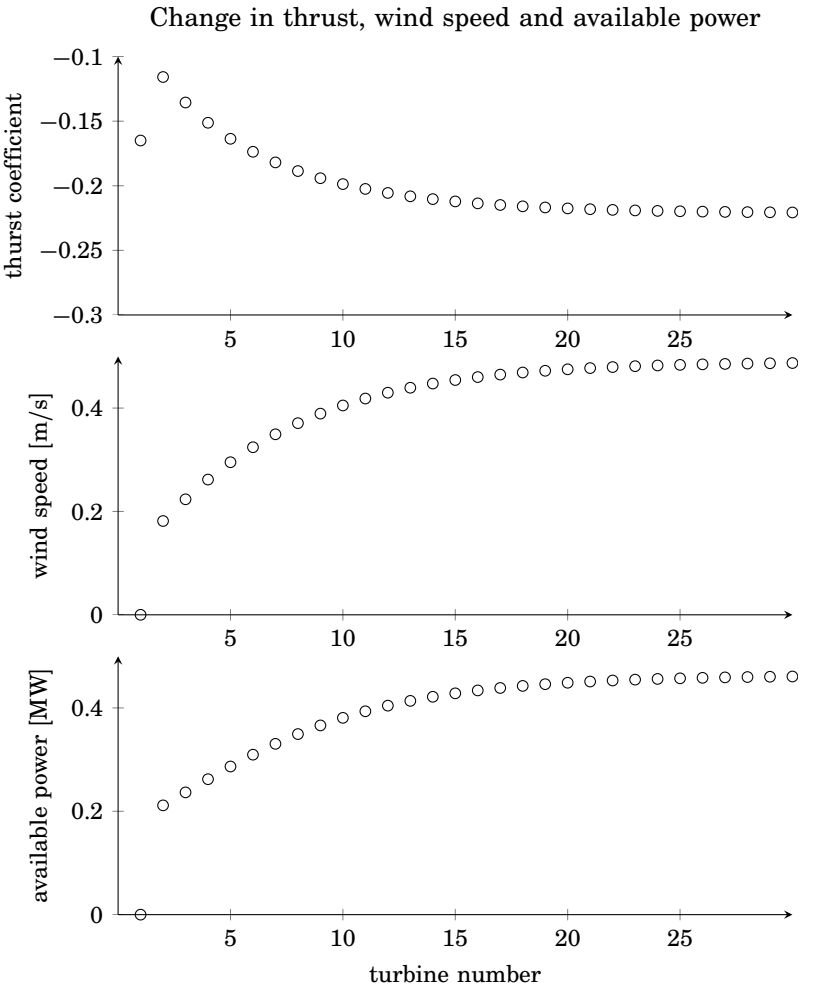


**Figure 7.** Result of decreasing power in turbine 1 by 0.5 MW, while maintaining the power capture in turbines 2-9. The values in the plots show the *change* relative to the case before the power decrease at turbine 1. Note that while $\Delta P_{a,i}$, and $\Delta v_i$ increase downwind, the same is not true for the *absolute* values $P_{a,i}$, and $v_i$.

of power production, to pose less of an obstacle for the wind. The second is that the increase in available power becomes larger further downwind. While the first effect is intuitive, the latter is due to the choice of of $k$, and $k'$. It occurs for large enough ratios, $k/k'$ (i.e small enough distances between the turbines). Whether this effect can be found in actual wind farms has to be concluded by experiments.

## 5. Future Work

Due to high confidentiality, and that real wind farms are mostly commercial, it takes time to obtain data for validation. However, efforts are being made on this front, and model validation will be carried out in the near future.

Another natural step is to examine to what extent the simplicity and distributed structure of the model can be exploited for distributed control purposes.

We would also like to extend the model to fit more complicated wind farm topologies, such as grids.

## Acknowledgements

This work was supported by the European Community's Seventh Framework Programme under grant agreement number 224548, acronym AEOLUS.

## References

Bossayani, E., C. Maclean, P. D. D. G. E. Whittle, N. Lipman, and P. Musgrove (1980). "The efficiency of wind turbine clusters". In: *Proceedings of the 3rd International Symposium on Wind Energy Systems*.

Burton, T., D. Sharpe, N. Jenkins, and E. Bossanyi (2001). *Wind Energy Handbook*. John Wiley & Sons, Chichester, UK.

Crespo, A., J. Hernández, and S. Frandsen (1999). "Survey of modeling methods for wind turbine wakes and wind farms". *Wind Energy* **2**:1, pp. 1–24.

Frandsen, S. (1992). "On the wind speed reduction in the centre of large clusters of wind turbines". *Journal of Wind Engineering and Industrial Aerodynamics* **39**:1–3, pp. 251–265.

Frandsen, S., R. Barthelmie, S. Pryor, O. Rathmann, S. ren Larsen, and J. rgen Hø jstrup (2006). "Analytical modelling of wind speed deficit in large offshore wind farms". *Wind Energy* **9**:1–2, pp. 39–53.

Frandsen, S. T. s (2007). *Turbulence and Turbulence Generated Structural Loading in Wind Turbine Clusters*. Ph.D. Thesis Risø-R-1188(EN). Risø National Laboratory.

Grunnet, J., M. Soltani, T. Knudsen, M. Kragelund, and T. Bak (2010). "Aeolus toolbox for dynamic wind farm modeling, simulation and control". In: *Proceedings of the 2010 European Wind Energy Conference*, pp. 3119–3129.

Jensen, N. (1983). *A Note on Wind Generator Interaction*. Tech. rep. Risø-M-2411. Risø National Laboratory, Roskilde, Denmark.

Jonkman, J., S. Butterfield, W. Musial, and G. Scott (2009). *Definition of a 5-MW Reference Wind Turbine for Offshore System Development*. Tech. rep. NREL/TP-500-38060. National Renewable Energy Laboratory, Golden, CO.

Pao, L. and K. Johnson (2009). "A tutorial on the dynamics and control of wind turbines and wind farms". In: *Proceedings of the 2009 American Control Conference*. St. Louis, MO, pp. 2076–2089.

# Paper VI

# On Using Wind Speed Preview to Reduce Wind Turbine Tower Oscillations

**Maxim Kristalny  Daria Madjidian  Torben Knudsen**

**Abstract**

We investigate the potential of using previewed wind speed measurements for damping wind turbine fore-aft tower oscillations. Using recent results on continuous-time $H^2$ preview control, we develop a numerically efficient framework for the feedforward controller synthesis. One of the major benefits of the proposed framework is that it allows us to account for measurement distortion. This results in a controller that is tailored to the quality of the previewed data. A simple yet meaningful parametric model of the measurement distortion is proposed and used to analyze the effects of distortion characteristics on the achievable performance and on the required length of preview. We demonstrate the importance of accounting for the distortion in the controller synthesis and quantify the potential benefits of using previewed information by means of simulations based on real-world turbine data.

## 1. Introduction

An evident trend in the area of wind energy during the past decades is a continuous growth of wind turbine dimensions. Modern day commercial turbines typically stand more than 90 m tall, with a blade span of over 120 m [Pao and Johnson, 2009]. As a consequence of such a large size, structural loads experienced by turbines becomes a central issue. These loads shorten the life span of the turbine and increase its maintenance costs. Alternatively, turbines with a higher tolerance to structural loads require a more rigid structure and, as a result, higher construction costs. For this reason, load reduction is an important factor in decreasing the cost of wind energy.

In this paper, we focus on exploiting wind speed preview for reducing tower fore-aft oscillations in wind turbines with collective pitch control. The idea of using preview in the control of wind turbines was discussed in [Pao and Johnson, 2009; Laks et al., 2009] and has been a subject of interest for many researchers in the last few years. The use of preview in cyclic pitch control was considered in [Schlipf et al., 2010]. Model predictive control with preview was studied in a collective pitch setting in [Korber and King, 2010; Soltani et al., 2011] and in an individual pitch setting in [Laks et al., 2011a]. The benefit of model predictive techniques is in their ability to account for hard input, output and state constraints, which is particularly useful when operating near rated conditions. These methods, however, may require heavy online computations and impede the analysis of the problem. The use of preview in individual pitch control was considered in [Laks et al., 2011b] using the LMI approach to $H^\infty$ optimization. In [Dunne et al., 2011; Wang et al., 2012], preview control for load reduction was studied using model inversion methods and adaptive control algorithms based on recursive least squares.

To the best of our knowledge, the methods proposed so far rely on time discretization. Availability of preview is typically handled by a state augmentation procedure, which leads to a finite-dimensional, yet, high-order optimization. In spite of its conceptual simplicity, this approach may have a number of drawbacks. In particular, it impedes direct analysis of the problem and is associated with a high computational burden, which grows with the increase of the preview length.

A different approach is proposed in this paper. We show that the problem can be conveniently formulated as an instance of the continuous-time two-sided $H^2$ model matching optimization with preview, which was recently solved in [Kristalny and Mirkin, 2012]. Unlike the commonly used discrete-time methods, the computational burden of the proposed solution does not depend on the preview length. The resulting optimal controller has an interpretable structure and is easy to implement. Moreover, the

proposed method facilitates the analysis of the problem, which is the main topic of this work.

A large part of the paper is devoted to the analysis of the effects of measurement distortion on the feedforward control. An important feature of the proposed method is that it allows us to include the distortion model in the problem formulation and to account for it in the controller synthesis procedure. This results in a feedforward controller that is tailored to the quality of the previewed information, and facilitates the analysis of the influence of distortion on the feedforward control. A simple and intuitive parametric model for the distortion is proposed and used to study the effects of distortion characteristics on the achievable performance and on the required length of preview. Using simulations based on real wind turbine measurements, we demonstrate that accounting for measurement distortion in the controller design is crucial in order to properly take advantage of the previewed wind speed information.

In the last part of the paper, we consider the possibility of obtaining a preview of the wind speed from upwind turbines in a wind farm. This idea was previously proposed in [Kristalny and Madjidian, 2011] as a possible alternative to the LIDAR based control. By analyzing data collected from a wind farm, we show that, at least in the setup proposed in [Kristalny and Madjidian, 2011], this idea is not likely to work. The results indicate that due to the large distance between neighboring turbines, the wind speed fluctuations experienced by two turbines are correlated only at lower frequencies, which are not pertinent to load reduction.

The paper is organized as follows: Section 2 describes the turbine model and the model of the wind speed. The problem formulation and solution are presented in Section 3. Section 4 constitutes the main part of this paper. It is devoted to analyzing the benefits of using previewed wind speed measurements and the effects of measurement distortion. In Section 5, we look into using previewed wind speed measurements from upwind turbines. Finally, some concluding remarks are provided in Section 6.

**Notation** The Frobenius norm of a matrix, $A$, is denoted by $\|A\|_{\mathrm{F}}$. The space of all proper and stable transfer matrices is denoted by $H^\infty$. The space of all rational transfer matrices in $H^\infty$ is denoted by $RH^\infty$. Given a transfer matrix $G(s)$, its conjugate is denoted by $G^\sim(s) := [G(-s)]'$. For any rational strictly proper transfer function given by its state-space realization

$$G(s) = C(sI - A)^{-1}B = \left[\begin{array}{c|c} A & B \\ \hline C & 0 \end{array}\right],$$

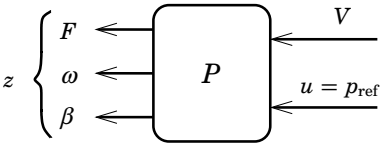


**Figure 1.** Turbine model

the completion operator, [Mirkin, 2003], is defined as

$$\pi_h\{G(s)\} := Ce^{-Ah}(sI - A)^{-1}B - e^{-sh}C(sI - A)^{-1}B$$

and is an FIR (finite impulse response) linear system.

## 2. Modeling

### 2.1 Turbine model

We adopt a nonlinear aeroelastic model of a 5 MW NREL wind turbine from [Jonkman et al., 2009]. The model consists of a tower with two fore-aft and two side-to-side bending modes, three blades with two flapwise and one edgewise bending modes each, a 3rd order drive train, as well as the internal controller described in [Jonkman et al., 2009] and modified according to [Grunnet et al., 2010]. In addition, the model has been augmented with a 1st order generator model and a 2nd order pitch actuator with an internal delay, which were both adopted from [Grunnet et al., 2010].

The internal controller manipulates the generator torque and blade pitch angle in order to meet a prescribed power demand. It has three main modes of operation, usually called “operating regions”. The first two modes are identical to those described in [Jonkman et al., 2009], whereas the third mode is extended according to [Grunnet et al., 2010] in order to provide the capability for derated operation.

The controller operates in the third (derated) mode if the power demand does not exceed the power that can be captured by the turbine. In this mode, excess wind power is curtailed in order to satisfy demand. This is achieved by keeping the rotor speed close to its rated value by adjusting the pitch angle, and manipulating the generator torque in order to maintain the desired power. Throughout this paper, we will assume that the power demand does not exceed the power available in the wind, which means that the internal controller operates in derated mode.

We use the full nonlinear turbine model described above for simulation purposes only. For analysis and controller synthesis, a simplified

linearized version of this model is adopted from [Spudić et al., 2010]. The nominal mean wind speed and power demand are denoted by $V_{\text{nom}}$ and $p_{\text{nom}}$, respectively. Throughout this paper, we assume that $V_{\text{nom}} = 10$ m/sec and $p_{\text{nom}} = 2$ MW. A continuous-time linearized wind turbine model can be described by the block depicted in Figure 1. It can be partitioned as

$$P = \begin{bmatrix} P_V & P_u \end{bmatrix}$$

with respect to the two input signals. The inputs $V$ and $p_{\text{ref}}$ denote deviations in the wind speed and the power demand from their nominal values. The second input will also be denoted as $u := p_{\text{ref}}$. Note that in the considered setting, $u$ is the only available control signal. The linearized model neglects generator dynamics, which makes the actual deviation in power production equal to $p_{\text{ref}}$.

The three outputs of $P$ are denoted by $F$, $\omega$, and $\beta$ and stand for the deviations in the thrust force, rotor speed, and pitch angle, respectively. The vector containing all outputs of the system is denoted by

$$z := \begin{bmatrix} F & \omega & \beta \end{bmatrix}'$$

. The state-space realization of $P$ for the aforementioned operating point is given by

$$P = \left[\begin{array}{ccc|cc} 0 & 1.2 \cdot 10^2 & -9.2 \cdot 10^{-1} & 0 & 0 \\ -8.4 \cdot 10^{-3} & -3.2 \cdot 10^{-2} & 0 & 1.6 \cdot 10^{-2} & -2.1 \cdot 10^{-8} \\ 0 & 1.5 \cdot 10^2 & -1.6 & 0 & 0 \\ \hline -5.8 \cdot 10^4 & -1.5 \cdot 10^5 & 0 & 7.4 \cdot 10^4 & 0 \\ 0 & 1 & 0 & 0 & 0 \\ 1 & 0 & 0 & 0 & 0 \end{array}\right],$$

where the three states correspond to the pitch angle, rotor speed and an internal controller state.

This linearized model neglects the influence of tower oscillations on the wind speed experienced by the turbine. Instead, we consider tower oscillations as an external dynamical mode excited by the thrust force. It is approximated by a second order system with static gain $k_{\text{twr}} = 3.58 \times 10^{-7}$, natural frequency $\omega_{\text{twr}} = 2$ rad/sec and damping coefficient $\zeta_{\text{twr}} = 0.08$, which is consistent with [Jonkman et al., 2009]. The tower deflection, i.e., the displacement of the nacelle, will hereafter be denoted by $y$.

Remark 2.1
Note that considering a turbine equipped with a standard internal controller is restrictive. This rules out direct access to the pitch and the generator torque, restricts us to work in a derated mode and leaves the power reference as the only available control signal. At the same time,

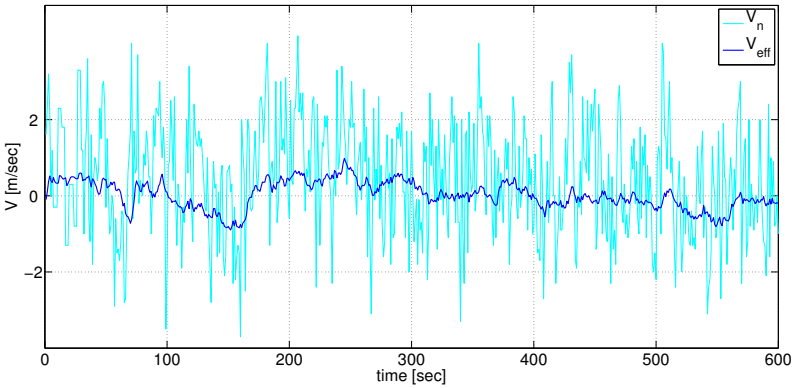


**Figure 2.** Comparison between measured nacelle wind speed, $V_n$, and estimated effective wind speed, $V_{eff}$. As expected, $V_{eff}$ fluctuates less than $V_n$.

this simplifies the problem and facilitates experiments on existing wind turbines. It is worth emphasizing that the ideas, the problem formulation and the solution techniques discussed in the paper can be extended to more general situations with no internal controller, individual pitch capabilities and a wide range of structural loads being in focus. □

## 2.2 Wind model

Since the relevant system variables such as rotor speed, thrust force and nacelle displacement depend on the wind speed variations along the entire rotor, we adopt the concept of *effective wind speed* (EWS) from [Knudsen et al., 2011]. It can be interpreted as a spatially constant wind field that produces a similar rotor torque and thrust force as the actual spatially varying wind flow. To model EWS at a turbine we use real wind turbine data collected from the Egmond aan Zee Offshore Wind Farm (OWEZ) [OWEZ, 2014]. During the period of data collection, the mean wind speed was 10 m/s, which is consistent with the operating point in Section 2.1. For more information on the data set we refer to [Knudsen et al., 2011] where it is described in detail.

To estimate EWS, we used the time varying extended Kalman filter described in [Knudsen et al., 2011]. A 10 minute sample of the estimated EWS deviation from its nominal value is shown in Figure 2, where it can be compared to the deviation of the measured nacelle wind speed. As expected, the EWS fluctuates less than the point wind speed measured on the nacelle.

Based on the estimated EWS a model was identified using a prediction error method [Ljung, 1999]. The model is given by a signal generator $M_V$, which takes white noise with unit intensity as input and provides the wind speed signal as the output. A first order model proved to be sufficient and is presented below:

$$M_V(s) = \frac{7.4476}{(1/0.0143)s + 1}.$$

## 3. Problem formulation and solution

The problem of using wind speed measurements for load reduction naturally falls into the open-loop disturbance attenuation scheme, depicted in Figure 3. The effective wind speed deviation $V$ acts as an external disturbance. Its frequency content is modeled by the filter $M_V$ as described in Section 2.2. The controller $K$ receives a measurement of the wind speed denoted by $V_m$. The delay $h$ in the first input of the plant corresponds to the length of preview available to the controller. Since the wind speed is measured some distance ahead of the turbine, there will aways be a mismatch between $V_m$ and the actual wind experienced by the turbine $V_i$. To account for this, we introduce the additive noise $n$, which, together with the filters $M_t$ and $M_n$, model distortion between the experienced and the measured wind speeds. A detailed discussion on the choice of $M_t$ and $M_n$ will be provided in Section 4.2. The aim of the controller is to keep the components of $z$ small. Pitch activity should be kept low to reduce wear on the pitch mechanism. Deviations of rotor speed from its rated

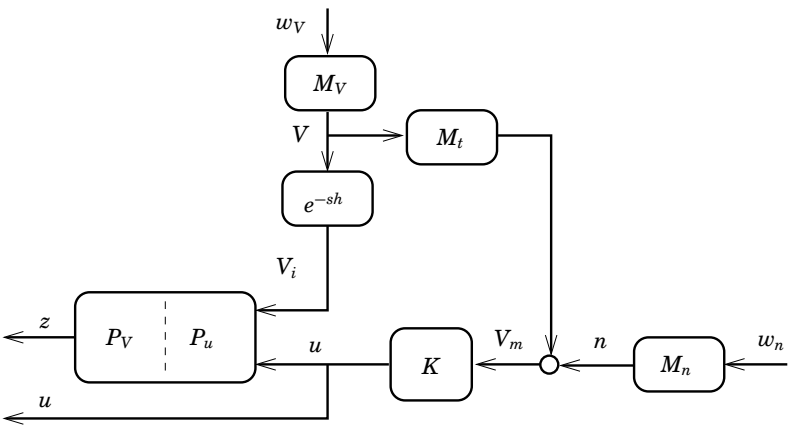


**Figure 3.** Turbine control scheme

value should not be large due to mechanical design constraints. Finally, fluctuations in thrust force should be alleviated, since they introduce oscillations, which cause damage to the tower, blades and other mechanical components [Burton et al., 2001]. To prevent large fluctuations in produced power, the control signal $u$ should also be penalized.

The relation between the input and output signals in Figure 3 is given by:

$$\begin{bmatrix} z/w_V & z/w_n \\ u/w_V & u/w_n \end{bmatrix} = \begin{bmatrix} e^{-sh}P_V M_V & 0 \\ 0 & 0 \end{bmatrix} + \begin{bmatrix} P_u \\ 1 \end{bmatrix} K \begin{bmatrix} M_t M_V \\ M_n \end{bmatrix}'.$$

We define the cost transfer function for the optimization as

$$T := \begin{bmatrix} W_z & 0 \\ 0 & W_u \end{bmatrix} \begin{bmatrix} z/w_V & z/w_n \\ u/w_V & u/w_n \end{bmatrix},$$

where $W_z = \mathrm{diag}\{W_F, W_w, W_\beta\}$ contains weights for all the components of $z$, and $W_u$ is the weight for the power reference. We choose the weight of the thrust force as

$$W_F = k_F \frac{s + \omega_{\mathrm{twr}}}{s^2 + 2\zeta_{\mathrm{twr}}\omega_{\mathrm{twr}} s + \omega_{\mathrm{twr}}^2}$$

in order to penalize tower oscillations. The weight for the rotor speed is static $W_w = k_w$. In order to penalize high pitch rates, we choose the weight for the pitch angle as a high-pass filter

$$W_\beta = k_\beta \frac{s}{s + \omega_\beta}.$$

Finally, we choose the weight for the power reference as

$$W_u = k_u \frac{(s + \omega_{\mathrm{twr}})^2}{s^2 + 2\zeta_{\mathrm{twr}}\omega_{\mathrm{twr}} s + \omega_{\mathrm{twr}}^2}$$

in order to prevent the controller from damping tower oscillations by means of oscillations in power production and, as a result, in the pitch angle.

Defining the transfer matrices

$$\left[\begin{array}{c|c} G_1 & G_3 \\ \hline G_2 & 0 \end{array}\right] := \left[\begin{array}{cc|c} W_z P_V M_V & 0 & W_z P_u \\ 0 & 0 & W_u \\ \hline M_t M_V & M_n & 0 \end{array}\right] \tag{1}$$

and choosing $||T||_2$ as the performance criterion, the problem can be formulated as model matching optimization.

**OP**: Given $G_1, G_2, G_3 \in RH^\infty$ as defined in (1) and the preview length $h \geq 0$ find $K \in H^\infty$, which guarantees

$$T = e^{-sh} G_1 - G_3 K G_2 \in H^2 \tag{2}$$

and minimizes $||T||_2$.

The formulation above can be considered as a special case of a more general problem, whose solution was recently obtained in [Kristalny and Mirkin, 2012]. Below, we tailor this solution to **OP**. Consider the composite *finite-dimensional* system given by its minimal state-space realization

$$\left[\begin{array}{cc} G_1 & G_3 \\ G_2 & 0 \end{array}\right] = \left[\begin{array}{c|cc} A & B_1 & B_2 \\ \hline C_1 & 0 & D_3 \\ C_2 & D_2 & 0 \end{array}\right].$$

Assume that

$\mathcal{A}_\mathbf{1}$: $D_2 D_2' = I$ and $D_3' D_3 = I$,

$\mathcal{A}_\mathbf{2}$: $G_2(s)$ and $G_3(s)$ have no j$\omega$-axis transmission zeros.

These are the standard assumptions in $H^2$ optimal control that rule out redundancy and singularity of the problem. The following result provides a complete state-space solution of **OP** in terms of two algebraic Riccati equations (AREs).

THEOREM 3.1
If the assumptions $\mathcal{A}_{\mathbf{1\text{-}2}}$ hold, then **OP** has a unique solution given by

$$K^{\text{opt}} = -e^{-sh} \left[\begin{array}{c|c} \bar{A} & L \\ \hline F & 0 \end{array}\right] - \left[\begin{array}{c|c} \bar{A} & B_2 \\ \hline F & I \end{array}\right] \pi_h\{\tilde{G}\} \left[\begin{array}{c|c} \bar{A} & L \\ \hline C_2 & I \end{array}\right],$$

where $\bar{A} := A + B_2 F + L C_2$ and

$$\tilde{G} := \left[\begin{array}{cc|c} -(A+B_2F)' & (C_1+D_3F)'C_1Y & XL \\ 0 & -(A+LC_2)' & C_2' \\ \hline B_2' & -D_3'C_1Y & 0 \end{array}\right]$$

with $F := -B_2'X - D_3'C_1$ and $L := -YC_2' - B_1D_2'$, ere $X \geq 0$ and $Y \geq 0$ are the stabilizing solutions of the algebraic Riccati equations

$$A'X + XA - (XB_2 + C_1'D_3)(B_2'X + D_3'C_1) + C_1'C_1 = 0$$
$$AY + YA' - (YC_2' + B_1D_2')(C_2Y + D_2B_1') + B_1B_1' = 0.$$

Moreover, the expression for the performance achieved by the optimal controller is given by

$$\left\|T^{\text{opt}}\right\|_2^2 = \left\| \left[\begin{array}{cc|c} A & B_2F & B_1 \\ -LC_2 & \bar{A} & -LD_2 \\ \hline C_1 & D_3F & 0 \end{array}\right] \right\|_2^2 - \left\|\pi_h\{\tilde{G}\}\right\|_2^2,$$

□

***Proof*** This is a special case of [Kristalny and Mirkin, 2012, Theorem 2] with stable $G_1$, $G_2$ and $G_3$. □

It is worth stressing that the computational load of the solution provided in Theorem 3.1 does not depend on the preview length. In fact, it is based on the standard AREs associated with the preview-free problem.

Also note that the solution provides an insight into the structure of the optimal controller. It is easy to see that the first term of $K^{\text{opt}}$ is based on the optimal controller for the preview-free problem. In fact, as manifested by the presence of the delay element, this term "ignores" the existence of previewed information. Availability of preview is accounted for solely by the second term, in which the only component that depends on the preview length is the FIR block $\pi_h\{\tilde{G}\}$.

Finally, the result in Theorem 3.1 facilitates the analysis of the influence of preview length on the achievable performance. Let $\mathcal{P}_h = \|T^{\text{opt}}\|_2$ be the optimal performances achieved with $h$ seconds of preview. It can be verified that $\mathcal{P}_h^2 := \mathcal{P}_0^2 - \|\pi_h\{\tilde{G}\}\|_2^2$. The first term in the above expression stands for the optimal performance with $h = 0$, while the second term corresponds to the performance improvement due to availability of preview. The latter can be computed using the integral $\|\pi_h\{\tilde{G}\}\|_2^2 = \int_0^h \|\tilde{G}^{\sim}(t)\|_{\text{F}}^2 dt$, where $\tilde{G}^{\sim}(t)$ refers to the impulse response of the stable finite-dimensional system $(\tilde{G})^{\sim}$. This shows that one can construct the curve of $\mathcal{P}_h$ versus $h$ without solving the problem for each value of preview length but only at the expense of solving two AREs.

Remark 3.1
Note that the proposed framework allows us to synthesize a preview controller for a specific operating point. In practice, the controller will need to be continuously adapted to the changes in operating point and, perhaps, also in the stochastic characteristics of the wind. The method of adding such adaptation capabilities to the controller deserves a separate discussion and is a possible direction for future work. □

## 4. Analysis and simulations

In this section, we use the mathematical framework described in Section 3 in order to assess the potential of exploiting previewed measurements of the effective wind speed for reducing tower oscillations. In particular, we examine the influence of the preview length and measurement distortion on the achievable performance.

All simulations in this section are performed on the complete nonlinear model[1] described in the beginning of Section 2.1. We choose the weight parameters used in the definition of the performance criteria in Section 3 as

$$k_V = 1,\ k_n = 1 \times 10^{-3},\ k_u = 1.8 \times 10^{-2},\ k_F = 0.5,\ k_w = 2 \times 10^{6}.$$

This section is divided into three parts. In Section 4.1, we assume that perfect measurements of the wind speed are available to the controller. This enables us to find an upper bound of the achievable performance. In Section 4.2, we introduce measurement distortion and observe its effect on the behavior of different controllers. In particular, we show the importance of taking distortion into account during the controller design. Finally, in Section 4.3, we analyze the influence of the distortion on the achievable performance and the required length of preview.

## 4.1 Preview control with perfect measurements

As a first step, let the distortion model be $M_t = 1$ and $M_n = 3 \times 10^{-3}$. This corresponds to the situation in which the controller receives (almost) perfect measurements of the incoming wind speed with a preview of $h$ seconds.

The natural questions when using preview are whether it can yield a noticeable performance improvement, and if so, what length of preview it requires. To address these questions, a curve of the achievable performance as a function of the preview length is presented in Figure 4. The values are normalized with respect to the performance of the original system without feedforward control. The figure indicates that in the considered setup with perfect measurements the reasonable scale of preview length is a number of seconds. In fact, 90% of all possible improvement is achieved with a preview of 0.75 sec.

Below we will compare the behaviour of the following three systems:

1. The original system without feedforward control, namely, with $K = 0$.

2. The system with feedforward controller based on local measurements without preview. This controller will be denoted by $K_0^p$ and is obtained by solving **OP** for $h = 0$.

[1] The model is implemented using NREL's FAST simulation package [FAST, 2014] and Simulink®. The FAST input files used in the simulation are described in detail in [Jonkman et al., 2009] and the parameter settings for the internal controller, pitch actuator, and generator can be found in [SimWindFarm, 2014].

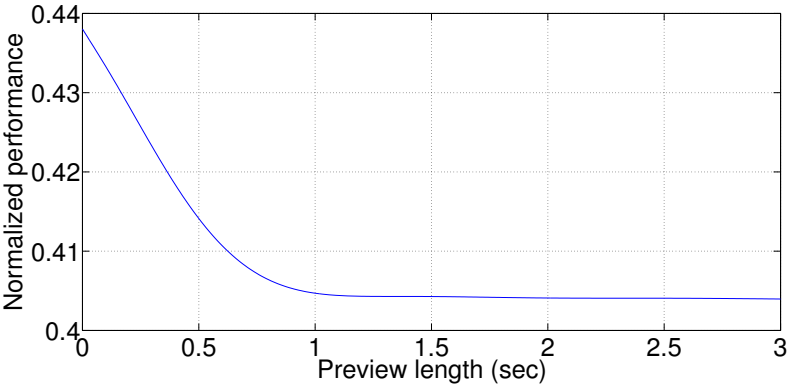


**Figure 4.** Achievable performance vs. preview length for the case of perfect measurement (normalized with respect to original system performance). We see that the reasonable scale of preview length is a number of seconds. In fact, 90% of all possible improvement is achieved with $h = 0.75$ sec.

3. The system with feedforward controller based on measurements with preview of $h = 1.3$ sec[2]. This controller will be denoted by $K_h^p$.

REMARK 4.1
The superscript $p$ in $K_0^p$, $K_h^p$ reflects that these controllers were synthesized assuming availability of perfect measurements. □

We simulate the response of these three systems to the effective wind speed estimated from real-world data as explained in Section 2.2. We run simulations on 10 different time series, each one minute long. The time series from one of the simulations are shown in Figure 5. The average outcome is presented in Table 1, where the DEL notation represents the 1 Hz *damage equivalent load*. This is a constant amplitude sinusoidal load that causes the same fatigue damage during one minute as the original load history does, see [Spudić et al., 2010; Hammerum et al., 2007; Burton et al., 2001] for more details. The DELs listed in Table 1 are for the fore-aft tower base bending moment, denoted $M_t$, and the flapwise blade root bending moment, denoted $M_b$. The tower base DEL was computed using an S/N-slope of 4 which is representative of steel structures, and the blade root DEL was computed with an S/N-slope of 10 which is representative of materials made out of glass fiber [Hansen, 2008]. DEL($M_b$) was included

[2] A relatively long preview ($h > 0.75$ sec) is chosen in order to facilitate comparison of the resulting controller with those designed in the following subsection.

**Table 1.** simulation results based on the nonlinear turbine model and ews estimated from real-world data. (feedforward based on perfect ews measurements.)

| | DEL($M_t$) kNm | DEL($M_b$) kNm | max($\dot{\beta}$) deg/sec | max($P$) kW | max($\omega$) rpm |
|---|---|---|---|---|---|
| $K = 0$ | 3581 | 996 | 0.33 | 0 | $5.5 \times 10^{-2}$ |
| $K_0^p$ | 1861 | 777 | 0.15 | 267 | $2.4 \times 10^{-2}$ |
| $K_h^p$ | 1280 | 734 | 0.17 | 222 | $2.7 \times 10^{-2}$ |

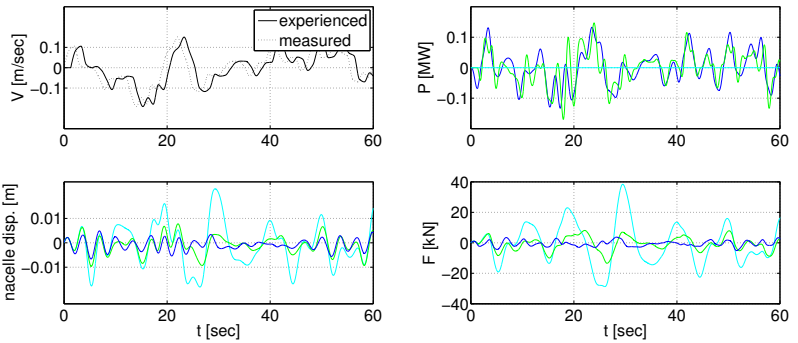


**Figure 5.** Simulation results based on the nonlinear turbine model and EWS estimated from real-world data. The results illustrate the behavior of controllers designed assuming perfect wind measurements. [cyan | $K = 0$; green | $K_0^p$; blue | $K_h^p$] The average results of 10 simulations of this kind are summarized in Table 1.

due to the coupling between tower and blade bending modes [Burton et al., 2001].

As expected, feedforward both with and without preview significantly reduces the tower bending moment. Both of these controllers also succeed in reducing the blade bending moment, the pitch rate, as well as the magnitude of the rotor speed deviations.

Inspecting the last two rows in Table 1, we see that the benefit of using previewed information is substantial. Comparing the tower bending moment for the two feedforward controllers, we see that preview offers improvement of approximately 31%.

## 4.2 Preview control with distorted measurements

The results so far were based on perfect measurements of the incoming wind speed. This assumption is not realistic, especially taking into account

that to obtain preview, one needs to measure the wind speed some distance ahead of the turbine. As the wind travels from the measuring location to the turbine, its high frequency content will be distorted, [Panofsky and Dutton, 1984]. As a result, one would expect that the longer the preview in our measurements, the more distortion they may experience. This question was investigated in [Panofsky and Dutton, 1984] in the context of LIDAR based wind speed measurements.

For the purposes of this work, we propose a simple, yet intuitive parameterized model for the distortion. To account for distant sensing, we may choose $M_t$ and $M_n$ as

$$M_t(s) = \frac{\omega_t}{s+\omega_t}, \tag{3}$$

$$M_n(s) = \frac{s}{s+\omega_t} M_V. \tag{4}$$

In this setup, the high-frequency component of $V$ is filtered out by $M_t$ and then replaced using the uncorrelated signal generator $n$, see Figure 3. The idea behind the parameterization (3)-(4) is to obtain equal spectral properties for the effective wind speeds at the measurement and the turbine locations. Indeed, with this choice of $M_t$ and $M_n$ the spectral densities of $V_i$ and $V_m$ will be equal, since

$$|M_t(jw)|^2|M_V(jw)|^2 + |M_n(jw)|^2 = |M_V(jw)|^2.$$

Note, however, that in addition to the distortion due to the distant sensing, the signal $V_m$ will inevitably be corrupted by some sensor noise. For simplicity, we assume that the sensor noise is white and account for it by adding a constant component to $M_n$, namely,

$$M_n(s) = \frac{s}{s+\omega_t} M_V + k_n. \tag{5}$$

From now on, the distortion model will be given by (3) and (5). The model is characterized by two parameters: the bandwidth limitation due to the distant measurement, $\omega_t$, and the sensor noise intensity, $k_n$. Note that perfect measurements correspond to $\omega_t = \infty$, and $k_n = 0$, and that the distortion increases with increasing $k_n$ and decreasing $\omega_t$. For illustration purposes, in this subsection, we set $\omega_t = 3.8$, $k_n = 3 \times 10^{-2}$ and investigate the influence of the resulting distortion on different aspects of preview control.

REMARK 4.2
In practice, the parameters of the measurement distortion model should be identified using experimental data obtained from a real-world measurement setup. One way to perform identification is by using a Box Jenkins model [Box and Jenkins, 1976] as discussed in Section 5. Some more

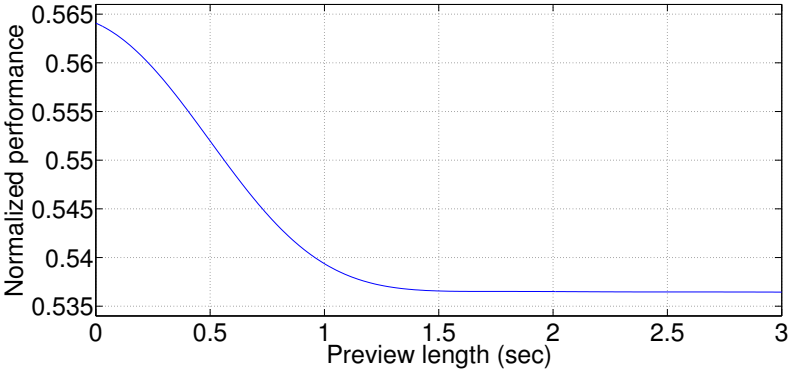


**Figure 6.** Performance ($\|T\|_2$) vs. $h$ (normalized with respect to the $\mathcal{H}_2$-norm of the original system). Compared to the case with pure measurements (Figure 4), the improvement due to availability of preview has decreased and the required preview length has increased.

evolved models for $M_t$ and $M_n$ may also be considered, as well as non-parametric identification methods for the construction of $M_t$ and $M_n$. □

As a first step, consider the curve of the achievable performance as a function of the preview length presented in Figure 6. As expected, the performance improvement due to availability of preview has decreased compared to the case with pure measurements described in Figure 4. Another important observation is that the length of preview required to obtain 90% of the possible improvement has increased to 1 sec.

To further investigate the impact of measurement distortion on the preview control, we compare the behavior of the following three systems:

1. The system with a feedforward controller based on local measurements without preview. This controller will be denoted by $K_0^d$ and is obtained by solving **OP** with $M_t = 1$ and $M_n = 3 \times 10^{-2}$, i.e., assuming that the measurements are corrupted with white additive noise only.

2. The system with a feedforward controller based on distant measurements with preview of $h = 1.3$ sec. This controller will be denoted by $K_h^d$ and is obtained by solving **OP** with $M_t$ and $M_n$ as in (3) and (5), respectively, with $\omega_t = 3.8$, $k_n = 3 \times 10^{-2}$.

3. The system with the a preview controller $K_h^p$ from the previous subsection, which was obtained assuming perfect measurements. This controller is considered to demonstrate that ignoring distortions in the controller design may lead to a poor controller behavior.

**Table 2.** simulation results based on the nonlinear turbine model and ews estimated from real-world data. (feedforward based on ews measurements with distortion.)

| | DEL($M_t$) kNm | DEL($M_b$) kNm | max($\dot{\beta}$) deg/sec | max($P$) kW | max($\omega$) rpm |
|---|---|---|---|---|---|
| $K_0^d$ | 1925 | 784 | 0.16 | 249 | $2.4 \times 10^{-2}$ |
| $K_h^d$ | 1768 | 774 | 0.28 | 189 | $2.8 \times 10^{-2}$ |
| $K_h^p$ | 2191 | 791 | 0.30 | 211 | $3.6 \times 10^{-2}$ |

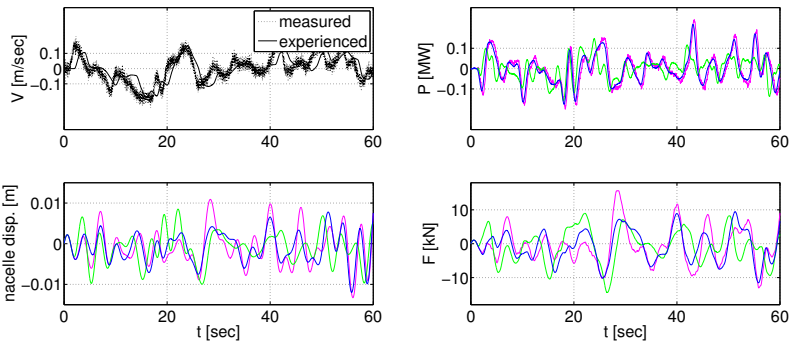


**Figure 7.** Simulation results based on the nonlinear turbine model and EWS estimated from real-world data. The EWS measurements are artificially corrupted with respect to the distortion model. [blue | $K_h^d$; green | $K_0^d$; magenta | $K_h^p$] The average results of 10 simulations of this kind are summarized in Table 2.

REMARK 4.3
The superscript $d$ in $K_0^d$, $K_h^d$ reflects that these controllers were synthesized accounting for the distortion in measurements. □

We compare the response of these three systems to the effective wind speed estimated from real-world experimental data as explained in Section 2.2. Note that in simulations we artificially distort the measurements with respect to the distortion model that corresponds to the preview length (i.e. to the distance between the turbine and the measurement location). Namely, in simulations with $K_h^d$ and $K_h^p$ the measurements are distorted with respect to (3), (5) with $\omega_t = 3.8$ and $k_n = 3 \times 10^{-2}$. In simulations with $K_0^d$, which uses the local measurements, the distortion is with respect to $M_t = 1$ and $M_n = 3 \times 10^{-2}$.

As before, we run simulations on 10 different time series, each one

minute long. The average outcome of these simulations is presented in Table 2 and the time series of one of the simulations are presented in Figure 7.

Comparing the behavior of $K_0^d$ and $K_h^d$ we see that, despite of the additional distortion associated with distant sensing, the use of preview is still beneficial. Note, however, that the decrease in the tower bending moment due to the use of preview is only 8.2%. This is substantially lower than the 31% that could be obtained in the previous subsection with perfect measurements.

Finally, the results obtained from the simulations with $K_h^p$ deserve a separate discussion. These results demonstrate that accounting for measurement distortion at the stage of controller synthesis is crucial for obtaining an adequate system behavior. Indeed, we see that $K_h^p$, which was obtained ignoring the distortion, is outperformed not only by $K_h^d$ but also by $K_0^d$. This suggests that in some situations not using preview might be better than using it without accounting for the distortion. Note, however, that the results still indicate that, in the considered example, having distorted previewed measurements might be advantageous if the distortion is taken into account.

## 4.3 Effects of measurement distortion on the achievable performance and the required preview length

Results from the previous subsection motivate further analysis of the relation between measurement distortion characteristics and different aspects of preview control. As a first step, we assume unlimited preview length, and plot the achievable performance as a function of the distortion model parameters, $\omega_t$ and $k_n$, see Figure 8. As expected, the performance monotonically improves with decreasing $k_n$ and increasing $w_t$. Also note that its normalized value approaches a value of approximately 0.4, which is consistent with Figure 4. The rapid deterioration in performance as $\omega_t$ decreases from 3 to 1 rad/sec can be related to the natural frequency of the tower, located at 2 rad/sec. Once $\omega_t$ decreases below this value, the frequencies responsible for tower excitation are filtered out of the measured signal $V_m$, which makes feedforward control based on these measurements irrelevant.

Another natural question is how the required preview length is affected by the distortion characteristics. Figure 9 shows the preview length required to attain 90% of all possible performance improvement as a function of $\omega_t$ and $k_n$. It shows that a longer preview is needed to cope with an increase in the sensor noise intensity. The same is true for a decrease in bandwidth $\omega_t$, but only up to a certain frequency after which there is a sharp decrease in the required preview length. The decrease starts

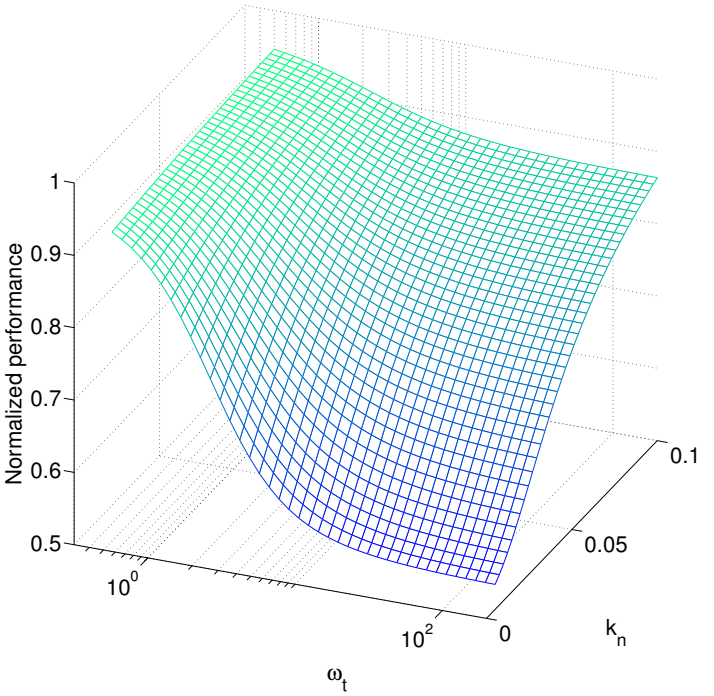


**Figure 8.** Normalized performance that can be achieved with unlimited preview as a function of the distortion parameters. As expected, the performance monotonically improves with decreasing $k_n$ and increasing $w_t$.

around $1-2$ rad/sec, indicating that there is less to be done once frequencies related to the system dynamics are filtered out of the measurement.

## 5. Preview from upwind turbines

So far, we have assumed that (possibly distorted) previewed effective wind speed measurements are available, but have said nothing about how to obtain them. One possibility would be to measure the wind field ahead of the turbine using LIDAR and estimate the effective wind speed from this data.

In wind farms, there is yet another possibility: upwind turbines could be used as sensors for their downwind neighbors. If successful, this option would offer several benefits. First, it is cheap since it does not require

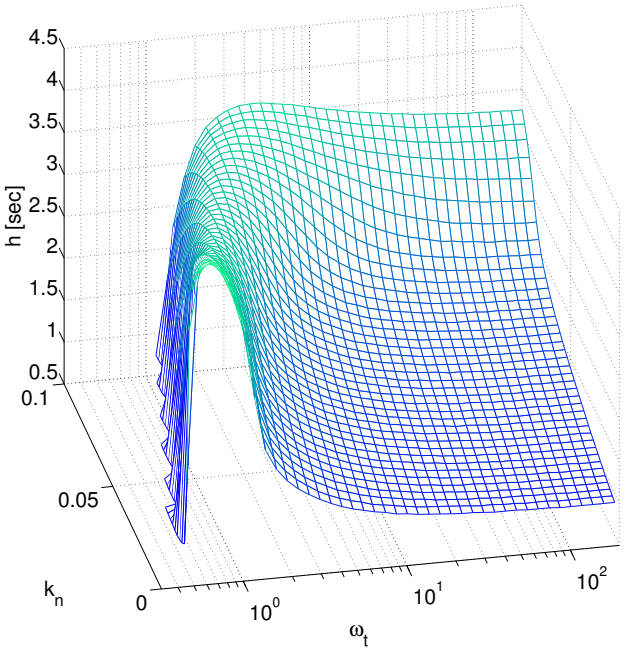


**Figure 9.** The preview length required to attain 90% of all possible performance improvement as a function of the distortion parameters. We see that a longer preview is needed to cope with an increase in the measurement noise intensity. The same is true for a decrease in the bandwidth $\omega_t$, but only up to a certain frequency after which there is a sharp decrease in the required preview length.

additional hardware. Second, by definition the effective wind speed is best estimated via a turbine.

To assess the potential of using upwind turbine measurements for preview control, we identify the corresponding measurement distortion model $M_n$ and $M_t$ based on real wind turbine data collected from OWEZ wind farm. The data was collected from two neighboring turbines. During the data collection the mean wind speed was 10 m/s and the mean wind direction was from one turbine to the other. For more information on the data set, see [Knudsen et al., 2011] where it is described in detail.

Effective wind speeds at both turbines were estimated from the data as described in [Knudsen et al., 2011] and used as inputs to the identification procedure. To be consistent with earlier notations, the effective wind speeds at the upwind and downwind turbines are denoted $V_m$ and $V_i$, respectively. See Figure 3. The relation between the signals is

$V_m = M_t V + M_n n = M_t e^{sh} V_i + M_n n$, where $h$ is the delay and $n$ is a white noise process, independent of $V$. The delay was estimated using covariance estimates and prewhitening [Ljung, 1999]. This resulted in a delay estimate of 60 sec, which is slightly smaller than the time it would take to travel between the turbines at mean wind speed. After setting $h = 60$ s, a prediction error method was used to fit $M_t$ and $M_n$ to a Box Jenkins model structure, [Box and Jenkins, 1976]. This resulted in a bandwidth for $M_t$ of $\omega_t = 0.015$, which is far below the 2 rad/sec needed to obtain a significant performance improvement. This shows that, effective wind speed estimates from a single upwind turbine are not useful for reducing tower oscillations, at least not for the wind conditions during the data collection. Indeed, substituting the identified $M_t$ and $M_n$ into the solution of **OP** yielded only an improvement of 0.8% in terms of the performance index.

Although the outcome of this section is negative, it provides us with insights for future research. The results suggest that in order to benefit from preview, effective wind speeds must be based on measurements close to the turbine. Note that, measuring closer to the turbine is feasible in terms of preview length, since the amount of preview needed is only a number of seconds.

## 6. Concluding remarks

In this paper, we considered the possibility of using previewed wind speed measurements for damping tower oscillations. Recent results on continuous-time $H^2$ preview control were used in order to develop a convenient framework for the analysis of the problem and for controller synthesis. The resulting controller performance was demonstrated by means of simulations based on the nonlinear NREL 5 MW turbine model described in [Jonkman et al., 2009], [Grunnet et al., 2010] and wind speeds obtained from real-world measurements.

We showed that in case of perfect measurements, a 31% improvement in terms of the damage equivalent load can be achieved due to availability of 1.3 sec preview. However, the benefit of using preview decreases in presence of measurement distortion. As expected, we saw that previewed measurements are useful only if their bandwidth exceeds the natural frequency of the tower. We also realized that, although the required length of preview grows due to the presence of measurement distortions, it does not exceed 5 sec for a reasonable range of distortion parameter values.

It is worth emphasizing that in the proposed control methodology, the model of the measurement distortion is naturally incorporated in the problem formulation. In other words, the distortion is explicitly taken into ac-

count during the controller synthesis. As demonstarted in Section 4, this is important for obtaining adequate controller behavior. In particular, we showed that in some cases it might be better not to use previewed information rather than using it without appropriately accounting for the distortion.

## Acknowledgments

This work was supported by the Swedish Research Council through the LCCC Linnaeus Center and by the European commission through the project AEOLUS.

## References

Box, G. E. P. and G. M. Jenkins (1976). *Time Series Analysis, Forecasting and Control*. Holden Day, San Fransisco, CA.

Burton, T., D. Sharpe, N. Jenkins, and E. Bossanyi (2001). *Wind Energy Handbook*. John Wiley & Sons, Chichester, UK.

Dunne, F., L. Y. Pao, A. D. Wright, B. Jonkman, and N. Kelley (2011). "Adding feedforward blade pitch control to standard feedback controllers for load mitigation in wind turbines". *Mechatronics* **21**:4, pp. 682–690.

FAST (2014). *NWTC computer-aided engineering tools (FAST by Jason Jonkman)*. Last modified: 2013-10-28. Retrieved 2014-04-16. URL: `http://wind.nrel.gov/designcodes/simulators/fast/`.

Grunnet, J., M. Soltani, T. Knudsen, M. Kragelund, and T. Bak (2010). "Aeolus toolbox for dynamic wind farm modeling, simulation and control". In: *Proceedings of the 2010 European Wind Energy Conference*, pp. 3119–3129.

Hammerum, K., P. Brath, and N. K. Poulsen (2007). "A fatigue approach to wind turbine control". *Journal of Physics: Conference Series* **75**:1.

Hansen, M. O. L. (2008). *Aerodynamics of Wind Turbines*. 2nd ed. Earthscan, London, UK.

Jonkman, J., S. Butterfield, W. Musial, and G. Scott (2009). *Definition of a 5-MW Reference Wind Turbine for Offshore System Development*. Tech. rep. NREL/TP-500-38060. National Renewable Energy Laboratory, Golden, CO.

Knudsen, T., M. Soltani, and T. Bak (2011). "Prediction models for wind speed at turbine locations in a wind farm". *Wind Energy* **14**:7, pp. 877–894.

Korber, A. and R. King (2010). "Model predictive control for wind turbines". In: *European Control Conference*.

Kristalny, M. and D. Madjidian (2011). "Decentralized feedforward control of wind farms: prospects and open problems". In: *Proceedings of the 50th IEEE Conference on Decision and Control and European Control Conference*. Orlando, FL, USA, pp. 3464–3469.

Kristalny, M. and L. Mirkin (2012). "On the $H^2$ two-sided model matching problem with preview". *IEEE Transactions on Automatic Control* **57**:1, pp. 204–209.

Laks, J., L. Y. Pao, E., Simley, A. D. Wright, N. Kelley, and B. Jonkman (2011a). "Model predictive control using preview measurements from lidar". In: *Proceedings of the 2011 AIAA Aerospace Sciences Meeting*. Orlando, FL.

Laks, J. H., L. Y. Pao, and A. D. Wright (2009). "Control of wind turbines: past, present, and future". In: *Proceedings of the 2009 American Control Conference*. St. Louis, MO, pp. 2096–2103.

Laks, J. H., L. Y. Pao, A. D. Wright, N. Kelley, and B Jonkman (2011b). "The use of preview wind measurements for blade pitch control". *Mechatronics* **21**:4, pp. 668–681.

Ljung, L. (1999). *System Identification, Theory for the User*. 2nd ed. PH, Upper Saddle River, NJ.

Mirkin, L. (2003). "On the fixed-lag smoothing: how to exploit the information preview". *Automatica* **39**:8, pp. 1495–1504.

OWEZ (2014). *Egmond aan zee offshore wind farm*. Retrieved 2014-04-16. URL: `http://www.noordzeewind.nl/`.

Panofsky, H. A. and J. A. Dutton (1984). *Atmospheric Turbulence*. John Wiley & Sons, NY.

Pao, L. and K. Johnson (2009). "A tutorial on the dynamics and control of wind turbines and wind farms". In: *Proceedings of the 2009 American Control Conference*. St. Louis, MO, pp. 2076–2089.

Schlipf, D., S. Schuler, F. Allgöwer, and M. Kuhn (2010). "Look-ahead cylcic pitch control with lidar". In: *Proceedings of the Science of Making Torque from Wind*. Heraklion, Greece.

SimWindFarm (2014). *Aeolus SimWindFarm Toolbox*. Retrieved 2014-04-16. URL: `http://www.ict-aeolus.eu/SimWindFarm/index.html`.

Soltani, M., R. Wisniewski, P. Brath, and S. Boyd (2011). "Load reduction of wind turbines using receding horizon control". In: *Proceedings of the 2011 IEEE International Conference on Control Applications*. Denver, CO.

Spudić, V., M. Jelavić, M. Baotić, and N. Perić (2010). "Hierarchical wind farm control for power/load optimization". In: *Proceedings of the Science of Making Torque from Wind*, pp. 681 –692.

Wang, N., K. E. Johnson, and A. D. Wright (2012). "FX-RLS-based feedforward control for LIDAR-enabled wind turbine load mitigation". *IEEE Transactions on Control Systems Technology* **20**:5, pp. 1212–1222.